Report on simulation work for crystalline-silicon based BIPV elements

Project report

NOBATEK, TECNALIA

November 2017

Summary

This document describes the results obtained from the simulation activities conducted at element and building level for the glass-glass products based on crystalline-silicon technology developed in WP3 "BIPV modules based on crystalline silicon technology" of PVSITES project.

The first part of the document describes the objectives and the methodology used for the modelling at element and building level. It also exposes the links with other activities within the project.

The second part of the report provides the main results obtained in terms of individual modules performance in the configurations designed for the experimental buildings and demo sites and the performance of each BIPV product for specific building typologies and different locations.

The results presented herein will feed directly tasks 2.3 "BIPV products portfolio" and task 9.8 "Implementation of the BIPV product portfolio", dedicated to the definition and implementation of a BIPV products portfolio.

Acknowledgements

Disclaimer

About the PVSITES project

PVSITES is an international collaboration co-funded by the European Union under the Horizon 2020 Research and Innovation program. It originated from the realisation that although building-integrated photovoltaics (BIPV) should have a major role to play in the ongoing transition towards nearly zero energy buildings (nZEBs) in Europe, the technology in new constructions has not yet happened. The cause of this limited deployment can be summarised as a mismatch between the BIPV products on offer and prevailing market demands and regulations.

The main objective of the PVSITES project is therefore to drive BIPV technology to a large market deployment by demonstrating an ambitious portfolio of building integrated solar technologies and systems, giving a forceful, reliable answer to the market requirements identified by the industrial members of the consortium in their day-to-day activity.

Coordinated by project partner Tecnalia, the PVSITES consortium started work in January 2016 and will be active for 3.5 years, until June 2019. This document is part of a series of public reports summarising the consortium's activities and findings, available for download on the project's website at www.pvsites.eu.

The PVSITES consortium:

Tecnalia Research & Innovation	CTCV	FormatD2
Onyx Solar	Flisom	Vilogia
BEAR-iD	Cricursa	R2M Solution Research to Market
Nobatek	CEA	CADCAMation
Film Optics	Acciona Infraestructuras	WIP - Renewable Energies

Contents

Tables

Figures

1 EXECUTIVE SUMMARY

1.1 Description of the deliverable content and purpose

This document is associated with task 3.6 "Modelling at element and building level". It provides the methodologies used for the simulation of the BIPV modules at element and building level and reports the corresponding results.

The aim of task 3.6 is to apply (and develop where needed) physical models for the BIPV products based on crystalline silicon technology, at element and building level, in order to characterize their main properties at different levels (optical, thermal, mechanical and electrical), make this information available for the manufacturer (Onyx Solar) and feed the BIPV products portfolio. In this sense, it complements the experimental work from task 3.7 (Performance validation testing).

The use cases associated with the demonstration sites have been simulated in the framework of task 8.1. "Design of demonstration installations". The main results in terms of impact of the BIPV products on the energy performance of the buildings and on the comfort (temperature and light level) are presented in deliverable D8.2 "Results of modelling and BIPV strategies for every demo site", which also includes a set of conclusions about the BIPV impact according to the technology used. For this deliverable, representative building configurations will be simulated for different climate zones, in order to get additional information on the technology performance.

1.2 Relation with other activities in the project

Table 1.1 depicts the main links of deliverable D3.7 to other activities (work packages, tasks, deliverables, etc.) within PVSITES project. The table should be considered along with the current document for further understanding of the deliverable contents and purpose.

Table 1.1 Relation between D3.7 and other activities in the project

Project activity	Relation with current deliverable
WP2 – T2.3 WP9 – T9.8	The results presented in D3.7 provide direct inputs to feed the BIPV product portfolio (tasks 2.3 and 9.8) and to generate useful information for dissemination materials.
WP3 – T3.7	The simulation work presented herein complements the laboratory testing in task 3.7 for the characterization of crystalline-silicon based glass-glass products.
WP4 – T4.3	Task 4.3 conducts a very similar approach as the one followed in task 3.6 but for the CIGS thin film technology provided by FLISOM.
WP7	Some of the algorithms developed within this task have been or are being implemented in the software tool. The information generated will feed the database of products within the software tool.
WP8 – T8.1	D8.2 provides the simulation results obtained for the demonstration sites in terms of impact of the BIPV products on the energy performance of buildings as well as on the comfort (temperature and lighting).

1.3 Reference material

D8.1 "Energy audit of buildings and identification of BIPV possibilities in every demo site", deliverable of the PVSITES project delivered at M15.

D8.2 "Results of modelling and BIPV strategies for every demo site", deliverable of the PVSITES project, in preparation, to be delivered in month 23.

1.4 Abbreviation list

BIPV: Building-integrated photovoltaics

CPR: Construction Products Regulation

EQE: External Quantum Efficiency

EVA: Ethyl-vinyl acetate

FEM: Finite Elements Method

IBC: Interdigitated Back Contact

IR: InfraRed

IQR: Inter Quartile Range

LVD: Low Voltage Directive

PV: Photovoltaics

PVR: PV Coverage Ratio

QCD: Quartile Coefficient of Dispersion

SHGC: Solar Heat Gain Coefficient

U: U value, thermal transmittance coefficient

WP: Work Package

WWR: Window-to-Wall Ratio

2 BIPV PRODUCTS

The aim of WP3 "BIPV modules based on crystalline silicon technology" is to take semi-transparent and opaque glass-glass BIPV technologies to a pre-industrial stage by providing a multiple answer to the market needs identified and defined in task 1.1. "Market and stakeholder analysis and needs". This section provides a short description of the different technologies developed by ONYX (sections 2.1 and 2.2) and Tecnalia, Film Optics and Onyx (section 2.3) within WP3 of PVSITES project. The calculations have been focused on the technologies and configurations selected for the experimental buildings (low concentration element in skylight and façade configuration, to be tested in Acciona and CEA facilities) and demo sites (semitransparent back-contact technology for Tecnalia building and opaque hidden bus bars and L-interconnections modules for Vilogia building).

2.1 Semitransparent modules with back-contact solar cells

The product is a glass-glass semitransparent solar PV module. It uses Sunpower Interdigitated Back Contact (IBC) solar cells encapsulated between two glass sheets with EVA polymer. The IBC technology has two main advantages:

-   Improved efficiency (from ~ 16% to ~25%) with zero shading loss and lower resistive loss,

-   Improved aesthetical aspect with invisible bus bar.

Figure 2.1: See-through back contact solar cell

Besides, depending on their architectural use, semi-transparent PV modules can play an important role in building energy use. When used as windows or shading devices, they affect the solar heat gain and natural lighting availability, and this has several consequences [1]:

-   During summer time, semitransparent modules reduce the cooling needs, or improve the occupant thermal comfort if the building temperature is uncontroled.

-   During winter time, the modules generally increase the heating needs.

-   Over the year, semitransparent BIPV reduces the natural lighting level and may increase artificial lighting consumption, depending on the regulation strategy.

Given these conflicting effects, several articles ([1], [2], [3]) indicate that the PV cell to transparent surface ratio has a strong impact on the energy performance and may be optimised. The objective is to get the appropriate balance between electricity production, thermal and lighting energy needs.

The impact of this product on the building overall energy needs will be analysed herein through appropriate state of the art models.

2.2 Hidden busbars and L-interconnections for opaque BIPV solutions

BIPV modules with visible bus bars or L-interconnections with a metallic aspect may cause unaesthetic effects when integrated in a building façade since these silver stripes present a marked contrast with the uniform appearance of the silicon cells. Therefore, ONYX has developed a technology where a black conductive ribbon is implemented over the welded cells in a string. Combined to black plastic sheets to hide the L-interconnections, and to a fully black frit patterned rear glazing, the final product will be a fully black PV glazing/glazing unit that will answer the aesthetic constraint, while maintaining the performance level.

Unlike conventional crystalline panels, hidden bus bar products display a uniform appearance. This aesthetical advantage allows architectural applications such as cladding or ventilated façade:

Figure 2.2: Front view of hidden busbar and L-interconnections product (2nd generation)

Figure 2.3: Vented cladding on Botanic garden of Denver

Being an opaque product, the fraction of solar radiation that is not either reflected or converted into electric energy is converted to thermal energy. Used as cladding, this product can affect the overall building performance. Therefore, modeling strategies are required to assess the impact of the product on the building heating/cooling needs and on occupant thermal comfort.

2.3 Low concentration, solar-control BIPV product for skylights and façades

These products are composed by semitransparent PV modules in conjunction with integrated optical elements (Fresnel lenses) that concentrate solar radiation onto the cells during the central part of the year and allow light passing towards the interior of the building during the winter with a double effect: (1) an increase in PV production in comparison with a traditional PV system of same installed

power (2) a decrease of the energy demand of the building during the summer. The details on system design can be found in deliverables D3.1 "Low-concentration, solar control system: report on lens and module designs and validity ranges" and D3.2. "Low-concentration, solar control system: report on architectural integration".
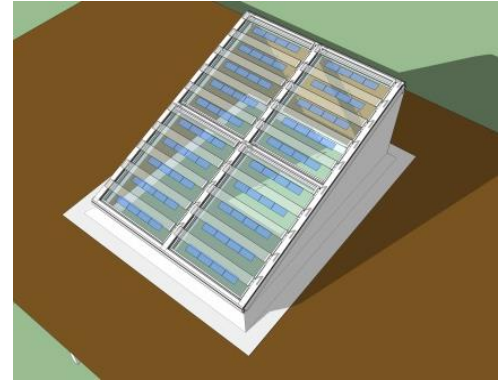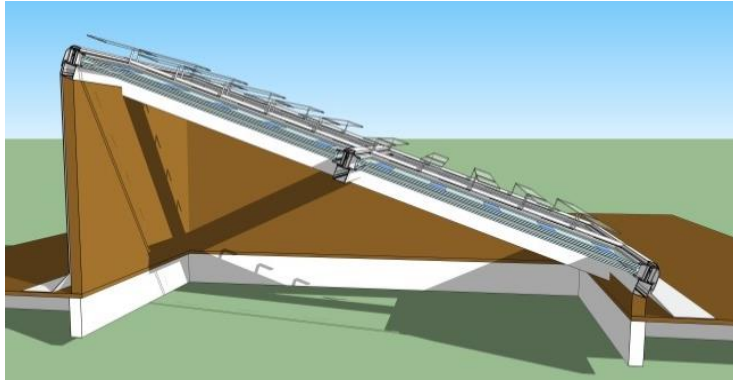
Figure 2.4: General view of low concentration element in skylight configuration
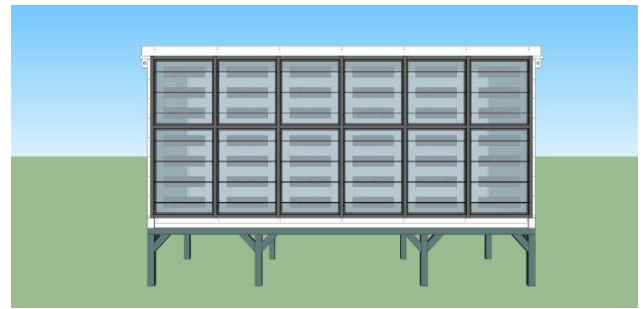
Figure 2.5: General view of low concentration element in façade configuration.

3 MODELLING OBJECTIVES

According to EN 50583 standard for BIPV modules and systems, photovoltaic modules are considered to be building-integrated if they constitute a construction product providing a function as defined in the European Construction Product Regulation CPR 305/2011. In this context, the term "function" refers to one or more of the following:

- Mechanical rigidity or structural integrity

- Primary weather impact protection: rain, snow, wind, hail

- Energy economy, such as shading, daylighting, thermal insulation

- Fire protection

- Noise protection

- Separation between indoor and outdoor environments

- Security, shelter or safety

As electrical systems, BIPV modules are subject to the applicable electro-technical requirements as stated in the Low Voltage Directive (LVD) 2006/95/EC and the corresponding CENELEC standards.

Any BIPV product entering the market needs, therefore, to demonstrate the fulfillment with these EU regulations, and both manufacturers and project designers need tools for a full characterization of BIPV products in this sense. The approach to show compliance with CPR and LVD is the testing according to the corresponding standards, as described in Tasks 1.3 "Standardization needs" and 3.7 "Performance validation testing" of PVSITES project. Additionally, some of these standards (e.g. for the optical and thermal properties of glazing systems) require a standardized calculation. In some cases, however, the calculation procedures in the standards are not suited to the specificities of a glazing system with encapsulated PV cells (e.g., the calculation of the solar factor as stated in EN 410 standard) and therefore novel and accurate procedures have to be developed to address these issues.

The general objective of the modeling activities proposed herein is to complement the experimental laboratory testing from Task 3.7 in order to provide a complete characterization of the BIPV products that can be used by the manufacturer for market activities and the architects and project designers in order to evaluate the potential performance of a building with integrated photovoltaic products. In addition to this, the newly developed calculation models will form part of the software tool developed in WP7 to support the design stages of BIPV products.

The simulation activities will be considered both at element and building levels in order to generate a complete set of information on the products performance and their influence on specific building and climate conditions.

4 SIMULATION AT ELEMENT LEVEL

4.1 Optical calculations at element level

The optical modelling includes the analytical calculation of transmittance, reflectance and absorptance of each product in different encapsulation conditions from a basic set of initial experimental UV-Vis-NIR spectrophotometry measurements. Analytical algorithms based on the transfer matrix-based method developed by T. Baenas and M. Machado (Solar Energy 125 (2016) 256-266) [4] for multilayer glazing systems and photovoltaic modules have been implemented and applied to the project products. The calculations allow a layer-by-layer study of the radiation absorption within the BIPV module, as an additional tool to define, from the glazing design phase, the thermal and mechanical processing needed for each glazing component. The absorptivity of the solar cells in a particular encapsulation condition can also be determined by calculation (M. Machado et al, Solar Energy 135 (2016) 77-83) [5]. This magnitude is directly related to the cell efficiency in a specific encapsulation condition. The analytical calculation for a range of glass panes types and thickness, as well as polymeric interlayer types and thickness is also possible from a reduced set of initial experimental UV-Vis-NIR spectrophotometry measurements.

Optical simulation is provided for the c-Si based glass-glass products developed within PVSITES project for demonstration sites, except the low concentration, solar control module, for which extensive optical simulations at element level formed part of the product design itself and were provided in deliverable 3.1.

4.1.1 Semitransparent modules with back-contact solar cells

In order to generate the optical data needed for the calculation of multiple encapsulation configurations, a basic experimental characterization was performed, as follows (all measurements in the 280-2200 nm wavelength range):

- Reflectance measurement of bare back-contact solar cell.
- Reflectance measurement of encapsulated back-contact solar cell + 1 layer EVA film + 4mm extraclear glass.
- Transmittance and reflectance of 4 mm extraclear glass.
- Transmittance and reflectance of a 4+4.1 laminated glass with no PV cells using a 0.45 mm EVA film.

All measurements were performed by TECNALIA using a JASCO V-670 spectrophotometer with a 150 mm integrating sphere, at normal incidence.

From these measurements, the optical properties of any laminated glass configuration using these components can be generated, including other glass thicknesses and number of EVA films (the internal transmittance of the used EVA film is calculated from the previous measurements so that it can be used in subsequent calculations for any other number of films). As an example, the properties of a 6+6.4 laminate (two 6 mm glass panes plus 4 EVA layers) are shown. This is the specific configuration chosen for the BIPV façade at Tecnalia demo site.

For completion, the external quantum efficiency (EQE) of the bare and encapsulated (4+4.2 configuration) back-contact solar cells has also been experimentally determined with a Bentham PVE 300. From these measurements, the external quantum efficiency and the short-circuit current of the cells in the encapsulation for Tecnalia demo site (6+6.4) have been calculated.

a) Results: solar cell experimental characterization and Jsc calculation
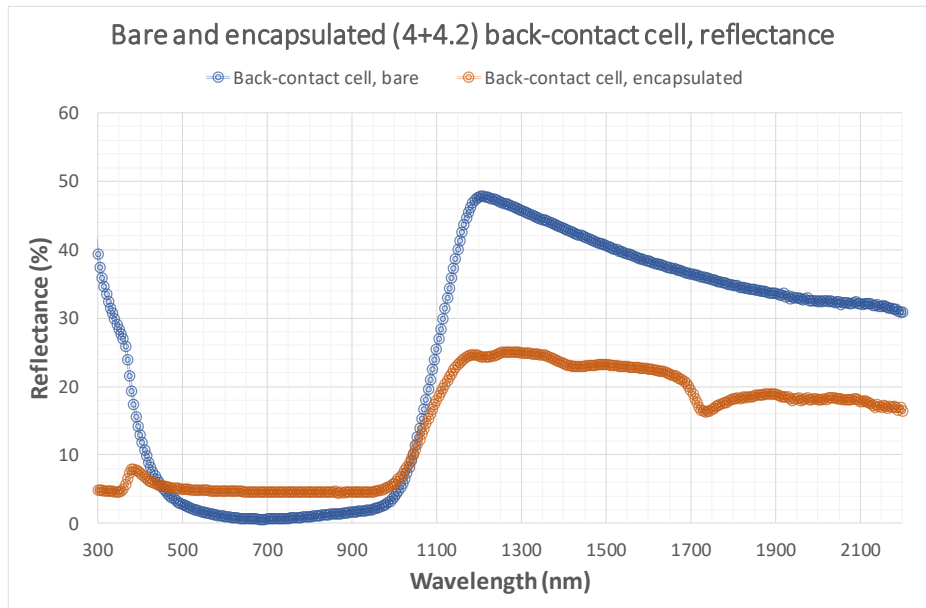
Figure 4.1: Experimental reflectance of a bare and encapsulated (in 4+4.2 configuration) back-contact solar cell.

It is interesting to remark that the glass-encapsulation reduces the reflectance in the visible range, due to the lower gradient of refraction indexes in the air-glass-encapsulant-cell system than in the air-cell system.
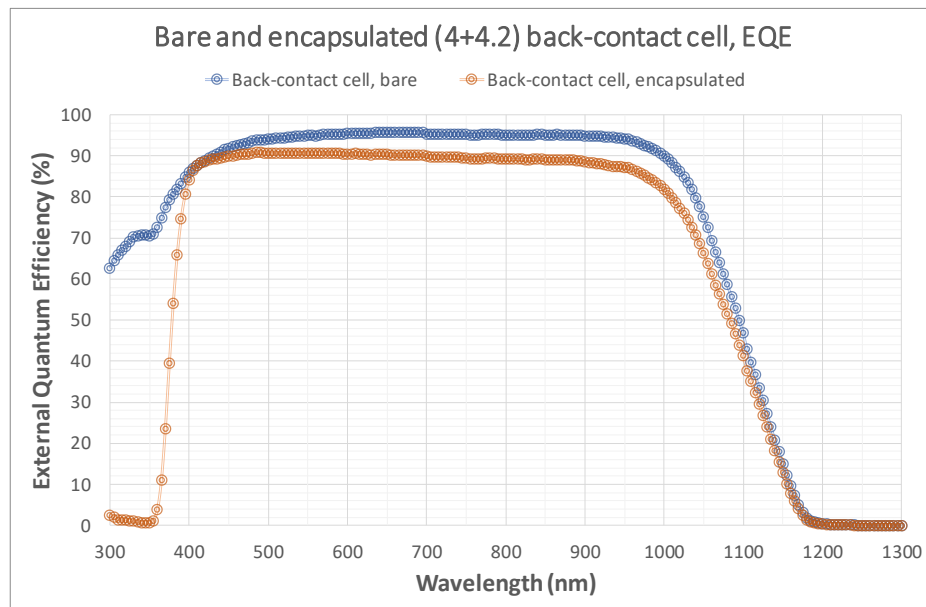
Figure 4.2: Experimental external quantum efficiency of a bare and encapsulated (in 4+4.2 configuration) back-contact solar cell.

From these curves, it is possible to calculate the short-circuit current of the back-contact cells used in the prototypes, both in bare and encapsulated conditions (i.e., calculating the corresponding Jsc for a 6+6.4) configuration), resulting in:

Bare cell: Jsc=40,68 mA/cm^2

Encapsulated cell (4+4.2): Jsc=37,61 mA/cm^2

Encapsulated cell (6+6.4)= 37,45 mA/cm^2

Encapsulation implies, therefore, a 7,9% reduction of the short-circuit current of the back- contact cells.

b) Results: Glazing system (glass and EVA polymer) experimental characterization
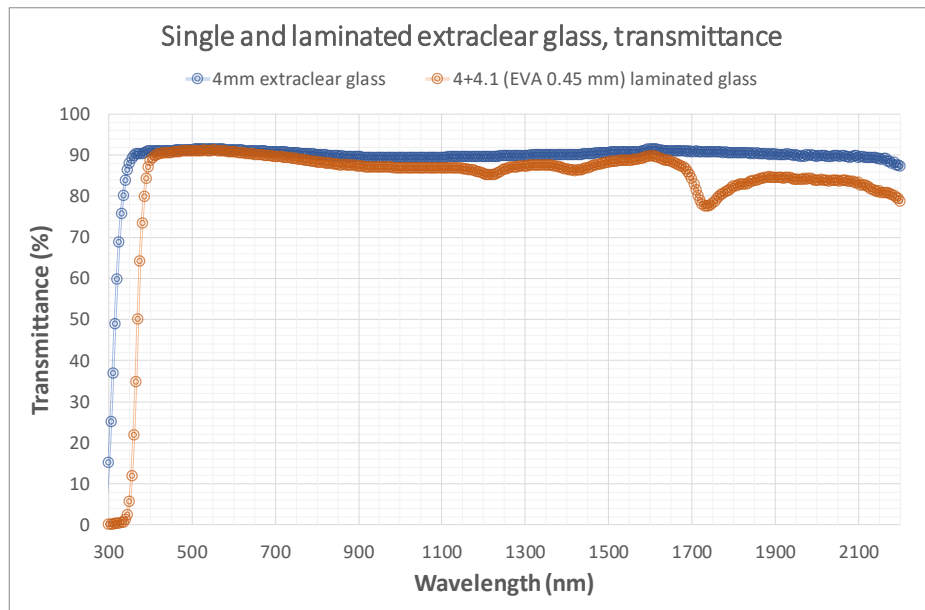
Figure 4.3: Experimental transmittance of a 4mm extraclear glass and a 4+4.1 laminated glass with 0.45 mm EVA film.
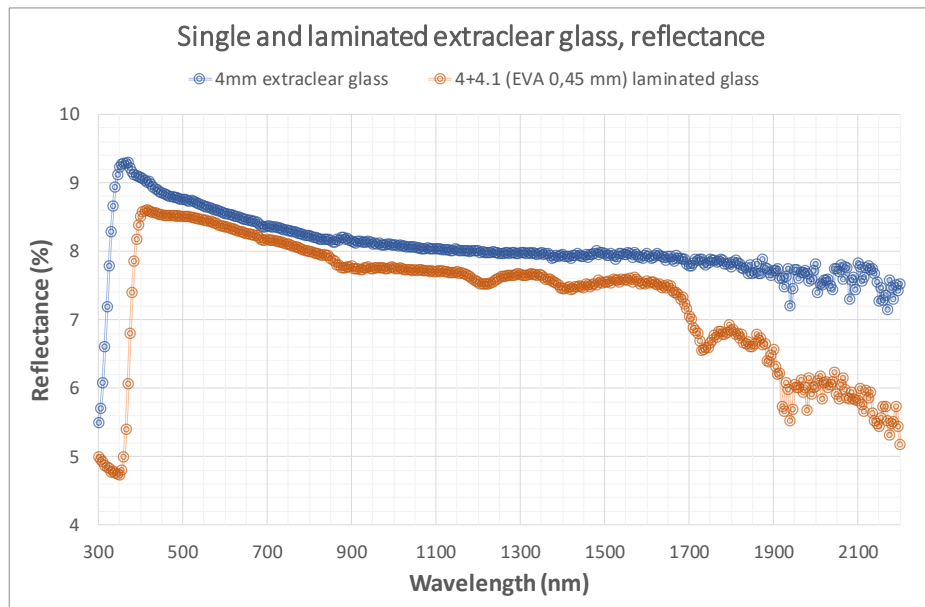
Figure 4.4: Experimental reflectance of a 4mm extraclear glass and a 4+4.1 laminated glass with 0.45 mm EVA film.
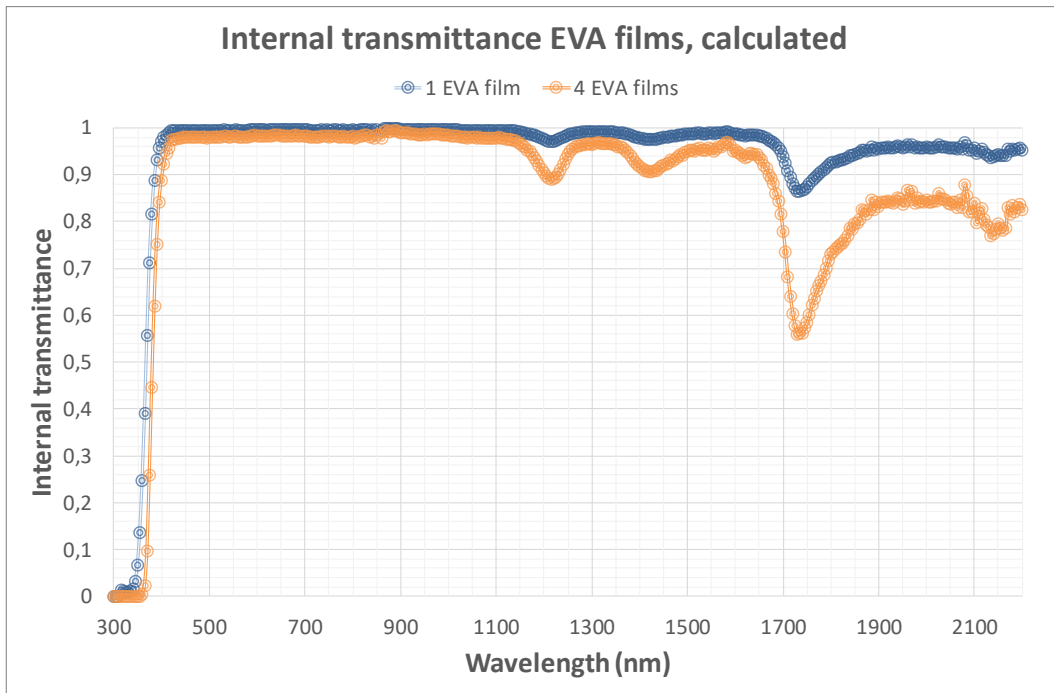
Figure 4.5: Calculated internal transmittance of 1 and 4 EVA films.

c) Results: laminated glass calculation in the demo-site configuration
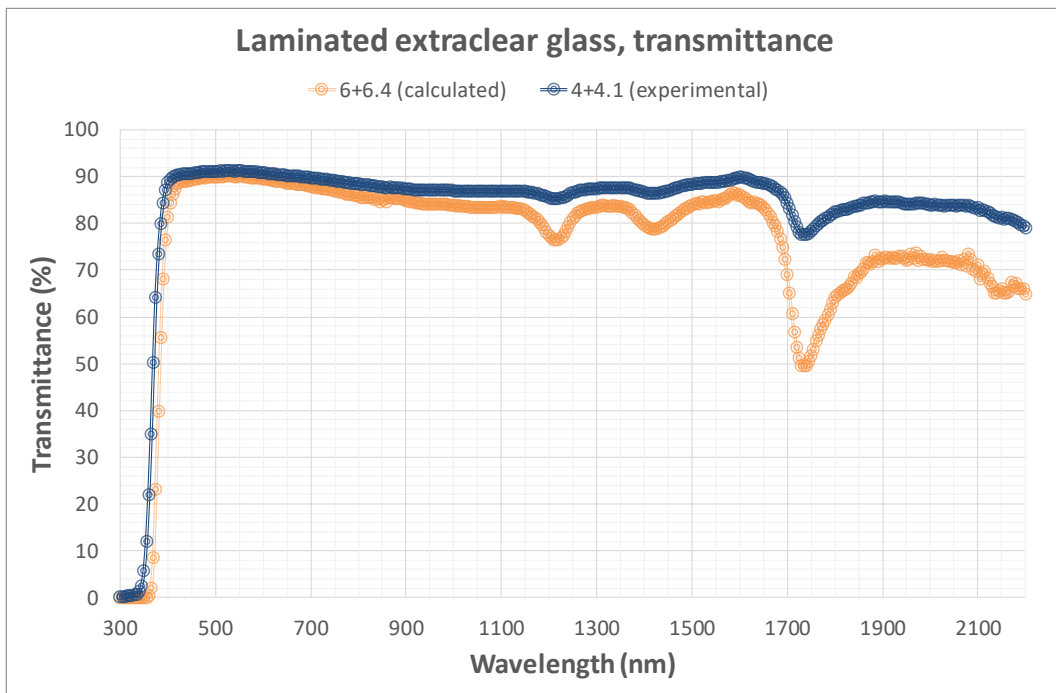
Figure 4.6: Calculated transmittance of a 6+6.4 laminated glass (configuration specified for Tecnalia demo site) shown together with the 4+4.1 experimental transmittance for comparison.
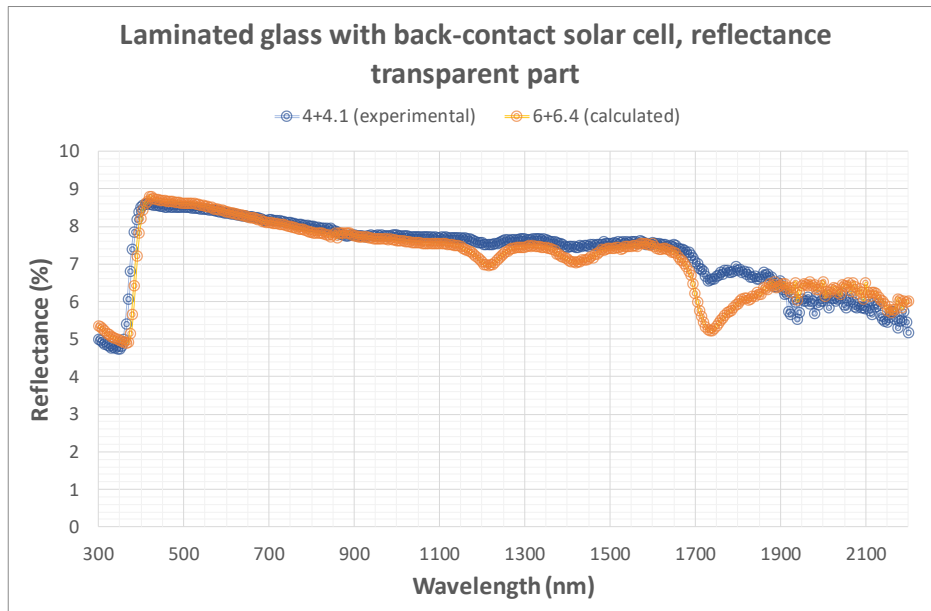
Figure 4.7: Calculated reflectance of the transparent part of a 6+6.4 laminated glass (configuration specified for Tecnalia demo site) shown together with the 4+4.1 experimental reflectance for comparison.
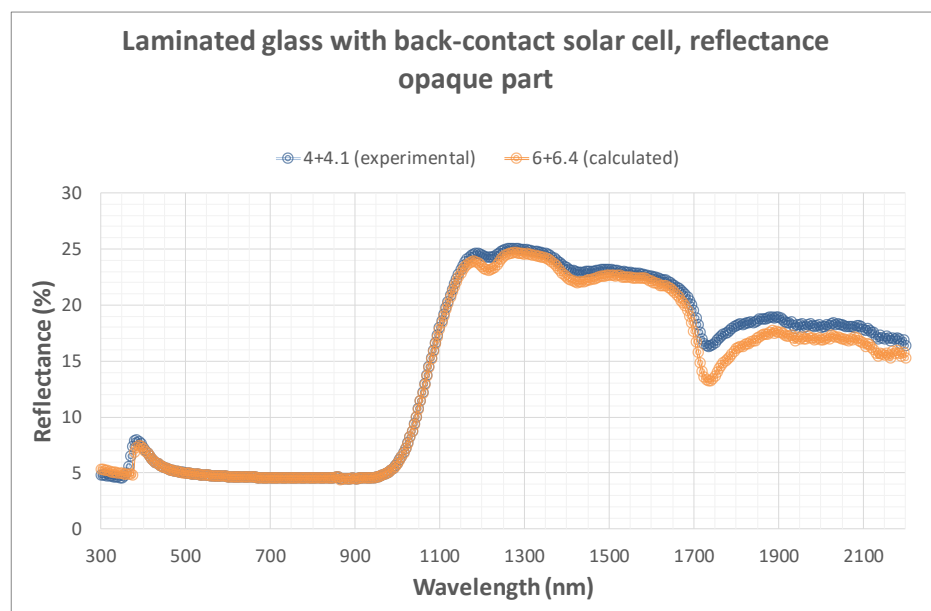
Figure 4.8: Calculated reflectance of the opaque parts (cell parts) of a 6+6.4 laminated glass (configuration specified for Tecnalia demo site) shown together with the 4+4.1 experimental reflectance for comparison.

The following table gathers the integrated transmittance and reflectance properties of the configurations considered, both for the transparent and opaque parts of the module.

Table 4.1 Optical simulation of the semi-transparent back-contact solar cell module, integrated values

Magnitude (%)	4+4.1	6+6.4
Solar transmittance	88,8	81,9
Visible transmittance	91,4	89,8
Solar reflectance - transparent part	7,9	7,8
Visible reflectance - transparent part	8,4	8,5
Solar reflectance - opaque part	8,2	8,3
Visible reflectance - opaque part	4,8	4,8

4.1.2 Hidden bus-bars and L-interconnections for opaque BIPV solutions

The first generation of modules (black frit and hidden bus bars) developed for Vilogia building have been considered for the calculation. Considering that this is an opaque product, the initial characterization does not consider transmittance measurement. It is not necessary to repeat the characterization of the cover glass either, so the needed measurements are the following:

- Reflectance measurement of bare crystalline silicon solar cell.
- Reflectance measurement of c-Si solar cell + 1 layer EVA film + 4mm extraclear glass.

All measurements were performed by TECNALIA using a JASCO V-670 spectrophotometer with a 150mm integrating sphere, at normal incidence.

From these measurements, the optical properties of any laminated glass configuration using these components can be generated, including other glass thicknesses and number of EVA films. As an example, the properties of a 6+6.4 laminate (two 6 mm glass panes plus 4 EVA layers) are shown. This is the specific configuration chosen for the BIPV façade at Vilogia demo site. However, the algorithms are ready to calculate any other configuration needed.

For completion, the external quantum efficiency (EQE) of the bare and encapsulated (4+4.2 configuration) solar cell used has also been experimentally determined with a Bentham PVE 300. From these measurements, the short-circuit current of the cells in the encapsulation conditions for Vilogia demo site (6+6.4) has been calculated.

a) Results: solar cell experimental characterization and Jsc calculation
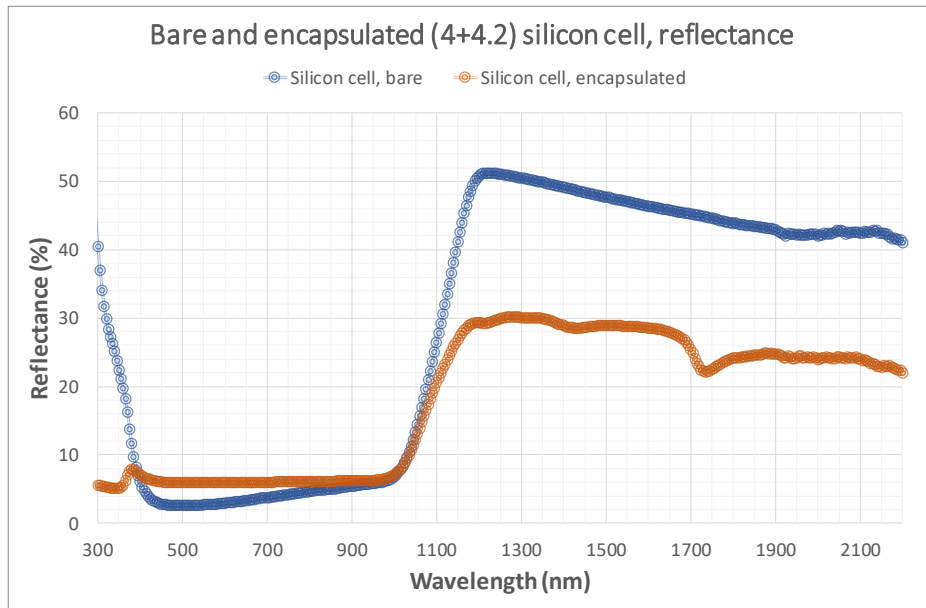
Figure 4.9: Experimental reflectance of a bare and encapsulated (in 4+4.2 configuration) crystalline silicon solar cell.
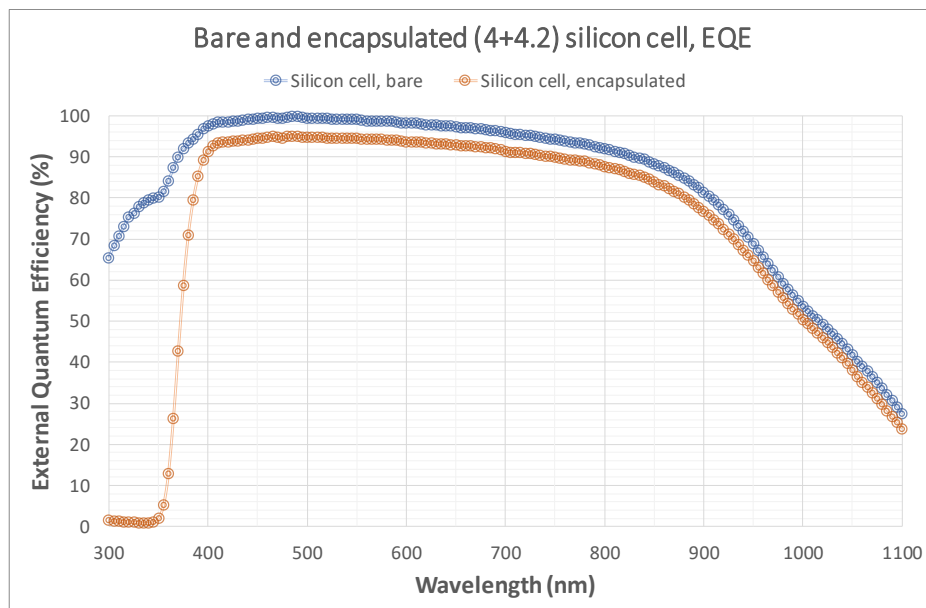
Figure 4.10: Experimental external quantum efficiency of a bare and encapsulated (in 4+4.2

The calculation of the Jsc from this input data, done for the encapsulation conditions decided for Vilogia building (6+6.4 laminated glass) results in the following values:

Bare cell: Jsc= 37,2 mA/cm^2

Encapsulated cell (4+4.2): Jsc=34,7 mA/cm^2

Encapsulated cell (6+6.4): Jsc= 35,7 mA/cm^2

The fact that the 4+4.2 configuration yields a slightly lower short-circuit current than the 6+6.4 is most probably due to inhomogeneities among different cells.

b) Results: Glazing system characterization

While the frontal glass is an extraclear, 6mm glass as used in the back-contact product, and EVA film is also the same and is therefore already characterized, the back cover in this case is a toughened glass with a black screen-printing, and therefore opaque. The characterization of EVA films was done for the back-contact cells module and there is no need to repeat it here.
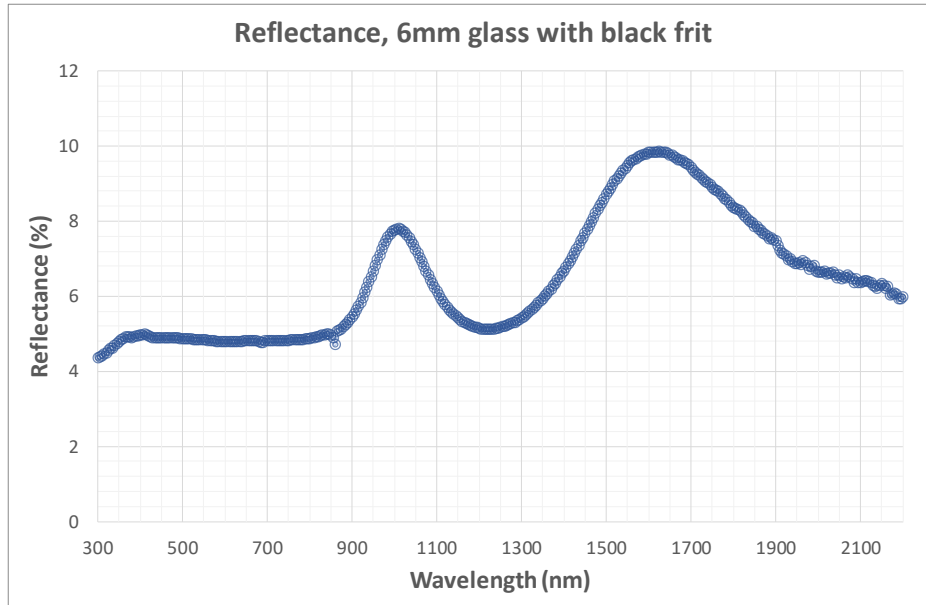
Figure 4.11: Reflectance of 6mm glass with black frit, used as back cover for BIPV modules with hidden bus-bars and L-interconnections.

c) Results: laminated glass calculation in the demo-site configuration
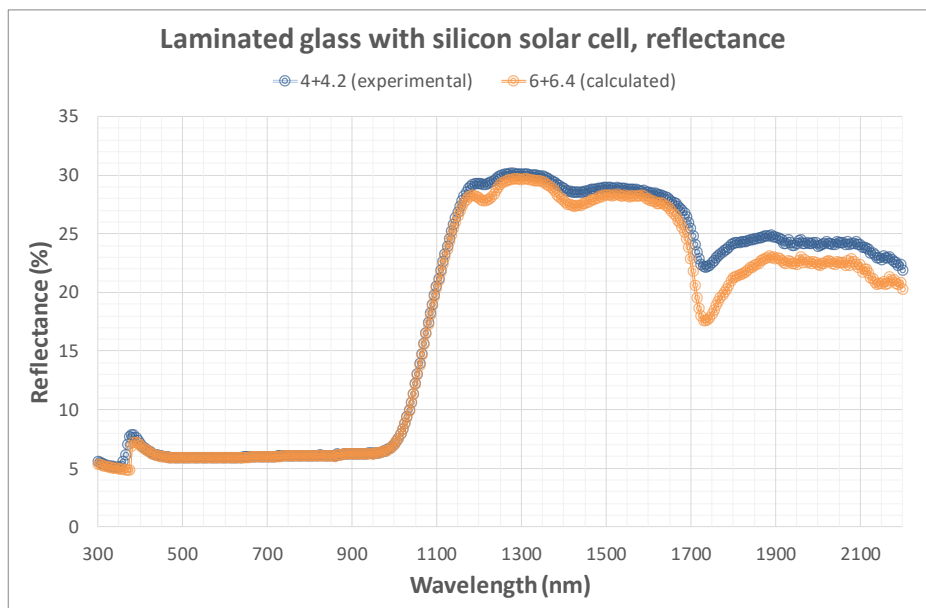
Figure 4.12: Calculated reflectance of the opaque parts (cell parts) of a 6+6.4 laminated glass (configuration specified for Vilogia demo site) shown together with the 4+4.2 experimental reflectance for comparison.

The following table gathers the integrated transmittance and reflectance properties of the configurations considered, for the opaque (cell) parts of the module.

Table 4.2 Optical simulation of the opaque module with hidden bus-bars and L-interconnections, integrated values

Magnitude (%)	4+4.1	6+6.4
Solar reflectance - opaque part (cells)	10,3	10,1
Visible reflectance - opaque part (cells)	5,9	5,9

4.2 Thermal calculations at element level

4.2.1 Thermal transmittance and solar factor

Thermal transmittance values have been calculated according to EN 673:2011 standard, "Glass in building. Determination of thermal transmittance (U value). Calculation method".

There are several standards (e.g. EN 410, ISO 9050) providing mathematical procedures for the calculation of the solar factor (or g value) of glazing systems with no PV cells embedded. However, they do not consider the case of a semi-transparent PV module in either open or short-circuit conditions. EN 50583:2016 standard, dealing with BIPV modules and systems, states the need to determine the g value for BIPV modules, but no specific calculation procedure is provided, beyond references to the glazing standards. For a correct determination of the solar factor of semi-transparent BIPV glass-glass modules, the analysis of heat transfer through the system should consider both the surface covered by the opaque PV cells and the transparent glazed part.

An analytical procedure for the determination of the g value of a glass-glass PV module has been developed in the framework of PVSITES project. This work has been published as T. Baenas and M. Machado, Energy and Buildings 151 (2017), 146-156 [6]. The work starts from the thermal study of a general system of any number of planar parallel layers with homogeneous absorption of solar radiation. An accurate description of the optical performance is included through the application of the optical model of Baenas and Machado [4] and Machado et al. [5]. The scope of this analytical model is in line with that of international standards for multiple glazing systems. However, it improves the accuracy of the optical and thermal modelling, with respect to the standardized simplified calculation, and it completes the description of the opaque region by introducing the effective short-wave absorptance of the solar cell. This effective absorptance takes into account the energy conversion at the solar cell.

The results of the calculations of U and g values for the laminated glass configurations to be used in Vilogia and Tecnalia demo sites are compiled in the table below.

Table 4.3 Thermal parameters of the laminated glass systems in the configuration established for demo sites.

Magnitude	6+6.4 laminated glass in demo site configuration
Solar factor – semitransparent back-contact cell module	0,44
U value - semitransparent back-contact cell module	5,12

Solar factor – opaque glazing with hidden busbars	0,23
U value - opaque glazing with hidden busbars	5,12

4.2.2 Finite element method thermal simulation of the hidden busbars and L-interconnections opaque product.

A simulation of the first generation fully black BIPV module (with hidden busbars, L-interconnectors and 86% cell occupancy) has been performed by TECNALIA using the SIEMENS NX platform, based on the finite element method (FEM), in order to calculate the expected thermal distribution of the PV module in a worst-case scenario for Wattignies (Lille). This is the only case in which potential thermal problems (overheating due to excessive absorption) might be expected. Previously to the FEM simulation, the absorptances of the solar cells and black glass were calculated with TECNALIA's internal algorithms and then used as an input for this thermal simulation.

The objective of the simulations was to determine whether the maximum temperature reached by the BIPV module was below the admissible threshold, when combining harsh ambient conditions such as high solar irradiation, high ambient temperature, natural ventilation (absence of wind) and open circuit conditions.

(a) Worst case scenario definition

The definition of the most unfavorable condition was performed calculating a simple analytical case of the system for the ambient conditions of August, September and October. August presented the highest ambient temperature and medium irradiation conditions derived from the sun elevation and the vertical façade configuration. September and October presented the opposite conditions, a lower ambient temperature but higher solar irradiation due to the lower sun elevation during those months.

The following table summarizes the boundary conditions studied in order to define the worst-case scenario for Wattignies.

Table 4.4 Boundary conditions considered to define the worst-case scenario.

Month	Irradiation (W/m^2)*	Ambient Temperature (°C)**
August	662	40
September	781	35
October	861	30

Calculated with PVGIS, ** *Taken from www.meteo-lille.net*

The following thermal system was considered:

h_{ext} = 5 W/m^2.K

h_{gap} = 7.5 W/m^2.K

T_{amb}: August= 40 °C / September= 35 °C / October= 30 °C

T_{sky}: August= 35 °C / September= 26 °C / October= 19 °C (calculated with Swinbank)[1]

Air gap temperature= 55 °C

---

[1] Tsky Swinbank =0,0552*(Tamb+273,15)^1,5

Wall temperature= 60 ºC

After solving the thermal system, the maximum temperatures obtained in the BIPV module for each case were:

$Tmax_{august}$= 74.8 ºC

$Tmax_{sept}$= 76.7 ºC

$Tmax_{oct}$= 77.6 ºC

Hence, based on the unidimensional calculation, <u>October</u> was set as the worst-case scenario.

Comments on the boundary conditions:

The ambient temperature records in Lille are in fact 3-4 degrees Celsius below the ones shown in the table, but for the purpose of this calculation it was decided to slightly increase them in order to study a more unfavorable situation.

Similarly, the irradiation condition refers to a direct radiation situation which is not truly realistic. Lille has an average diffuse to global ratio of 0.55, which means that 55% of the radiation is based on a diffuse component.

(b) FEM simulation in SIEMENS NX

The simulation was simplified to a model based on a single photovoltaic module. Three cases were studied. Two of them were simple cases in which the convection coefficients, air temperature in the gap and the wall temperature were assumed to be known. A third case was built, including a CFD analysis of the air gap, in order to confirm that the previously made assumptions (convection coefficient, air temperature in the gap and wall temperatures) were admissible.

Geometric model

A 1700 x 1000 mm glass-glass module was built in NX, maintaining the real cell layout and distances to the edge of the original module (86% cell occupancy). The configuration was 66.4, i.e., 6 mm external glass, 6 mm internal glass, and 4 EVA sheets (1.8 mm total).
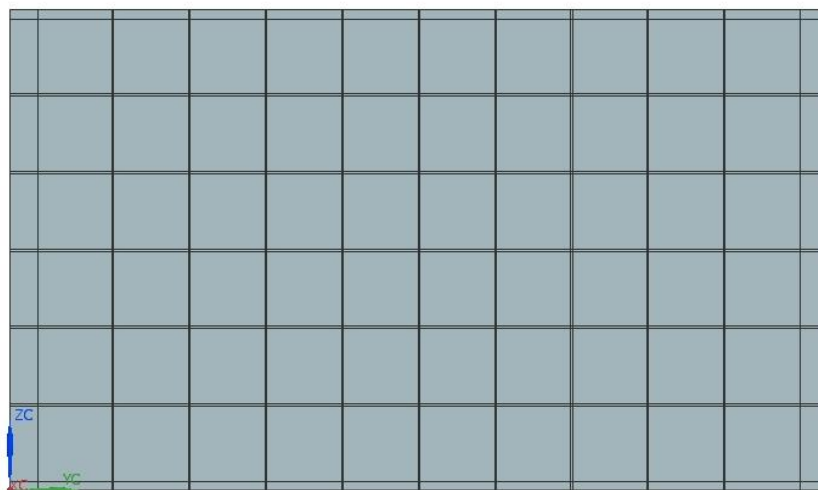
Figure 4.13: Geometry of the PV module for the simplified case (not CFD)

For the CFD analysis case, in addition to the PV module, the geometries of the air gap behind the module, an isolation layer and a concrete wall were included in the model. A 50 mm air gap, 50 mm isolation layer and 100 mm concrete wall were considered.
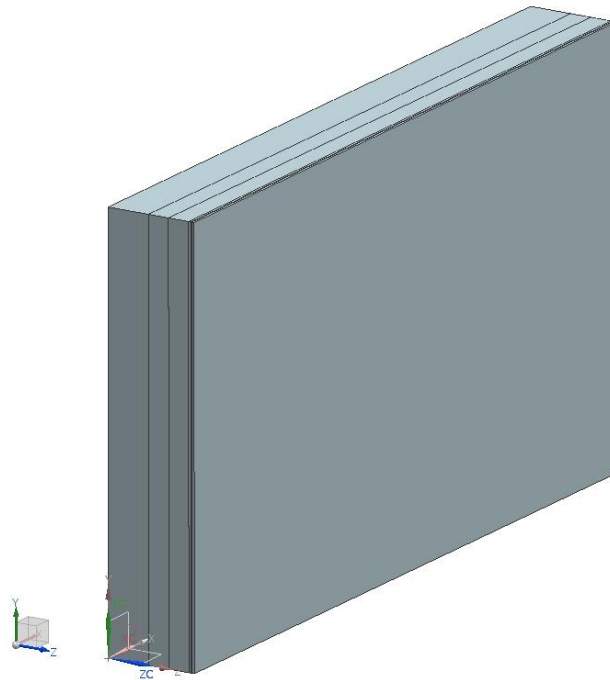
Figure 4.14: Geometry of the PV module for the CFD case, including PV module, air gap, isolation and wall.

Mesh

Hexahedral elements of 3 mm size were used to mesh the model of the simplified case. For the CDF model, 5 mm elements were used for the PV module, and 10, 20 and 30 mm for the air, isolation and concrete wall, respectively.
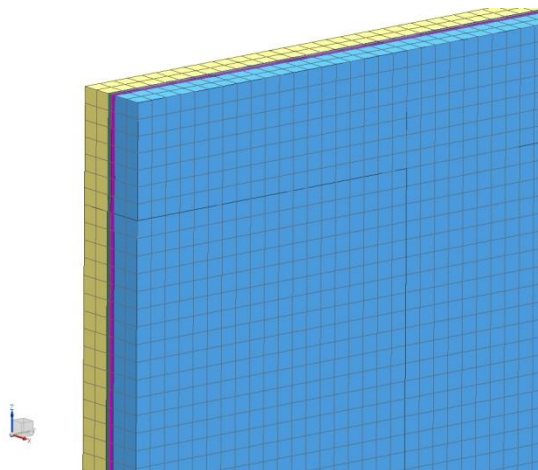
Figure 4.15: Detail of the mesh of the simplified case
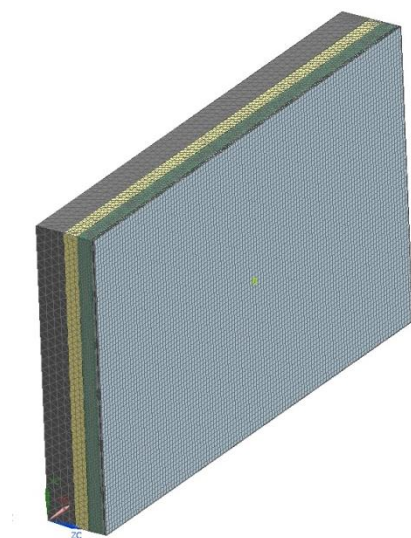
Figure 4.16: CFD model mesh

Report on simulation work for crystalline-silicon based BIPV elements

Simulation and boundary conditions

The thermal properties of the materials involved in the calculation are gathered in the table below.

Table 4.5 Thermal properties of the materials used in the calculation.

Material	Conductivity (W/m.K)	Emissivity
Glass	1	0.84
EVA	0.24	-
Isolation	0.037	0.9
Concrete wall	2	0.9

As for the boundary conditions used:

Case 1. Air gap temperature 55ºC and wall temperature 60 ºC

- Solar irradiation: 861 W/m^2
- Ambient temperature: 30 ºC
- Air gap temperature: 55 ºC
- Convection coefficient (ambient): 5 W/m^2.K
- Convection coefficient (cavity): 7.5 W/m^2.K
- Sky temperature: 19 ºC (calculated with the Swinbank expression)
- Wall temperature: 60 ºC
- Solar cell absorptance: 0.917 (calculated with internal procedures according to the relevant standards)
- Black glass absorptance: 0.937 (calculated with internal procedures according to the relevant standards)
- Open circuit condition

Case 2. Air gap temperature 65ºC and wall temperature 70 ºC

- Solar irradiation: 861 W/m^2
- Ambient temperature: 30 ºC
- Air gap temperature: 65 ºC
- Convection coefficient (ambient): 5 W/m^2.K
- Convection coefficient (cavity): 7.5 W/m^2.K
- Sky temperature: 19 ºC (calculated with the Swinbank expression)
- Wall temperature: 70 ºC
- Solar cell absorptance: 0.917 (calculated with internal procedures according to the relevant standards)
- Black glass absorptance: 0.937 (calculated with internal procedures according to the relevant standards)
- Open circuit condition

Case 3. CFD analysis

Two cases were studied, assuming 0.1 m/s and 0.5 m/s air velocities in the inlet part of the model. Both of them can be considered natural ventilation conditions thus representing unfavorable situations.

- Solar irradiation: 861 W/m^2
- Ambient temperature: 30 ºC
- Air gap temperature: calculated (inlet temperature: 30 ºC)
- Air velocity (inlet): 0.1 m/s and 0.5 m/s
- Convection coefficient (ambient): 5 W/m^2.K
- Convection coefficient (cavity): calculated
- Sky temperature: 19 ºC (calculated with the Swinbank expression)
- Wall temperature: calculated
- Solar cell absorptance : 0.917 (calculated with internal procedures according to the relevant standards)
- Black glass absorptance: 0.937 (calculated with internal procedures according to the relevant standards)
- Open circuit condition

(c) Results

Case 1. Air gap temperature 55ºC and wall temperature 60 ºC
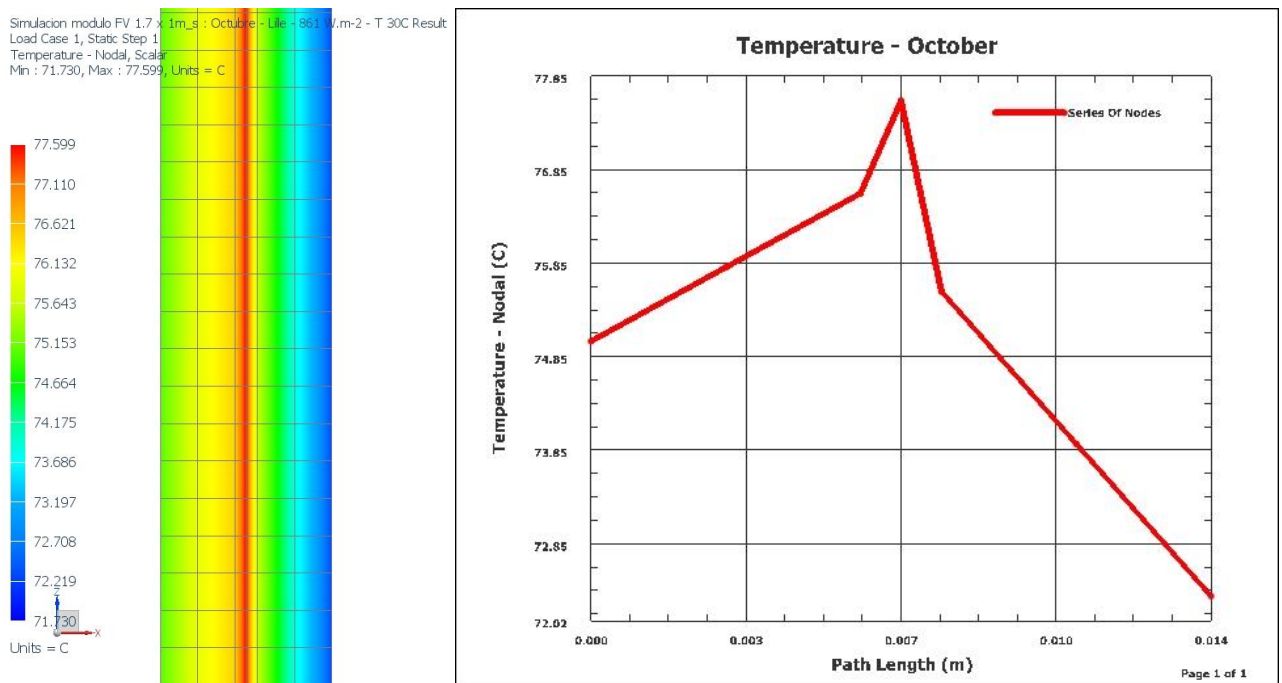
Figure 4.17: Temperature profiles for the cross section of the PV glass-glass module.

Case 2. Air gap temperature 65⁰C and wall temperature 70 ⁰C
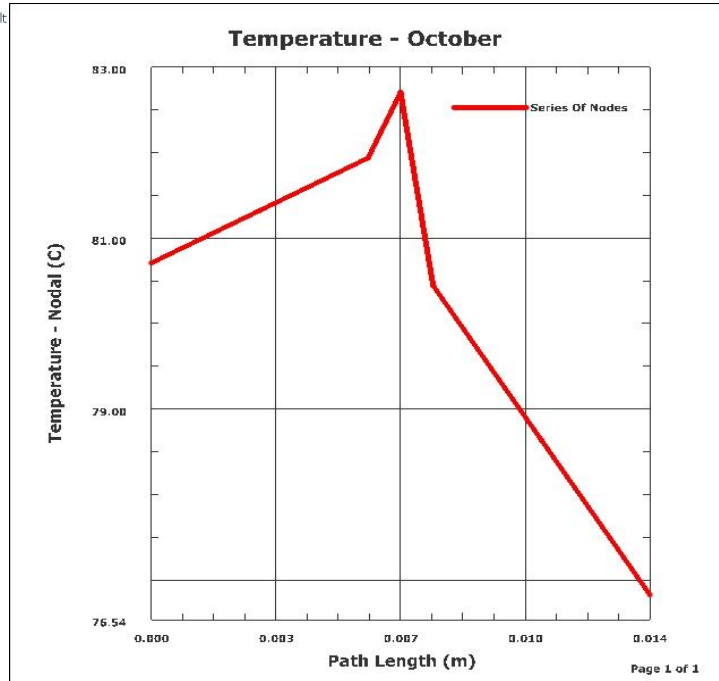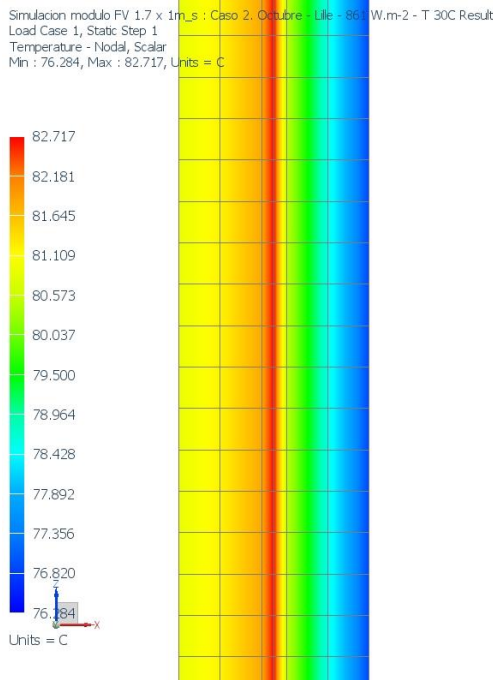
Figure 4.18: Temperature profiles for the cross section of the PV glass-glass module.

Case 3. CFD analysis

Case 3.1. Air velocity 0.5 m/s

System temperature distribution	Module temperature
Cell zone temperature	Isolation
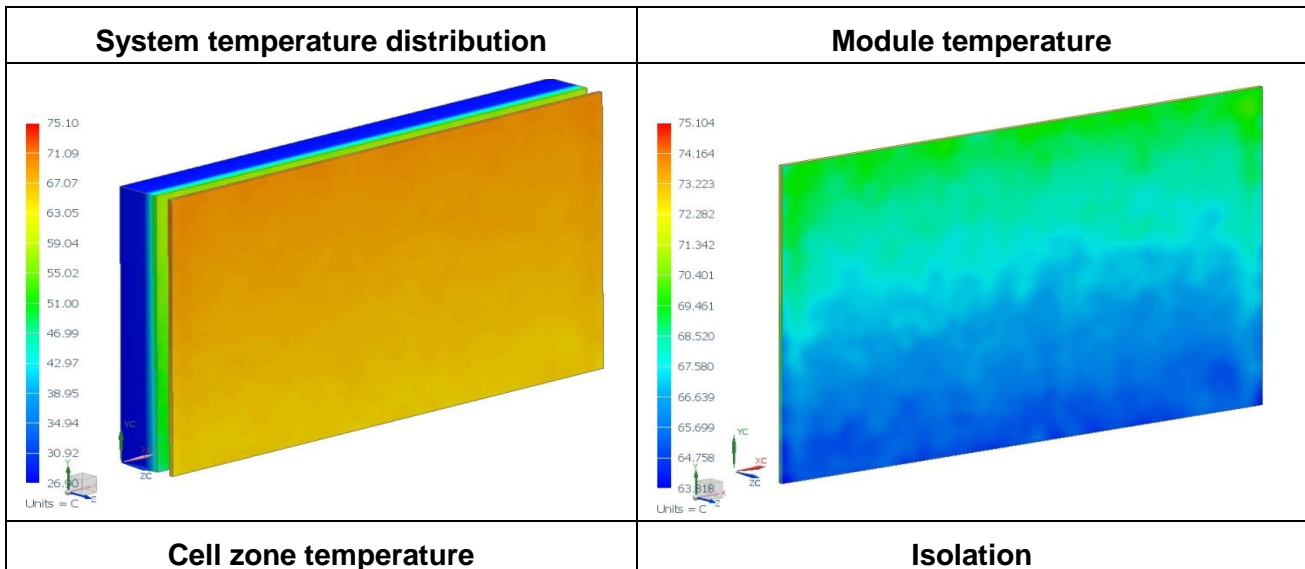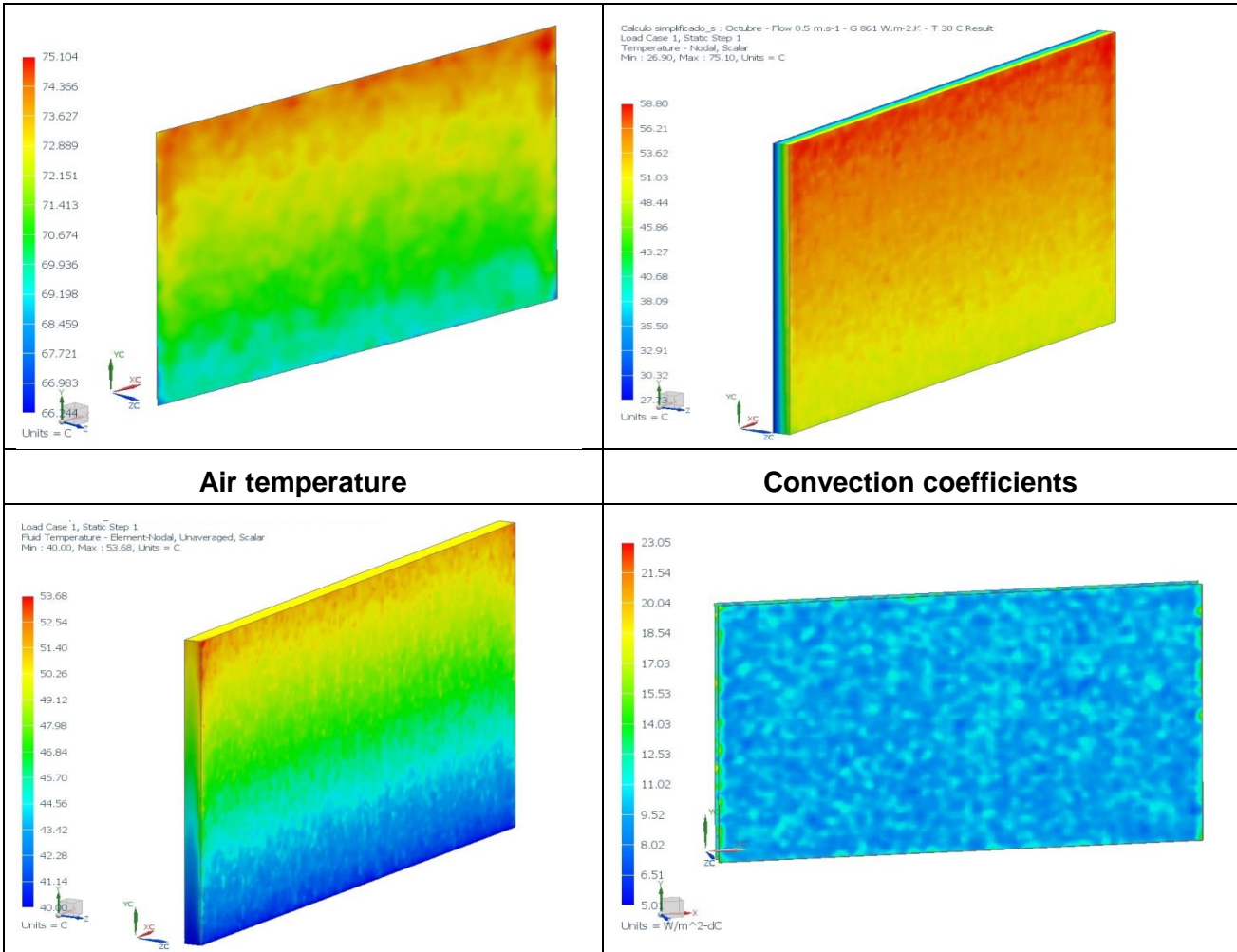
Figure 4.19: CFD analysis results

Case 3.2. Air velocity 0.1 m/s

| Air temperature | Convection coefficients |
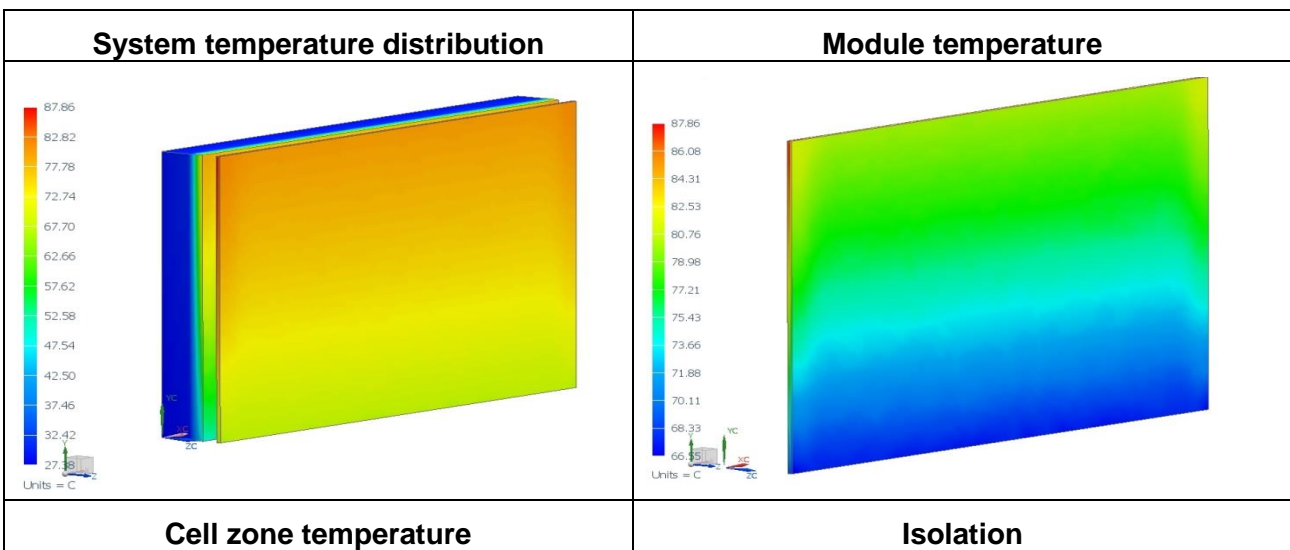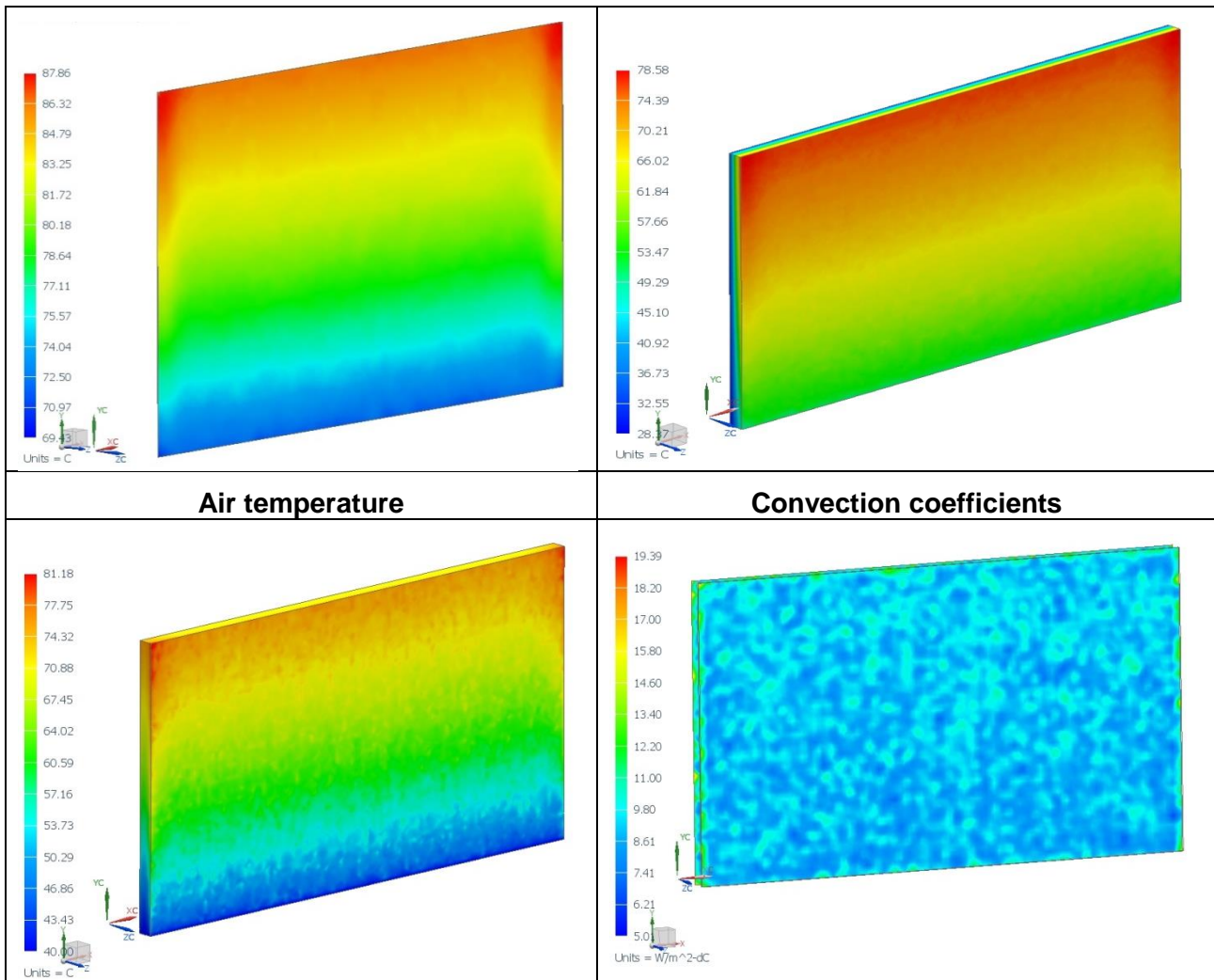
Figure 4.20: CFD analysis results

The following table summarizes the results for Case 3.

Table 4.6 Summary of results for case 3.

CASE 3	T_{max}	T_{wall} (average)	$T_{out\ air}$ (average)	h_{wall} (average)
Case 3.1 - 0.5 m/s	75.1	53.7	50.44	9.6
Case 3.2 - 0.1 m/s	87.9	66.2	73.8	9.0

(d) Conclusions

A series of thermal simulations have been performed, with the aim of determining the maximum temperatures that could be reached in the BIPV module in a worst-case scenario, when simultaneously experiencing high solar irradiation, high ambient temperature, natural ventilation (absence of wind) and open circuit conditions, in the city of Wattignies (Lille, France).

The approach started with a first simplified unidimensional analytical calculation for the determination of the worst-case scenario, later set in the month of October as a result of this calculation. The

thermal simulations performed using SIEMENS NX were addressed in two different ways. The first simulation was based on a detailed cell layout and simplified boundary conditions, where the air temperature in the gap, the resulting convection coefficients and the wall temperature itself were assumed to be known and introduced as an input for the simulation. Two situations were modeled, considering 55 / 65 ºC for the air temperature inside the cavity and 60 / 70 ºC for the wall temperature, respectively. A second approach based on a simple CFD analysis was used to confirm that the assumptions and results of the previous simulations were indeed correct, as the results would later confirm.

It is noteworthy to underline that a series of simplifications have been taken in order to ease the simulation process. A detailed thermal simulation would have required the calculation of, at least, a complete row of modules of the façade system, in order to account for the temperature increase of the air inside the cavity. By using CFD analysis, the path and thermal transfer between the module and the air flowing in the cavity would have been simulated, thus allowing the calculation of the exact thermal distribution of such system under the given boundary conditions (air is meshed and convection coefficients are calculated). However, representing and modelling in a realistic way the boundary conditions of the façade is not easy, since the ventilated façade is not fully air tight. In fact, it is not air tight at all, since there is a distance between each module, both in the horizontal and vertical directions. These air gaps will therefore contribute to cool down the air temperature as it goes increasing due to the natural flow created by the existing pressure difference between the bottom and the top parts of the façade.

However, since the purpose of this simulation is to determine if the thermal distribution obtained in a worst-case scenario leads to temperatures under the admissible threshold, a simpler simulation could be suggested. This simulation represents a more unfavorable case, since the air only enters through the bottom part of the façade, and was considered a valid approach to fulfil the objective of the simulation with an important safety coefficient.

The results show a maximum temperature in the solar cells of 87.9 ºC for the most unfavorable condition, which occurs in the month of October when applying the following boundary conditions: solar irradiation of 861 W/m^2, ambient temperature of 30 ºC and an air velocity of 0.1 m/s. This maximum temperature does not represent a problem in terms of absolute value, and nor it does in terms of absolute gradient temperature in the module, since the ~20 ºC gradient is admissible in tempered glass configurations.

The studied cases tried to address adverse thermal situations that combined extreme effects such as high solar irradiation, high ambient temperature, natural ventilation and absence of air inflow between modules (which lead to unfavorable situations that won't occur in reality) and open circuit conditions. In real operation conditions, the open circuit condition will only occur in punctual moments of the year that will rarely coincide with the assumed extreme boundary conditions at the same time. Thus, a lower maximum temperature will be certainly reached in case those extreme conditions would happen with the BIPV installation working in normal operation conditions since more than >15% of the absorbed solar radiation would be transformed into electricity, and not heat, as it was considered in the performed simulations.

In terms of maximum temperatures, the studied fully black glass-glass BIPV (86% cell occupancy) module won't differ much from a standard glass-glass BIPV module with a higher cell occupancy (close to 100%).

4.3 Mechanical performance simulation at element level

Mechanical calculations of the glass-glass products make sense at a system level and are being performed as part of the design of each installation in WP8 "Large scale demonstration and assessment of BIPV systems in real buildings". At element level, however, it does make sense to simulate the mechanical performance of Fresnel lenses (and their supporting elements) of the low concentration, solar control product both in skylight and façade configurations, in order to determine their resistance when subjected to wind and their own weight. Simulations have been performed with SIEMENS NX tool for Finite Element analysis.

4.3.1 Skylight configuration

Description of system and model

The analysed system consists of the lamella and its two supporting ends, each one including a square hollow section profile made of duraluminium 7075.
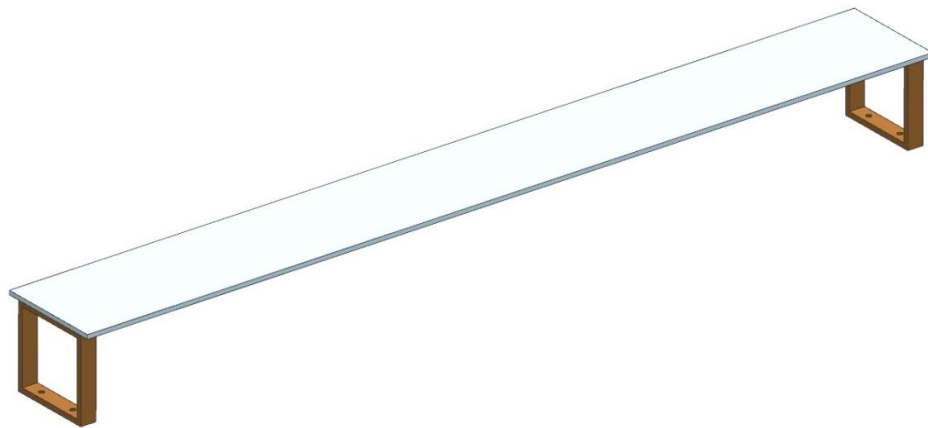
Figure 4.21: Schematics of the analysed system
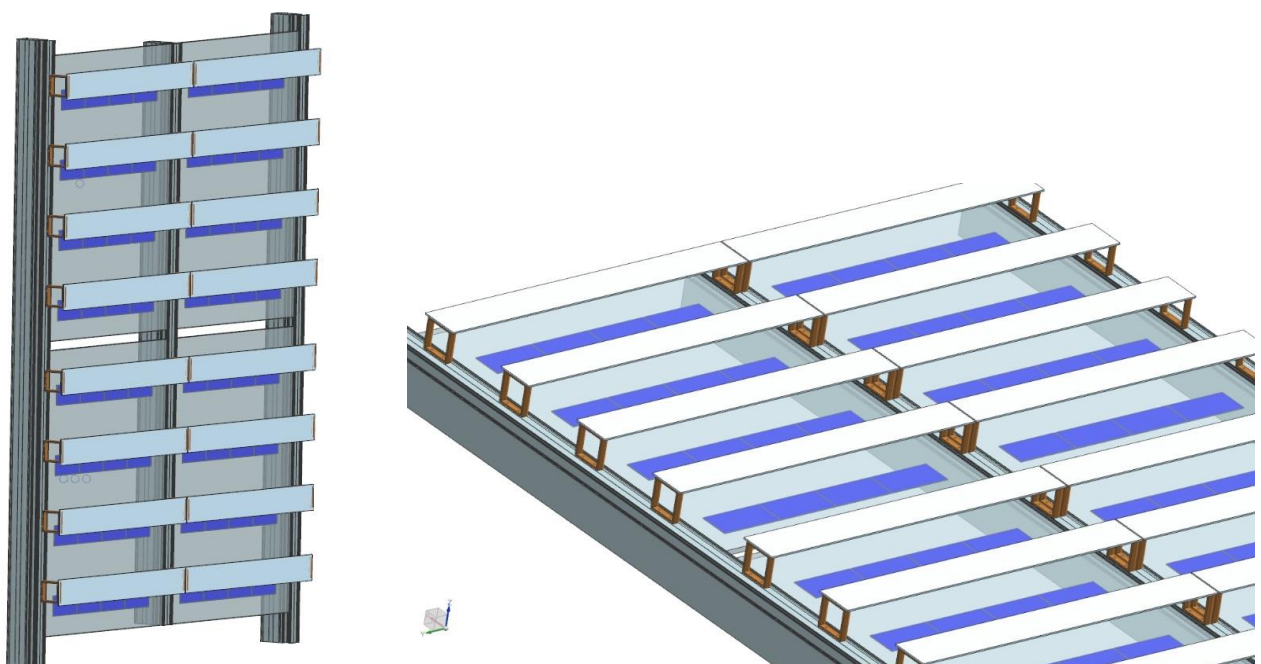
Figure 4.22: Skylight general views

The described structure is modelled by means of solid elements and consists of 396620 nodes and 240378 elements.

Mesh mating conditions are defined between every two components in contact.
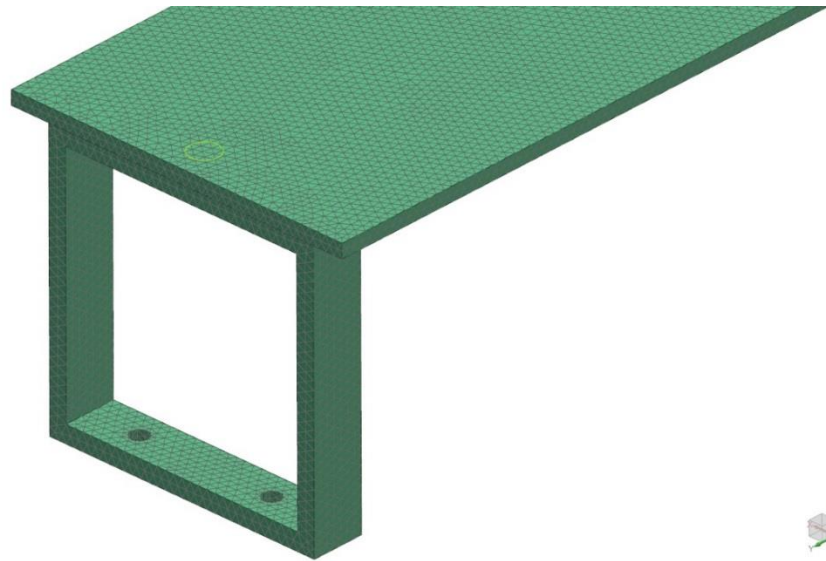
Figure 4.23: Detail of the finite element mesh of the skylight configuration

Regarding materials, the lamella is considered to be made of tempered glass and the square profile is considered to be made of duraluminium 7075.

Table 4.7 Material properties.

Property	Units	Tempered glass	Al. 7075
Density	kg/m^3	2500	2700
Yield stress	MPa	120	450
Young's modulus	MPa	70000	70000
Poisson's ratio	-	0,22	0.33

Boundary conditions: The square profiles are considered to be fixed in a 10mm diameter area surrounding the two bolts. This corresponds to the effect of the bolted joint with a washer. The outer diameter of a M5 washer is 10 mm.

The lamella is glued to the square profile.

The applied loads are:

- Wind load: 2000 Pa, both pressure and suction.

- Weight of the lamella.

Both loads are applied as distributed loads in the lamella, normal to its upper surface.
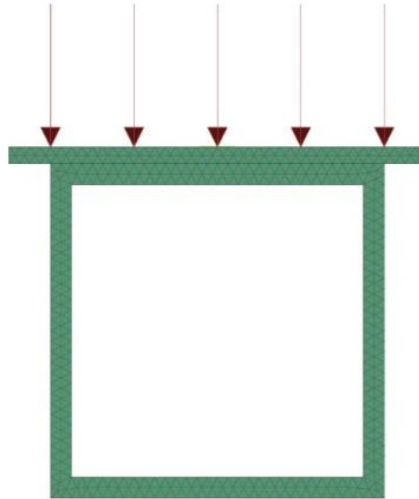
Figure 4.24: Simultaneous action of pressure wind load and weight over the skylight configuration

Numerical results obtained for each load case assessed are presented below.

The most restrictive load case is that in which the weight of the lamella and the pressure wind load are simultaneously applied.

Table 4.8 Main results for mechanical performance, skylight configuration.

Magnitude	Wind (pressure) + Weight
Maximum deformation (mm)	6,5
Maximum stress in lamella (MPa)	77,1
Maximum stress in aluminium parts (MPa)	64,3

SKYLIGHT ASSEMBLY_fem1_sim1 : SOLUCIÓN 1 Result
VIENTO + PESO PROPIO, Static Step 1
Displacement - Nodal, Magnitude
Min : 0.000, Max : 6.514, Units = mm
Deformation : Displacement - Nodal Magnitude

6.514
5.971
5.428
4.885
4.342
3.800
3.257
2.714
2.171
1.628
1.086
0.543
0.000

Units = mm
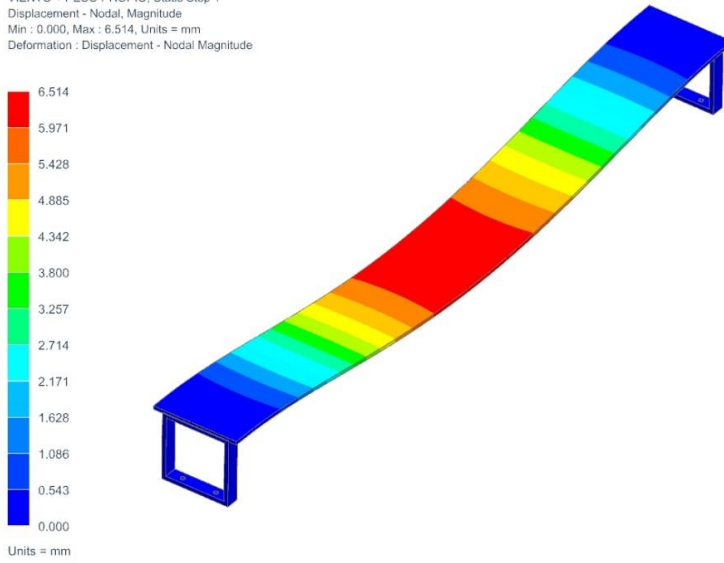
Figure 4.25: Deformation results, skylight case

SKYLIGHT ASSEMBLY_fem1_sim1 : SOLUCIÓN 1 Result
VIENTO + PESO PROPIO, Static Step 1
Stress - Element-Nodal, Unaveraged, Von-Mises
Min : 0.01, Max : 77.10, Units = N/mm^2(MPa)
Deformation : Displacement - Nodal Magnitude

77.10
70.68
64.25
57.83
51.40
44.98
38.55
32.13
25.71
19.28
12.86
6.43
0.01
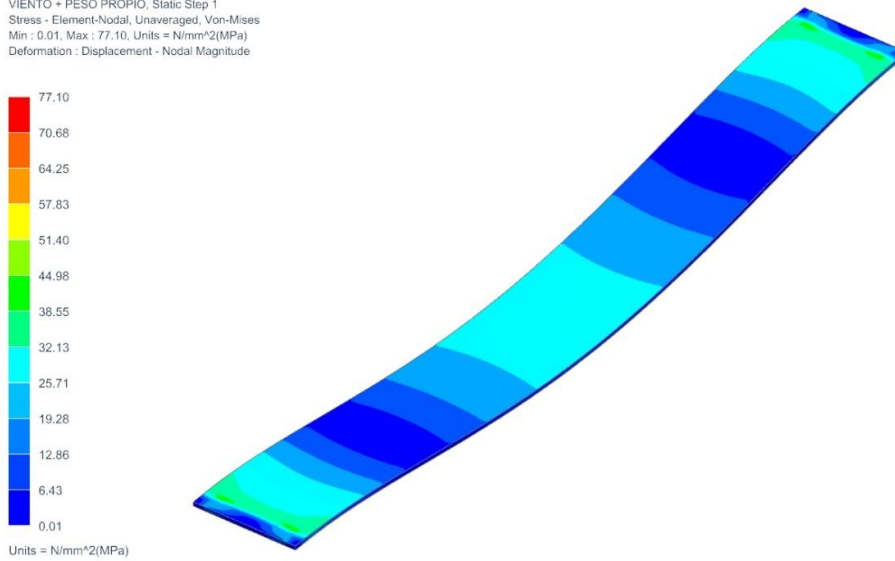
Units = N/mm^2(MPa)

Figure 4.26: Stress distribution in the lamella

SKYLIGHT ASSEMBLY_fem1_sim1 : SOLUCIÓN 1 Result
VIENTO + PESO PROPIO, Static Step 1
Stress - Element-Nodal, Unaveraged, Von-Mises
Min : 0.01, Max : 77.10, Units = N/mm^2(MPa)
Deformation : Displacement - Nodal Magnitude

77.10
70.68
64.25
57.83
51.40
44.98
38.55
32.13
25.71
19.28
12.86
6.43
0.01
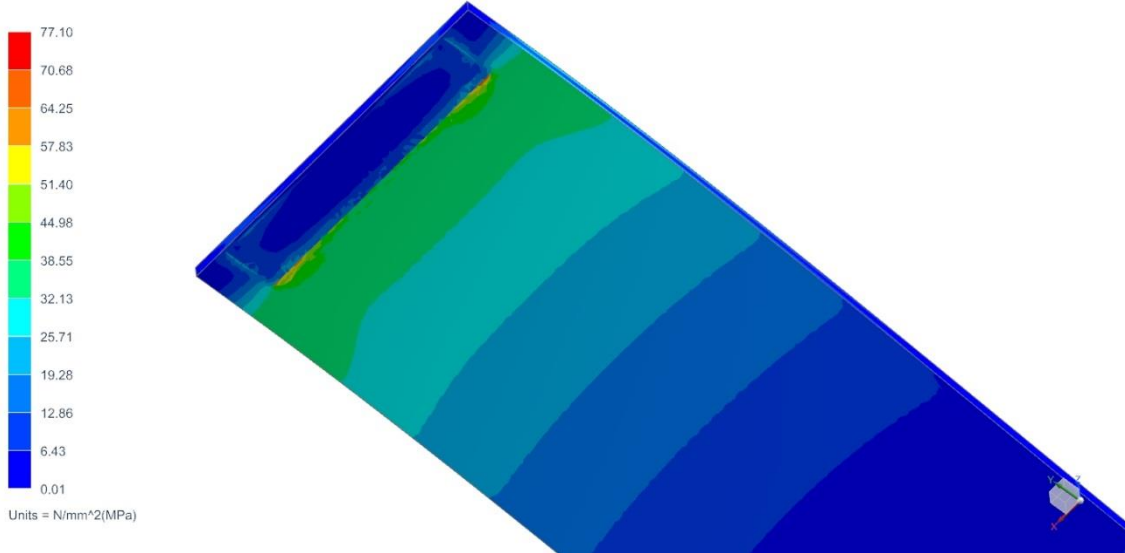
Units = N/mm^2(MPa)

Figure 4.27: Von Mises stress distribution in the lamella (lower surface)

SKYLIGHT ASSEMBLY_fem1_sim1 : SOLUCIÓN 1 Result
VIENTO + PESO PROPIO, Static Step 1
Stress - Element-Nodal, Unaveraged, Min Principal
Min : -102.52, Max : 14.27, Units = N/mm^2(MPa)
Deformation : Displacement - Nodal Magnitude

14.27
4.53
-5.20
-14.93
-24.66
-34.39
-44.13
-53.86
-63.59
-73.32
-83.06
-92.79
-102.52
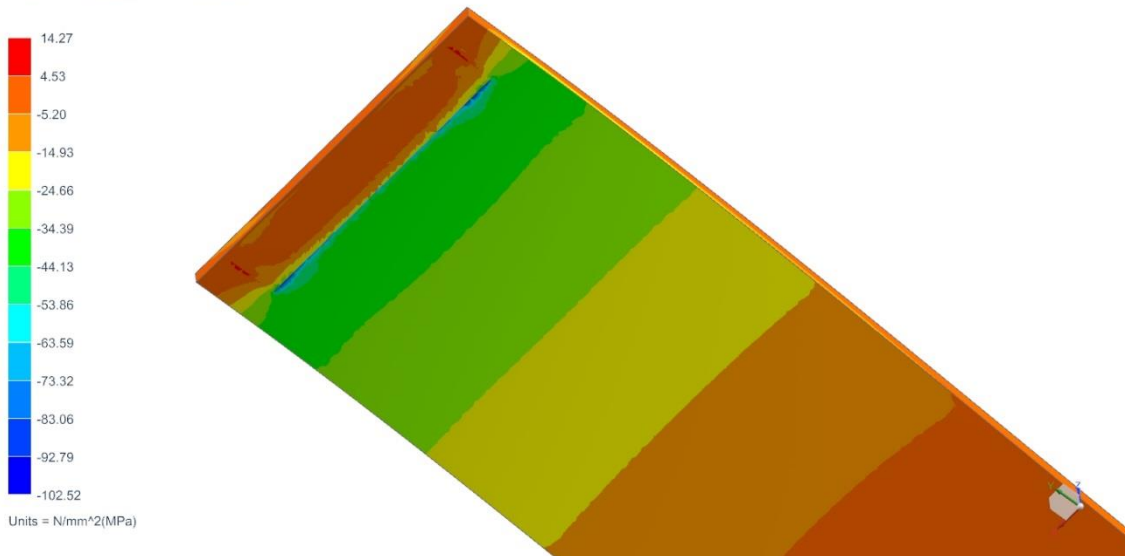
Units = N/mm^2(MPa)

Figure 4.28: Compressive stresses in lower surface of the lamella

Report on simulation work for crystalline-silicon based BIPV elements

SKYLIGHT ASSEMBLY_fem1_sim1 : SOLUCIÓN 1 Result
VIENTO + PESO PROPIO, Static Step 1
Stress - Element-Nodal, Unaveraged, YY
Min : -89.75, Max : 51.30, Units = N/mm^2(MPa)
Deformation : Displacement - Nodal Magnitude
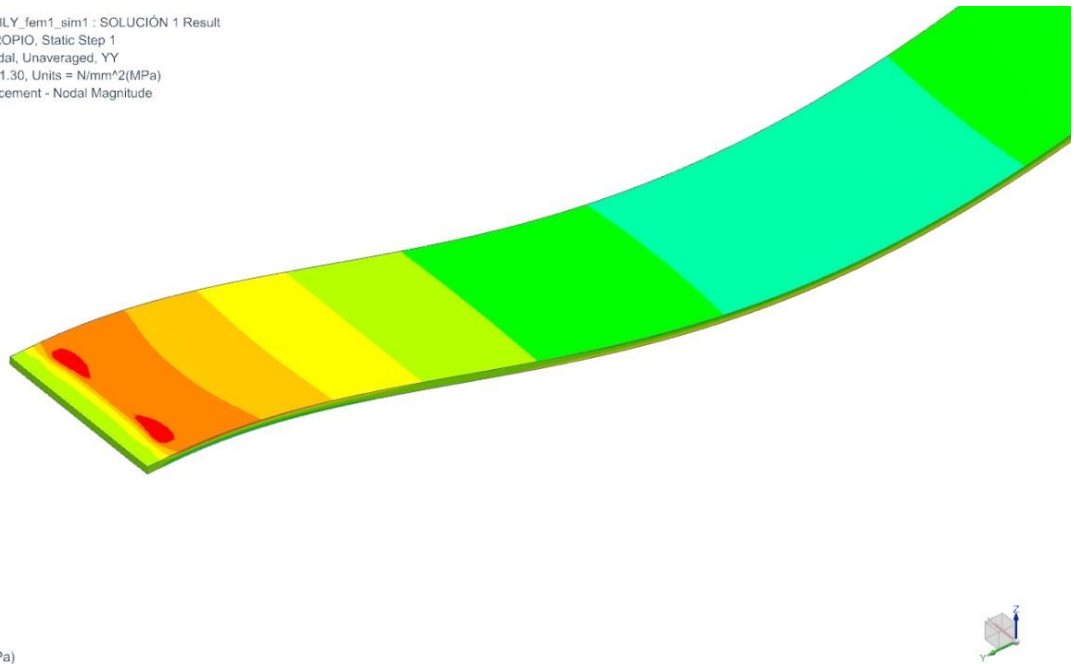
Figure 4.29: Tensile stresses in upper surface of the lamella

SKYLIGHT ASSEMBLY_fem1_sim1 : SOLUCIÓN 1 Result
VIENTO + PESO PROPIO, Static Step 1
Stress - Element-Nodal, Unaveraged, Von-Mises
Min : 0.01, Max : 77.10, Units = N/mm^2(MPa)
Deformation : Displacement - Nodal Magnitude
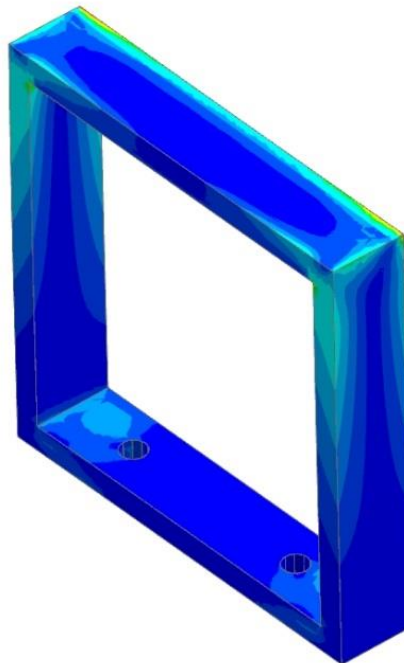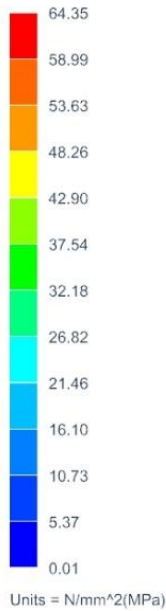
Figure 4.30: Stress distribution in U profiles

Analysis of glued joints between the U profiles and the glass lamella:

The glass lamellas are joined to the aluminium U profiles by means of glue, so analytical calculations have been done in order to evaluate the forces involved in the system. 2000 Pa is considered as wind load in both sense (upwards and downwards) but the most problematic will be upwards wind load. Considering the area of lamella (832 cm^2), each joint will be subjected to 83,2 N. Taking into account the joint area (1200 mm^2), the expected upwards pressure is 0.07 MPa. Adhesives are organic compounds and their adhesion force may decrease with time, especially under external conditions. Thus, a high security factor should be used which in our case is 10. Thus, the minimum adhesion strength considering a high security factor is 0.7 MPa.

Currently two options are being considered to join glass lamellas with aluminium wedge, one of them is based on especial tape for structural applications with performance of 0.450 MPa, and a second one based on epoxy adhesive with 17.5 MPa@80ºC.

The following **conclusions** can be drawn:

- Stress values are below their allowable value for all the parts involved in the system.

- Regarding deformations due to self-weight (constant deformations) they will not affect significantly the optical performance of the system. The deformation under strong wind conditions are not an issue from the optical point of view because they are applied for short periods of time.

- The expected maximum stresses are always below the yield strength of materials. The only remarkable situation is that the difference between yield strength of glass (120 MPa) and maximum stress registered (102,5 MPa compressive stress) is not as high as desired (glass normally requires security factor from 3 to 5). However, the glass normally breaks due to tensile forces (not compressive), which in our simulations have a maximum value of 51,3 MPa. Thus, the glass lamellas should withstand with a reasonable security factor wind loads of 2000 MPa.

- In addition, calculations have been made to evaluate the joint between glass lamella and aluminium wedge. Two adhesion solutions have been selected and both of them are strong enough for the application.

- Finally, it should be remarked that mechanical tests are being performed in Tecnalia's laboratories, in order to complement these simulations. The results of this testing activity will be reported in deliverable D3.9 "Report on indoor validation tests crystalline-silicon based BIPV elements".

4.3.2 Façade configuration

Description of system and model

The analysed system consists of the lamella and its two supporting ends, each one including an L profile and a wedge. Both elements are made of duraluminium 7075.
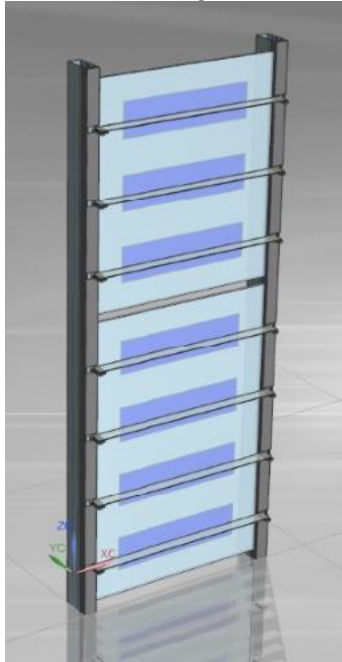
Figure 4.31: Low concentration system for façade integration including lamellas
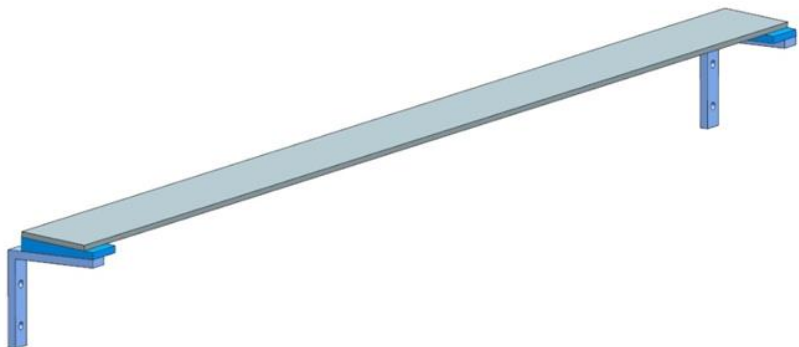
Figure 4.32: Description of a lamella system subjected to mechanical analysis
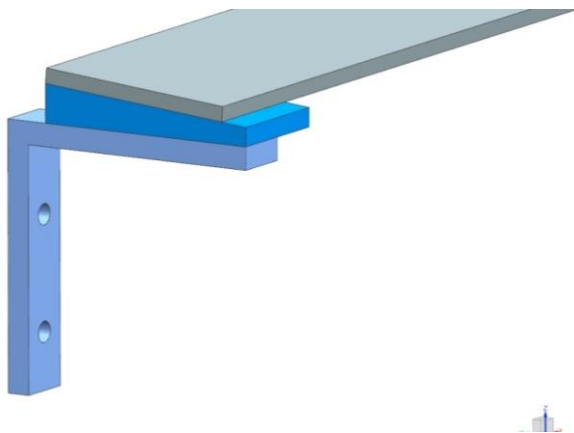
Figure 4.33: Detail of the support of the lamella

Figure 4.34: Detail of the finite element mesh of the lamella

The described structure is modelled by means of solid elements and consists of 198460 nodes and 114127 elements. Mesh mating conditions are defined between every two components in contact.

Regarding materials, the lamella is considered to be made of tempered glass and both the L profile and the wedge are considered to be made of duraluminium 7075.

Table 4.9 Material properties

Property	Units	Tempered glass	Al. 7075
Density	kg/m^3	2500	2700
Yield stress	MPa	120	450
Young's modulus	MPa	70000	70000
Poisson's ratio	-	0,22	0.33

The L profiles are considered to be fixed in a 10mm diameter area surrounding the two bolts. This corresponds to the effect of the bolted joint with a washer. The outer diameter of a M5 washer is 10 mm.

L profile and wedge are also joined by means of bolts, while the lamella is glued to the wedge. This joint will be further analysed in order to evaluate the required glue adhesion force.

The applied loads are:

- Wind load: 2000 Pa, both pressure and suction.
- Weight of the lamella.

Both loads are applied as distributed loads in the lamella.
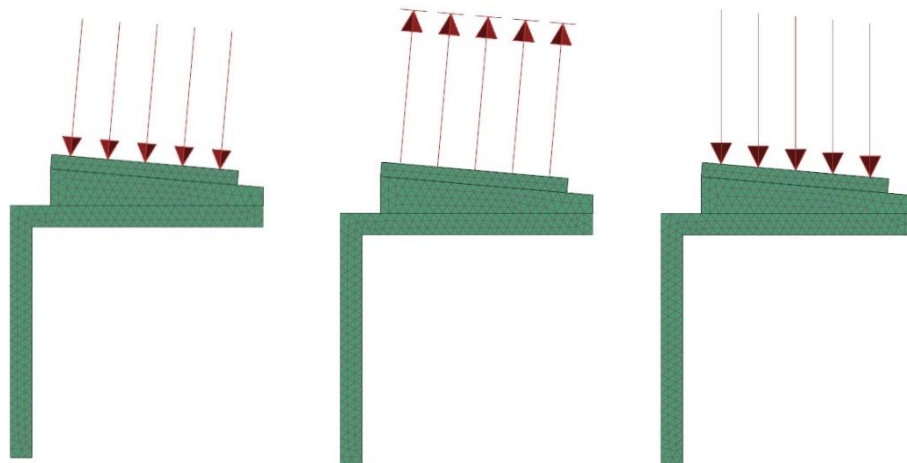
Figure 4.35: From left to right: pressure wind load, suction wind load and weight over the lamella system

Results

Numerical results obtained for each load case assessed are presented below.

The most restrictive load case is that in which the weight of the lamella and the pressure wind load are simultaneously applied.

Table 4.10 Main results for mechanical performance, façade configuration

Magnitude	WIND (PRESSURE) + WEIGHT
Maximum deformation (mm)	9.5
Maximum stress in lamella (MPa)	82.1
Maximum stress in aluminium parts (MPa)	100.3
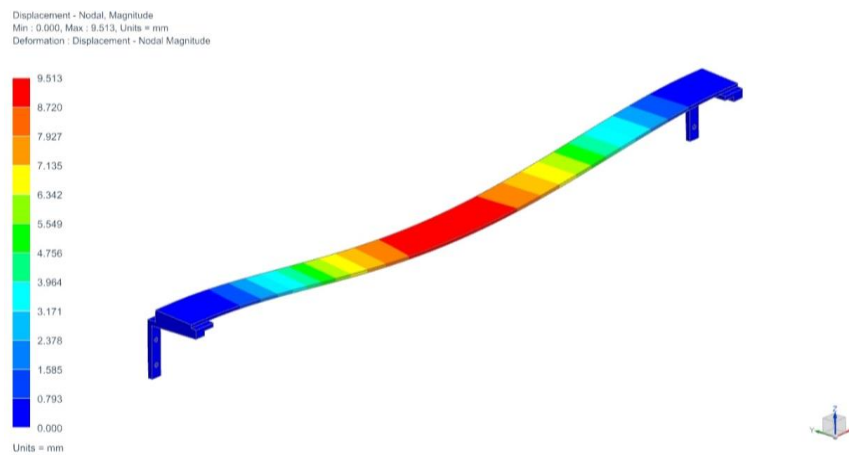
Figure 4.36: Deformation results, lamella system case

Figure 4.37: Von Misses stress distribution in the lamella

ASSEMBLY DISENO SIN MARCO 2_fem1_sim1 : VIENTO 2000 Pa Result
PRESION 2000 Pa+PESO PROPIO, Static Step 1
Stress - Element-Nodal, Unaveraged, XX
Min : -82.07, Max : 62.92, Units = N/mm^2(MPa)
Deformation : Displacement - Nodal Magnitude
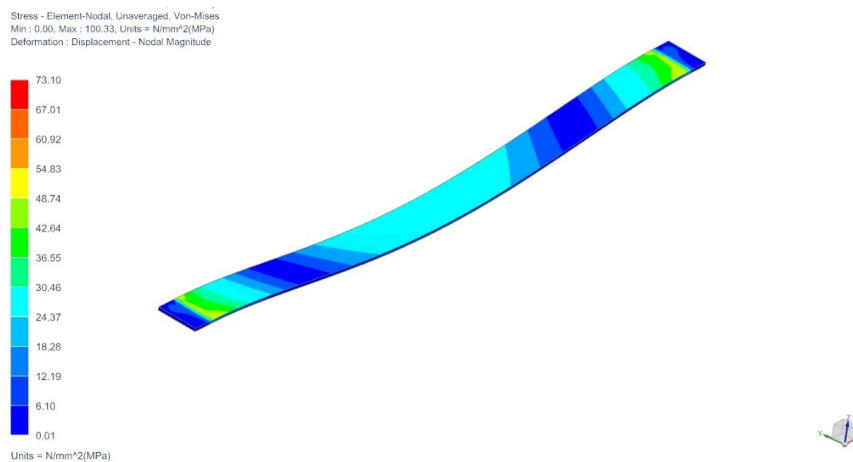
62.92
50.84
38.76
26.67
14.59
2.51
-9.58
-21.66
-33.74
-45.83
-57.91
-69.99
-82.07
Units = N/mm^2(MPa)
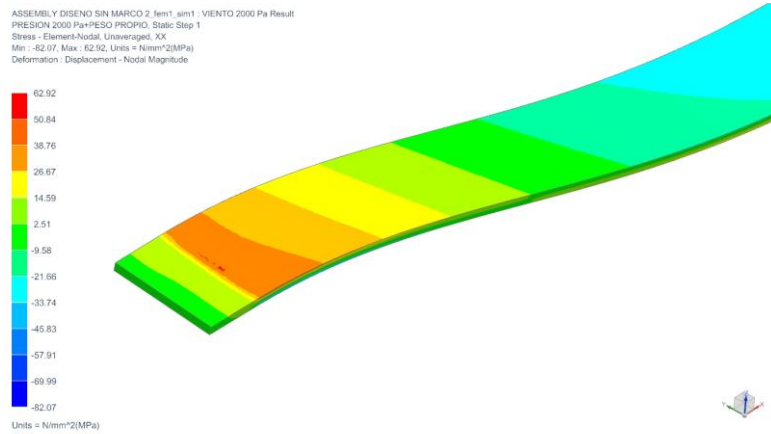
Figure 4.38: Tensile stresses in the upper side of the lamella

ASSEMBLY DISENO SIN MARCO 2_fem1_sim1 : VIENTO 2000 Pa Result
PRESION 2000 Pa+PESO PROPIO, Static Step 1
Stress - Element-Nodal, Unaveraged, XX
Min : -82.07, Max : 62.92, Units = N/mm^2(MPa)
Deformation : Displacement - Nodal Magnitude

62.92
50.84
38.76
26.67
14.59
2.51
-9.58
-21.66
-33.74
-45.83
-57.91
-69.99
-82.07
Units = N/mm^2(MPa)
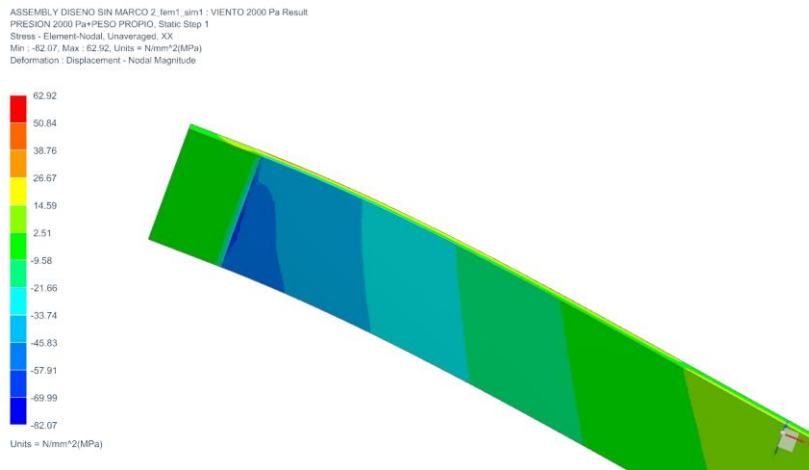
Figure 4.39: Compressive stresses in the lower side of the lamella

ASSEMBLY DISENO SIN MARCO 2_fem1_sim1 : VIENTO 2000 Pa Result
PRESION 2000 Pa+PESO PROPIO, Static Step 1
Stress - Element-Nodal, Unaveraged, Von-Mises
Min : 0.00, Max : 100.33, Units = N/mm^2(MPa)
Deformation : Displacement - Nodal Magnitude

100.33
91.97
83.61
75.25
66.89
58.53
50.17
41.80
33.44
25.08
16.72
8.36
0.00
Units = N/mm^2(MPa)
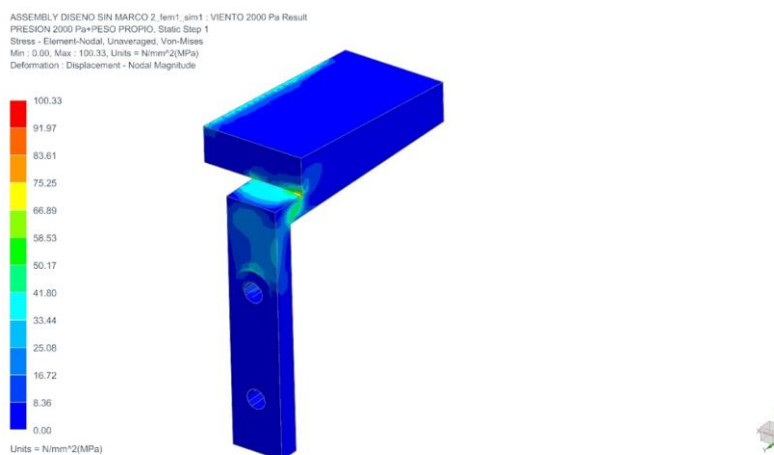
Figure 4.40: Stress distribution in L profile and wedge

Report on simulation work for crystalline-silicon based BIPV elements

Analysis of glued joint between the wedge and glass lamella

The glass lamellas are joined to the aluminium wedge by means of glue, so analytical calculations have been done in order to evaluate the forces involved in the system.

2000 Pa is considered as wind load in both senses (upwards and downwards) but the most problematic will be upwards wind load. Considering the area of lamella (488 cm^2), each joint will be subjected to 49N. Taking into account the joint area (1560 mm^2), the expected upwards pressure is 0.0314 MPa.

Adhesives are organic compounds and their adhesion force may decrease with time, especially under external conditions. Thus, a high security factor should be used which in our case is 10. Thus, the minimum adhesion strength considering a high security factor is 0.314 MPa.

Currently two options are being considered to join glass lamellas with aluminium wedge, one is based on especial tape for structural applications with performance of 0.450 MPa, and a second one based on epoxy adhesive with 17.5 MPa@80ºC.

The following **conclusions** can be drawn:

Stress values are well below their allowable value for all the parts involved in the system.

Regarding deformations due to self-weight (constant deformations) they will not affect significantly the optical performance of the system. The deformation under strong wind conditions are not an issue from the optical point of view because they are applied for short periods of time.

The expected maximum stresses are always below the yield strength of materials. The only remarkable situation is that the difference between yield strength of glass and maximum stress registered is not as high as desired (glass normally requires security factor from 3 to 5). However, the glass normally brakes due to tensile forces (not compressive), which in our simulations have a maximum value about 40 MPa. Thus, the glass lamellas should withstand, with a reasonable security factor, wind loads of 2000 MPa.

In addition, calculations have been made to evaluate the joint between glass lamella and aluminium wedge. Two adhesion solutions have been selected and both of them are strong enough for the application.

Finally, it should be remarked that mechanical tests are being performed in parallel in order to complement these simulations.

4.4 Electrical calculations

The purpose of these calculations was to obtain the PV production of the proposed solutions. Thus, several simulations have been performed for different locations, orientations, window to wall ratio (WWR) and PV ratio (PVR). This work uses the same building file and parameters defined in sections 6.2 and 6.3 in order to get a complete energy study on the same cases analysed at building level in section 6.

The simulations include an idealized building, described in section 6.2, with glazed areas facing North, East, West and South. Glazed areas have been replaced by PV glazing with different number of cells according to specific values of WWR and PVR. An image of the model is shown in Figure 4.41.
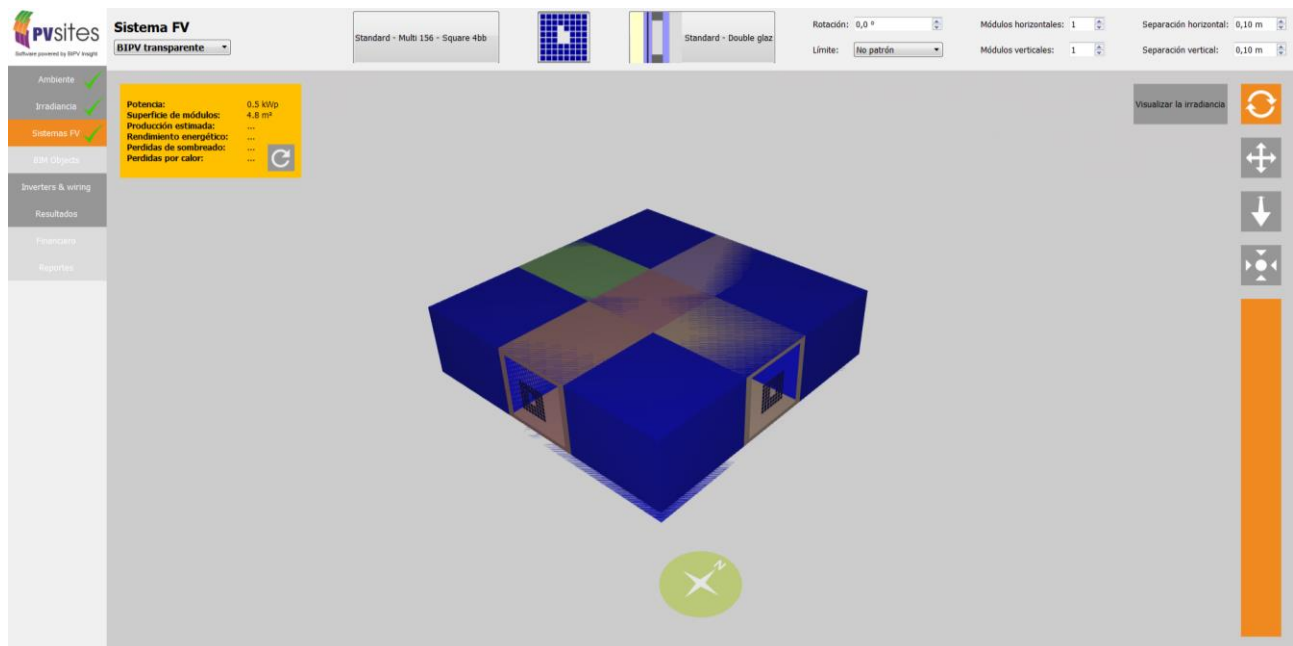
Figure 4.41: Image of building configuration and integration of BIPV glazing

The simulations have been carried out using PVSITES software (developed in the context of WP7). The software allows to easily import the IDF file coming from EnergyPlus, which describes the building geometry and all the characteristics related with its energy performance. Then, under the BIPV mode, the specific BIPV glazing was described as double-glazing including 4BB polycrystalline silicon solar cells, 4.59 Wp each. The model considers also a ground albedo of 20%.

The studied cases include three locations (Copenhagen, Lyon and Madrid), five WWR values (0.2, 0.4, 0.6, 0.8, 1), four PVR values (0.2, 0.4, 0.6, 0.8) and four orientations (N, E, W, S). The simulations were performed for every combination of input parameters, and the results are described in Figure 4.43, Figure 4.44 and Figure 4.45.

As expected, the PV production is strongly related to the WWR and PVR and the location radiation conditions. In this sense, Madrid shows the higher PV production values for every orientation.

Table 4.11 shows the PV production decrease for PV systems located in Lyon and Copenhagen locations, compared to Madrid. North orientation shows lower differences, given that diffuse irradiation is similar in every location, while the differences in direct irradiation are higher.

Figure 4.42 shows the monthly PV production for the three locations and orientations. The different behavior of the PV production of South oriented systems (black line) along the year, depending on location, should be remarked. For instance, a South oriented system in Copenhagen shows its maximum production during May-June, while in Madrid the same system has a local minimum during the same period due to the different solar paths.

In addition, Table 4.12 shows the average decrease of PV production compared to South oriented PV glazing, for which the maximum production values can be found. The different results are linked with differences between diffuse and direct irradiation, solar position and air temperature.

The validation of PVSITES software performance and accuracy is foreseen from month 30 (task 7.3 "Validation of software results"), once reliable weather and production data are available from the project demonstration sites. Meanwhile, several assessments are in progress using other PV simulation tools such as PVSyst. Some discrepancies have been found, however, the fact that it has not been possible to use the same weather data has to be taken into consideration. A thorough check of the correct and complete implementation of the physical models developed for the software

is also in progress in order to have an optimized tool before the final assessment from month 30 of project development.

Table 4.11 Decrease of PV production in northern European locations compared to Madrid

Orientation	Lyon vs Madrid	Copenhagen vs Madrid
North	-5,8%	-17,9%
East	-25,8%	-41,1%
West	-19,4%	-37,7%
South	-25,3%	-33,0%
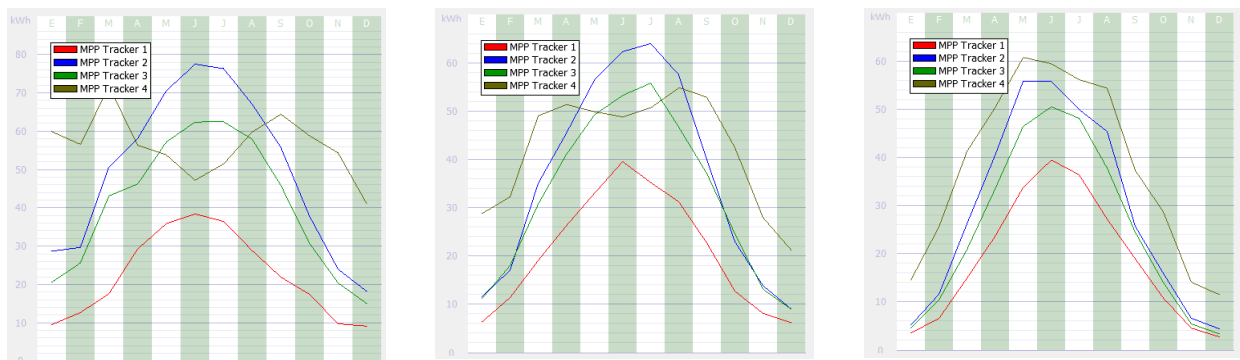
Figure 4.42: Monthly PV production. From left to right: Madrid, Lyon, Copenhagen. Orientations: North (red), East (blue), West (green) and South (black). WWR = 0.6; PVR = 0.8

Table 4.12 Average decrease of PV production compared to South oriented PV glazing

Orientation	Madrid	Lyon	Copenhagen
North	-60,6%	-50,3%	-51,7%
East	-10,3%	-10,8%	-21,1%
West	-26,9%	-21,2%	-32,1%

Copenhagen						
Inputs				Outputs		
WWR	PVR	Orientation	# solar cells	Annual production (kWh)	Losses vs South	Images monthly production
0,2	0,2	N	20	18,1	-51,5%	
0,2	0,2	E		30,3	-18,8%	
0,2	0,2	W		26,1	-30,0%	
0,2	0,2	S		37,3	0,0%	
0,2	0,4	N	40	37,3	-51,3%	
0,2	0,4	E		60	-21,7%	
0,2	0,4	W		50,9	-33,6%	
0,2	0,4	S		76,6	0,0%	
0,2	0,6	N	59	53,9	-52,0%	
0,2	0,6	E		88,8	-20,9%	
0,2	0,6	W		75,1	-33,1%	
0,2	0,6	S		112,2	0,0%	
0,2	0,8	N	79	73,8	-52,4%	
0,2	0,8	E		118,1	-23,8%	
0,2	0,8	W		105,9	-31,6%	
0,2	0,8	S		154,9	0,0%	
0,4	0,2	N	40	37,3	-51,3%	
0,4	0,2	E		60	-21,7%	
0,4	0,2	W		50,9	-33,6%	
0,4	0,2	S		76,6	0,0%	
0,4	0,4	N	79	73,8	-52,4%	
0,4	0,4	E		118,1	-23,8%	
0,4	0,4	W		105,9	-31,6%	
0,4	0,4	S		154,9	0,0%	
0,4	0,6	N	118	106,4	-52,6%	
0,4	0,6	E		176,4	-21,4%	
0,4	0,6	W		151,9	-32,3%	
0,4	0,6	S		224,5	0,0%	
0,4	0,8	N	157	147,9	-49,9%	
0,4	0,8	E		236,8	-19,8%	
0,4	0,8	W		200,7	-32,0%	
0,4	0,8	S		295,3	0,0%	
0,6	0,2	N	59	53,9	-52,0%	
0,6	0,2	E		88,8	-20,9%	
0,6	0,2	W		75,1	-33,1%	
0,6	0,2	S		112,2	0,0%	
0,6	0,4	N	118	106,4	-52,6%	
0,6	0,4	E		176,4	-21,4%	
0,6	0,4	W		151,9	-32,3%	
0,6	0,4	S		224,5	0,0%	
0,6	0,6	N	176	163,8	-51,5%	
0,6	0,6	E		268,2	-20,5%	
0,6	0,6	W		227,6	-32,6%	
0,6	0,6	S		337,5	0,0%	
0,6	0,8	N	235	210,4	-52,7%	
0,6	0,8	E		357,9	-19,5%	
0,6	0,8	W		307,4	-30,9%	
0,6	0,8	S		444,7	0,0%	
0,8	0,2	N	79	73,8	-52,4%	
0,8	0,2	E		118,1	-23,8%	
0,8	0,2	W		105,9	-31,6%	
0,8	0,2	S		154,9	0,0%	
0,8	0,4	N	157	147,9	-49,9%	
0,8	0,4	E		236,8	-19,8%	
0,8	0,4	W		200,7	-32,0%	
0,8	0,4	S		295,3	0,0%	
0,8	0,6	N	235	210,4	-52,7%	
0,8	0,6	E		357,9	-19,5%	
0,8	0,6	W		307,4	-30,9%	
0,8	0,6	S		444,7	0,0%	
0,8	0,8	N	315	300	-50,2%	
0,8	0,8	E		486,2	-19,2%	
0,8	0,8	W		410,4	-31,8%	
0,8	0,8	S		601,9	0,0%	
1	0,2	N	95	88,9	-51,4%	
1	0,2	E		140,7	-23,2%	
1	0,2	W		125,5	-31,5%	
1	0,2	S		183,1	0,0%	
1	0,4	N	190	177,9	-50,6%	
1	0,4	E		290,6	-19,3%	
1	0,4	W		249,4	-30,8%	
1	0,4	S		360,2	0,0%	
1	0,6	N	285	267,2	-52,1%	
1	0,6	E		420,8	-24,5%	
1	0,6	W		370,1	-33,6%	
1	0,6	S		557,6	0,0%	
1	0,8	N	380	335,8	-53,3%	
1	0,8	E		585,4	-18,6%	
1	0,8	W		488	-32,2%	
1	0,8	S		719,6	0,0%	

Figure 4.43: PV production results for Copenhagen

Report on simulation work for crystalline-silicon based BIPV elements

Lyon						
Inputs				Outputs		
WWR	PVR	Orientation	# solar cells	Annual production (kWh)	Losses vs South	Images monthly production
0,2	0,2	N		21,2	-51,2%	
0,2	0,2	E	20	37,9	-12,7%	
0,2	0,2	W		33,7	-22,4%	
0,2	0,2	S		43,4	0,0%	
0,2	0,4	N		42,6	-49,4%	
0,2	0,4	E	40	76,4	-9,3%	
0,2	0,4	W		67,4	-20,0%	
0,2	0,4	S		84,2	0,0%	
0,2	0,6	N		63,7	-49,0%	
0,2	0,6	E	59	112,6	-9,9%	
0,2	0,6	W		100,6	-19,5%	
0,2	0,6	S		125	0,0%	
0,2	0,8	N		82,8	-51,4%	
0,2	0,8	E	79	151,9	-10,8%	
0,2	0,8	W		130,9	-23,1%	
0,2	0,8	S		170,3	0,0%	
0,4	0,2	N		42,6	-49,4%	
0,4	0,2	E	40	76,4	-9,3%	
0,4	0,2	W		67,4	-20,0%	
0,4	0,2	S		84,2	0,0%	
0,4	0,4	N		82,8	-51,4%	
0,4	0,4	E	79	151,9	-10,8%	
0,4	0,4	W		130,9	-23,1%	
0,4	0,4	S		170,3	0,0%	
0,4	0,6	N		127	-49,5%	
0,4	0,6	E	118	223,8	-11,0%	
0,4	0,6	W		197,7	-21,4%	
0,4	0,6	S		251,6	0,0%	
0,4	0,8	N		166,5	-50,1%	
0,4	0,8	E	157	298	-10,7%	
0,4	0,8	W		265,1	-20,6%	
0,4	0,8	S		333,8	0,0%	
0,6	0,2	N		63,7	-49,0%	
0,6	0,2	E	59	112,6	-9,9%	
0,6	0,2	W		100,6	-19,5%	
0,6	0,2	S		125	0,0%	
0,6	0,4	N		127	-49,5%	
0,6	0,4	E	118	223,8	-11,0%	
0,6	0,4	W		197,7	-21,4%	
0,6	0,4	S		251,6	0,0%	
0,6	0,6	N		188,3	-49,4%	
0,6	0,6	E	176	337,8	-9,3%	
0,6	0,6	W		296	-20,5%	
0,6	0,6	S		372,5	0,0%	
0,6	0,8	N		246,2	-50,6%	
0,6	0,8	E	235	445,3	-10,7%	
0,6	0,8	W		396,7	-20,5%	
0,6	0,8	S		498,7	0,0%	
0,8	0,2	N		82,8	-51,4%	
0,8	0,2	E	79	151,9	-10,8%	
0,8	0,2	W		130,9	-23,1%	
0,8	0,2	S		170,3	0,0%	
0,8	0,4	N		166,5	-50,1%	
0,8	0,4	E	157	298	-10,7%	
0,8	0,4	W		265,1	-20,6%	
0,8	0,4	S		333,8	0,0%	
0,8	0,6	N		246,2	-50,6%	
0,8	0,6	E	235	445,3	-10,7%	
0,8	0,6	W		396,7	-20,5%	
0,8	0,6	S		498,7	0,0%	
0,8	0,8	N		334,1	-50,4%	
0,8	0,8	E	315	590,1	-12,4%	
0,8	0,8	W		520,1	-22,8%	
0,8	0,8	S		673,4	0,0%	
1	0,2	N		97,4	-51,4%	
1	0,2	E	95	179,8	-10,3%	
1	0,2	W		158,2	-21,1%	
1	0,2	S		200,5	0,0%	
1	0,4	N		201	-50,2%	
1	0,4	E	190	362,9	-10,0%	
1	0,4	W		316,7	-21,5%	
1	0,4	S		403,4	0,0%	
1	0,6	N		291,1	-52,7%	
1	0,6	E	285	533	-13,3%	
1	0,6	W		477,7	-22,3%	
1	0,6	S		615	0,0%	
1	0,8	N		410,1	-49,8%	
1	0,8	E	380	710,1	-13,0%	
1	0,8	W		646,9	-20,7%	
1	0,8	S		816,2	0,0%	

Figure 4.44: PV production results for Lyon

Madrid						
Inputs				Outputs		
WWR	PVR	Orientation	# solar cells	Annual production (kWh)	Losses vs South	Images monthly production
0,2	0,2	N		22,3	-61,1%	
0,2	0,2	E	20	50,8	-11,3%	
0,2	0,2	W		42	-26,7%	
0,2	0,2	S		57,3	0,0%	
0,2	0,4	N		45,3	-60,4%	
0,2	0,4	E	40	101,6	-11,2%	
0,2	0,4	W		81,5	-28,8%	
0,2	0,4	S		114,4	0,0%	
0,2	0,6	N		66,2	-60,6%	
0,2	0,6	E	59	151,6	-9,7%	
0,2	0,6	W		123,2	-26,6%	
0,2	0,6	S		167,9	0,0%	
0,2	0,8	N		90,4	-59,9%	
0,2	0,8	E	79	201,5	-10,7%	
0,2	0,8	W		163,2	-27,7%	
0,2	0,8	S		225,6	0,0%	
0,4	0,2	N		45,3	-60,4%	
0,4	0,2	E	40	101,6	-11,2%	
0,4	0,2	W		81,5	-28,8%	
0,4	0,2	S		114,4	0,0%	
0,4	0,4	N		90,4	-59,9%	
0,4	0,4	E	79	201,5	-10,7%	
0,4	0,4	W		163,2	-27,7%	
0,4	0,4	S		225,6	0,0%	
0,4	0,6	N		132,2	-60,5%	
0,4	0,6	E	118	304,2	-9,1%	
0,4	0,6	W		246,7	-26,3%	
0,4	0,6	S		334,6	0,0%	
0,4	0,8	N		172,7	-61,5%	
0,4	0,8	E	157	404,3	-9,8%	
0,4	0,8	W		331,1	-26,1%	
0,4	0,8	S		448	0,0%	
0,6	0,2	N		66,2	-60,6%	
0,6	0,2	E	59	151,6	-9,7%	
0,6	0,2	W		123,2	-26,6%	
0,6	0,2	S		167,9	0,0%	
0,6	0,4	N		132,2	-60,5%	
0,6	0,4	E	118	304,2	-9,1%	
0,6	0,4	W		246,7	-26,3%	
0,6	0,4	S		334,6	0,0%	
0,6	0,6	N		196,7	-60,9%	
0,6	0,6	E	176	451,5	-10,3%	
0,6	0,6	W		375,5	-25,4%	
0,6	0,6	S		503,2	0,0%	
0,6	0,8	N		270,3	-60,0%	
0,6	0,8	E	235	601	-11,0%	
0,6	0,8	W		491,3	-27,3%	
0,6	0,8	S		675,5	0,0%	
0,8	0,2	N		90,4	-59,9%	
0,8	0,2	E	79	201,5	-10,7%	
0,8	0,2	W		163,2	-27,7%	
0,8	0,2	S		225,6	0,0%	
0,8	0,4	N		172,7	-61,5%	
0,8	0,4	E	157	404,3	-9,8%	
0,8	0,4	W		331,1	-26,1%	
0,8	0,4	S		448	0,0%	
0,8	0,6	N		270,3	-60,0%	
0,8	0,6	E	235	601	-11,0%	
0,8	0,6	W		491,3	-27,3%	
0,8	0,6	S		675,5	0,0%	
0,8	0,8	N		345,3	-61,6%	
0,8	0,8	E	315	807,5	-10,2%	
0,8	0,8	W		650,3	-27,7%	
0,8	0,8	S		898,9	0,0%	
1	0,2	N		107	-60,0%	
1	0,2	E	95	240,7	-10,0%	
1	0,2	W		196,8	-26,4%	
1	0,2	S		267,4	0,0%	
1	0,4	N		211,1	-61,2%	
1	0,4	E	190	486,3	-10,6%	
1	0,4	W		396,7	-27,1%	
1	0,4	S		544	0,0%	
1	0,6	N		322,4	-60,1%	
1	0,6	E	285	738,4	-8,7%	
1	0,6	W		601,8	-25,6%	
1	0,6	S		809	0,0%	
1	0,8	N		424,3	-61,1%	
1	0,8	E	380	971,4	-10,8%	
1	0,8	W		796,8	-26,9%	
1	0,8	S		1089,5	0,0%	

Figure 4.45: PV production results for Madrid

Report on simulation work for crystalline-silicon based BIPV elements

5 OPTICAL AND THERMAL MODELLING OF PV GLAZING SYSTEMS AT BUILDING LEVEL

5.1 Modelling objectives at building level

Depending on the technology, BIPV products may have different impact on the building. Using see-through modules as glazing for windows or sun screen can reduce the amount of solar radiation entering the building. The solar heat gains will be reduced impacting both heating/cooling needs and occupant thermal comfort. It will also reduce the amount of available natural light.

The opaque BIPV modules should have a smaller impact as it won't affect transmitted solar radiation. These kinds of products will be used as cladding system and will be mounted on a building opaque surface. The building thermal behavior may be impacted as the system will modify conductive and radiative heat transfer.

At building level, the objective of simulation is to propose simplified model adapted to building scale, able to accurately reproduce the impact of the modules on the building thermal/lighting behavior.

For building simulation, the EnergyPlus software has been selected in agreement with WP7 activities (BIPV software tool development).

A parametric study is performed for an ideal office building and for different European climates. The impact of different parameters is studied: windows to wall ratio, PV cells ratio, room orientation and climate (Copenhagen, Lyon and Madrid). The results shall help the designers to conceive adapted BIPV installation that will find the best compromise between electricity generation, thermal energy uses and artificial lighting needs. It will provide a methodology to assess and compare several design performances.

The EnergyPlus simulation code has been selected to perform this task. This tool is the same which is currently being coupled to the project BIPV software tool for the simulation of buildings energy performance. This section of D3.7 describes the methods used to model the c-Si semi-transparent and opaque BIPV products manufactured by Onyx to be used in PVSITES demonstration installations (the low concentration product for demonstration in test benches was simulated in deliverables D3.1 and D3.2 and will not be included herein).

The effects of the BIPV products on the building performance are assessed using specific indicators related to energy needs:

- Artificial lighting consumption,
- Heating needs,
- Cooling needs.

The Onyx BIPV modules can be used and simulated in 3 different ways:

- As an external system that is not part of the thermal envelop (Tecnalia demo site): in this configuration, a simple external shading device with the appropriate solar transmission is defined in EnergyPlus.
- As a single or double glazing system integrated to the building envelop (this is used in the parametric study): in this case, the semitransparent module is modeled as an equivalent glazing. This is described in the next chapter.
- As a cladding system for opaque BIPV (Vilogia demo site): In this configuration, a specific object call external vented cavity is used. This is described in a following chapter.

The modelling method is being implemented in the PVSITES software tool (WP7). Similarly, the energy needs and thermal comfort indicators used in this work package have been defined in WP7.

5.2 Semitransparent BIPV modelling

The integration of PV cells in glass substrates allows a semi-transparent photovoltaic glazing that can be embedded in a multilayer solution such as double or triple glazing system and combined with added coatings or coloured elements to provide improved aesthetics, shading during the summer, natural lighting and thermal insulation during the winter, etc. Below is a scheme of a standard semitransparent PV glazing [7]:
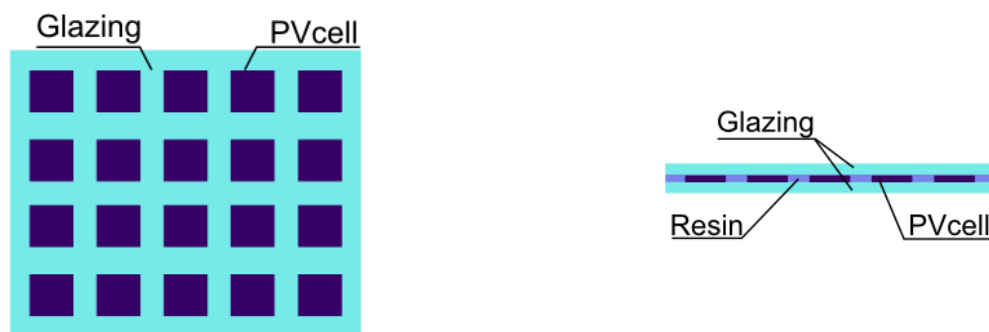
Figure 5.1: A typical structure of a semi-transparent glazing

Though most of the time, the modules are frameless, in some cases, the modules are assembled using specific framing system hosting the electrical connections. This system is quite complex to model as it implies radiative, convective and conductive heat transfer for both the glazing complex and the framing system. The chosen model has to describe the conductive, convective, and radiative heat transfers. It also has to model the solar radiation transmission, reflection and absorption properties.

5.2.1 EnergyPlus multiple-glazing system model

In EnergyPlus the most appropriate way to simulate see-through BIPV products is to consider them as a glazing with "equivalent" properties [3]. The software proposes two related modeling approaches [8]. The first one is a layer by layer description. The second one, which is the simplest approach, re-uses the same model and converts the performance of a given multilayer glazing into an equivalent single layer.

For task 3.6, we propose to use the multi-layer windows model. Its configuration requires the specifications of the following elements:

- **Glazing**: it consists of one or more plane/parallel glass layer(s). If there is more than one glass layer, it should be separated by a gap filled with gas.
- **Gaps**: they separate two glazing layers and are filled with gas.
- **Frame**: opaque material that holds and surrounds the glazing on four sides.
- **Divider**: horizontal or vertical element that divides the glazing.
- **Shading device**: it can be considered as a separate layer such as drapery, roller or blind. It can be located inside, or outside the glazing. Its purpose is to reduce the amount of solar gain, the heat loss or to control daylight.

To take heterogeneous PV glazing into account, simplifications or assumptions have to be made. The objective is to get an "equivalent" layer defined by the same properties as a standard glazing

(thermal conductivity, short wave transmittance, short wave reflectance, emissivity, visible properties, etc.). These properties are derived from:

- The models at element level described in the previous chapter,

- The experimental campaign carried out on specific ONYX products.

The following figure describes the main heat transfer modelled in EnergyPlus for double glazing window.
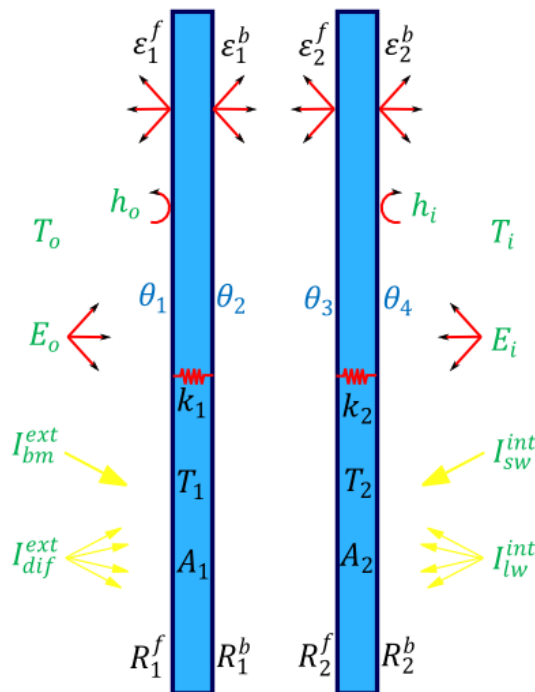
Figure 5.2: Schematic of a double-glazing system showing variables used in heat balance equations

The window temperatures at several points are calculated at each time step. The following equations are given for a double-glazing window. However, the approach is equivalent for single, triple or N glazing windows.

Several assumptions are made for calculation:

- Glass layers are thin, heat storage is neglected,

- The heat flow is one dimensional and perpendicular to the glazing. Edge of glass effect and separator are considered separately.

- The glass layers are opaque to IR radiation.

- Glass faces are isothermal.

For a double-glazing product, the four heat balance equations may be written under the following form:

$$E_0\varepsilon_1^f - \varepsilon_1^f\sigma\theta_1^4 + k_1(\theta_2 - \theta_1) + h_0(T_0 - \theta_1) + S_1 = 0 \qquad \textbf{Eq. 1}$$

$$k_1(\theta_1 - \theta_2) + h_1(\theta_3 - \theta_2) + \sigma\frac{\varepsilon_1^b\varepsilon_2^f}{1 - \left(1 - \varepsilon_1^b\right)\left(1 - \varepsilon_2^f\right)} + (\theta_3^4 - \theta_2^4) + S_2 \qquad \textbf{Eq. 2}$$
$$= 0$$

$$h_1(\theta_2 - \theta_3) + k_2(\theta_4 - \theta_3) + \sigma\frac{\varepsilon_1^b\varepsilon_2^f}{1 - \left(1 - \varepsilon_1^b\right)\left(1 - \varepsilon_2^f\right)} + (\theta_2^4 - \theta_3^4) + S_3 \qquad \textbf{Eq. 3}$$
$$= 0$$

$$E_i\varepsilon_2^b - \varepsilon_2^b\sigma\theta_4^4 + k_2(\theta_4 - \theta_3) + h_i(T_i - \theta_4) + S_4 = 0 \qquad \textbf{Eq. 4}$$

The internal convection coefficient h_i is computed according to the ISO 15099 [9] correlation for still room air.

S_i is the radiation absorbed on the ith face. It gathers short-wave and long-wave radiation from inside and outside the building (solar, lights, equipment). The radiations are assumed to be absorbed uniformly along a glass layer. The glass panes are opaque to IR, inside radiation (lights, equipment) are assigned to the inside surface of the inside glass. For N glass layers, S_i is given by:

$$S_{2j-1} = S_{2j} = \frac{1}{2}\left(I_{bm}^{ext}cos\emptyset A_j^f(\emptyset) + I_{dif}^{ext}A_j^{f,dif} + I_{sw}^{int}A_j^{b,dif}\right), j = 1\ to\ N \qquad \textbf{Eq. 5}$$

$$S_{2N} = S_{2N} + \varepsilon_{2N}^b I_{lw}^{int} \qquad \textbf{Eq. 6}$$

Where

ε_{2N}^b : emissivity of room side face inside glass layer,

A_j^f Front beam solar absorptance of glass layer j

$A_j^{f,dif}$, $A_j^{b,dif}$ front and back diffuse solar absorptance of layer j.

5.2.1.1 Glazing system optical properties

In the multilayer model, the optical properties are calculated for a glazing system consisting of several glass layers separated by non-absorbing gas layers. They are determined by solving the recursion relations for $T_{i,j}$, the transmittance; $R_{i,j}^f$ and $R_{i,j}^b$, the front and back reflectance, through layers i to j; and A_j, the absorption in layer j. Below is an example for a double-glazing system:
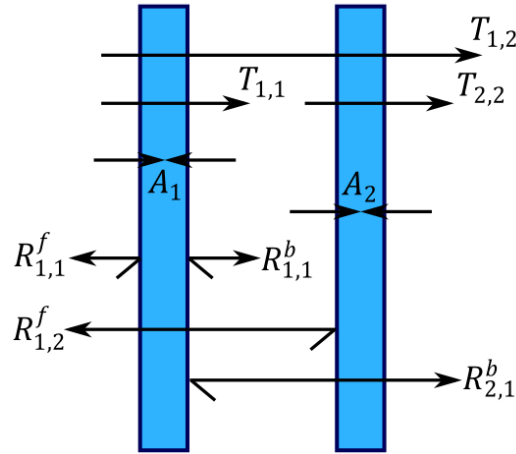
Figure 5.3: Schematic of transmission, reflection and absorption of solar radiation within a double-glazing system

$$T_{1,2} = \frac{T_{1,1}T_{2,2}}{1 - R^f_{2,2}R^b_{1,1}}$$ **Eq. 7**

$$R^f_{1,2} = R^f_{1,1} + \frac{T^2_{1,1}R^f_{2,2}}{1 - R^f_{2,2}R^b_{1,1}}$$ **Eq. 8**

$$R^b_{2,1} = R^b_{2,2} + \frac{T^2_{2,2}R^b_{1,1}}{1 - R^f_{2,2}R^b_{1,1}}$$ **Eq. 9**

$$A^f_1 = \left(1 - T_{1,1} - R^f_{1,1}\right) + \frac{T_{1,1}R^f_{2,2}(1 - T_{1,1} - R^b_{1,1})}{1 - R^f_{2,2}R^b_{1,1}}$$ **Eq. 10**

$$A^f_2 = \frac{T_{1,1}(1 - T_{2,2} - R^f_{2,2})}{1 - R^f_{2,2}R^b_{1,1}}$$ **Eq. 11**

In EnergyPlus, transmittance and reflectance can be defined as a function of wavelength. For "simple" calculation the above calculated properties are integrated over wavelength.

$$P_s = \frac{\int P(\lambda)E(\lambda)d\lambda}{\int E_s(\lambda)d\lambda}$$ **Eq. 12**

In the above equation, P_s designates the spectral-average value of a solar property $P(\lambda)$. E_s is the solar irradiance function.

The glazing optical parameters that need to be defined for non-spectral data are gathered and explained in the following table:

Table 5.1 Glazing optical parameters that need to be defined for non-spectral data

Optical parameters	Definition
Solar transmittance at normal incidence	Short wave transmittance at normal incidence averaged over the solar spectrum. This should be an "equivalent transmittance" taking into account transparent and solar cell part.
Front side solar reflectance at normal incidence	Front side short wave reflectance at normal incidence averaged over the solar spectrum. This should be an "equivalent reflectance" taking into account transparent and solar cell part. This coefficient should also integrate the part of solar radiation absorbed by the PV cells and converted into electricity. This way, this fraction of solar radiation is removed from the heat conservation equation.
Back side solar reflectance at normal incidence	Back side short wave reflectance at normal incidence averaged over the solar spectrum. This should be an "equivalent reflectance" taking into account transparent and solar cell part.
Visible transmittance at normal incidence	This should be an "equivalent transmittance" taking into account transparent and solar cell part.
Visible transmittance at normal incidence	This should be an "equivalent transmittance" taking into account transparent and solar cell part.
Front side visible reflectance at normal incidence	This should be an "equivalent reflectance" taking into account transparent and solar cell part.
Back side visible reflectance at normal incidence	This should be an "equivalent reflectance" taking into account transparent and solar cell part.
Infrared transmittance at normal incidence	This should be an "equivalent transmittance" taking into account transparent and solar cell part.
Front side infrared hemispherical emissivity	This should be an "equivalent emissivity" taking into account transparent and solar cell part.
Back side infrared hemispherical emissivity	This should be an "equivalent emissivity" taking into account transparent and solar cell part.

5.2.2 Conductive heat transfer

See-through BIPV glazing is a heterogeneous material composed of silicon cells, encapsulated into polymer, inserted between 2 layers of glass. To get an equivalent glazing that can be imported into EnergyPlus, simplification must be made to get equivalent properties. Xu [1] proposes the following 1D model:
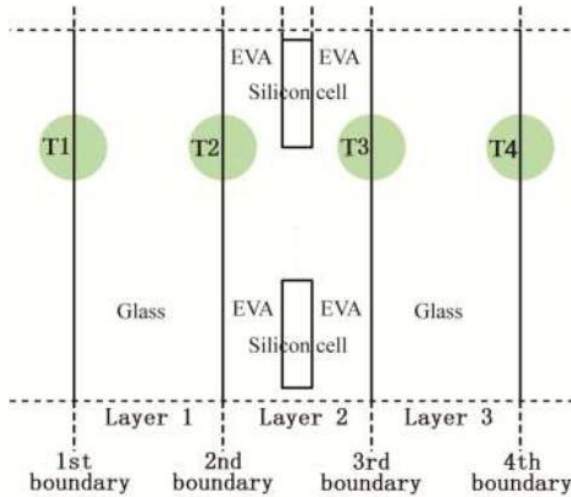
Figure 5.4: Schematic of a semi-transparent BIPV [1]
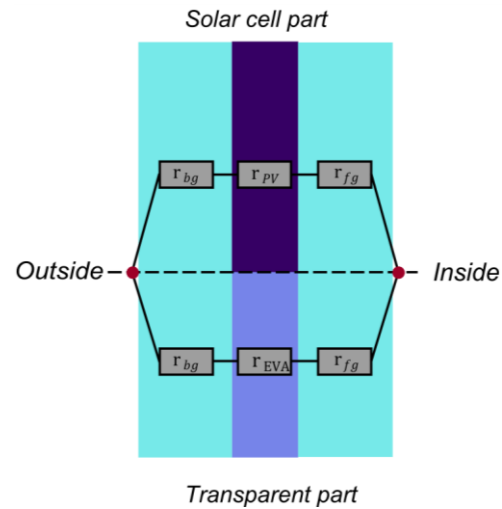
Figure 5.5: Equivalent thermal resistance model

At 1st and 4th boundaries, convection, conduction and long wave radiation are considered. They will not be detailed here as these transfers have been described in the previous chapter. According to [10], heat transfer between the encapsulation polymer and the photovoltaic cells (vertical axis on the above scheme) can be neglected. Finally, Wong *et al* [2] use a simple equivalent thermal resistance model to compute the encapsulation polymer/cells layer thermal conductivity. From Figure 5.4, it can be written:

$$K_{\text{mod}ule} = \frac{A_{pv}}{R_{pv}} + \frac{A_{eva}}{R_{eva}}$$ **Eq. 13**

$$R_{pv} = \frac{e_{bg}}{k_{bg}} + \frac{e_{pv}}{k_{pv}} + \frac{e_{fg}}{k_{fg}}$$ **Eq. 14**

$$R_{eva} = \frac{e_{bg}}{k_{bg}} + \frac{e_{eva}}{k_{eva}} + \frac{e_{fg}}{k_{fg}}$$ **Eq. 15**

With K_{module} being the equivalent thermal conductivity, A_{PV} and A_{eva} the PV and transparent area, and e_x the thickness of the different element (front and back glass, photovoltaic cells and polymer).

The obtained conductivity is an EnergyPlus model input:

Table 5.2: relevant parameters for EnergyPlus model input.

Conductivity	W/m.K	Equivalent BIPV glazing thermal conductivity

5.2.3 Frame, divider and edge of glass effects calculation

The conductance of the glazing near the frame or the divider is higher than in its center, due to thermal bridging effects. This phenomenon is taken into account in EnergyPlus. However, the corresponding equations are not relevant for the project, and will not be displayed in this document.

5.3 Opaque BIPV with cladding system model

EnergyPlus proposes a model to simulate exterior naturally vented cavity. On a thermal point of view, it modifies the boundary conditions on the building envelop. The solar radiation and the convective heat transfers happen between the external environment and a surface named "baffle". The building external wall interacts with the baffle through long wave heat exchanges, and with the air gap between the baffle and the wall through convection and conduction heat exchanges. The air gap is naturally vented by buoyancy effects [8].
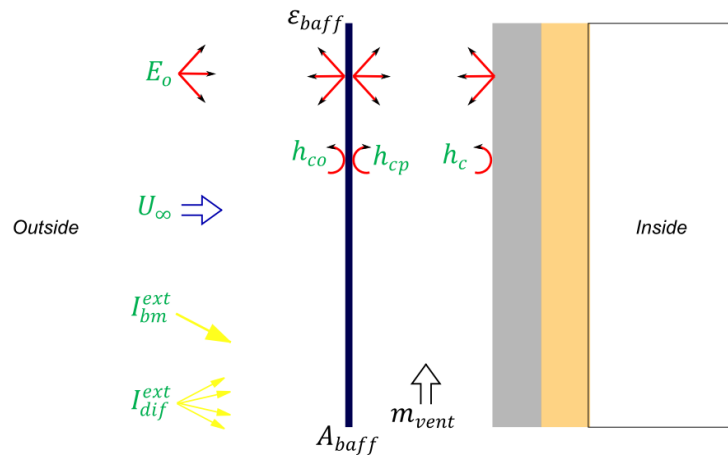
Figure 5.6: Schematic of the vented cavity showing variables relative to heat thermal transfer

Several hypothesis are made:

- The baffle is assumed to be sufficiently thin and high conductive so that it can be modelled with a single temperature (1D model).

- The baffle is opaque to both short wave and long wave radiations.

The heat balance on the baffle surface's control volume is:

$$q_{\alpha sol} + q_{LWR,Env} + q_{conv,Env} + q_{LWR,cav} + q_{conv,cav} + q_{source} = 0 \qquad \textbf{Eq. 16}$$

With

$q_{\alpha sol}$: the absorbed direct and diffuse radiation (short wave),

$q_{LWR,Env}$: the long wave exchange with air and surrounding,

$q_{conv,Env}$: the convection flux exchange with outside air,

$q_{LWR,cav}$: the long wave exchange with the building underlying surface,

$q_{conv,cav}$: the convection flux exchange with the cavity air,

q_{source}: a sink that accounts for the solar energy transformed into electric energy and exported out of the control volume.

The heat balance in the cavity is written as follows:

$$\dot{Q}_{vent} + \dot{Q}_{co} + \dot{Q}_{c,baff} = 0$$

<div align="right">**Eq. 17**</div>

Where

$\dot{Q}_{vent}$ is the net energy added from natural ventilation (in this case buoyancy),

$\dot{Q}_{co}$ is the net energy transfer from the building wall to the cavity by convection,

$\dot{Q}_{c,baff}$ is the net energy transferred from the baffle to the cavity by convective heat transfer.

In Energyplus, the vented cavity interacts with the envelop by modifying a surface boundary condition. It is configured with the following inputs:

Table 5.3 Input parameters for the simulation

Internal heat gains		
Area Fraction of Openings [-]	0 - 1	It indicates the amount of "hole" in the baffle in term of a ration expressed by hole surface/total surface.
Thermal Emissivity of Exterior Baffle Material [-]	0 - 1	The thermal emissivity of the PV solar panel. This is a known limit of the model as only one emissivity can be specified. Front face and back face emissivity cannot be specified. Energyplus considers a uniform material.
Solar Absorptivity of Exterior Baffle [-]	0 - 1	The PV panel solar absorbance. With this model, the amount of radiation that is not absorbed is reflected (the material is opaque so there is no transmission). When specifying the absorbance one must take into account that in solar PV, a fraction of the radiation is converted into electricity.
Effective Thickness of Cavity Behind Exterior Baffle [m]	0.05	The thickness of the air gap
Roughness of Exterior Surface	Smooth - Rough	A qualitative value describing the PV panel surface.
Effectiveness for Perforations with Respect to Wind	0 - 1	A coefficient describing the impact of the wind driven air change rate in the air gap. Energyplus documentation provides more detailed information
Discharge Coefficient for Openings with Respect to Buoyancy Driven Flow	0 - 1	A coefficient describing the impact of buoyant air change rate in the air gap. Energyplus documentation provides more detailed information

6 PARAMETRIC STUDY OF SEMI-TRANSPARENT SOLAR PV IN AN OFFICE BUILDING

At building scale; BIPV products impact the amount of solar radiation received by the building, or the way these radiations are transferred to the indoor. For opaque BIPV, simulations performed for demo site in Task 8.2 "Manufacturing of prototypes" show that this kind of product have nearly no impact on the building thermal behaviour. But the effect is negligible regarding the other thermal transfer (wall conduction, HVAC equipment, solar and internal heat gain, etc.) except the fraction of solar radiation that is converted into electricity; the BIPV modules behave like a "normal" cladding.

On the other hand, semitransparent solar PV strongly affects the solar heat gains and the lighting level inside the building. Depending on the PV coverage ratio (PVR), a fraction of the solar radiation (short and visible wavelength) is absorbed and converted into electric energy. The remaining part is reflected to the outside or transmitted to the inside of the building. Therefore, the fraction of the wall covered by the module and the PVR are two parameters that will strongly impact the building energy demand.

6.1 Defining the indicators

When it comes to building design, engineers often have to find a tradeoff between 3 main preoccupations/criteria:
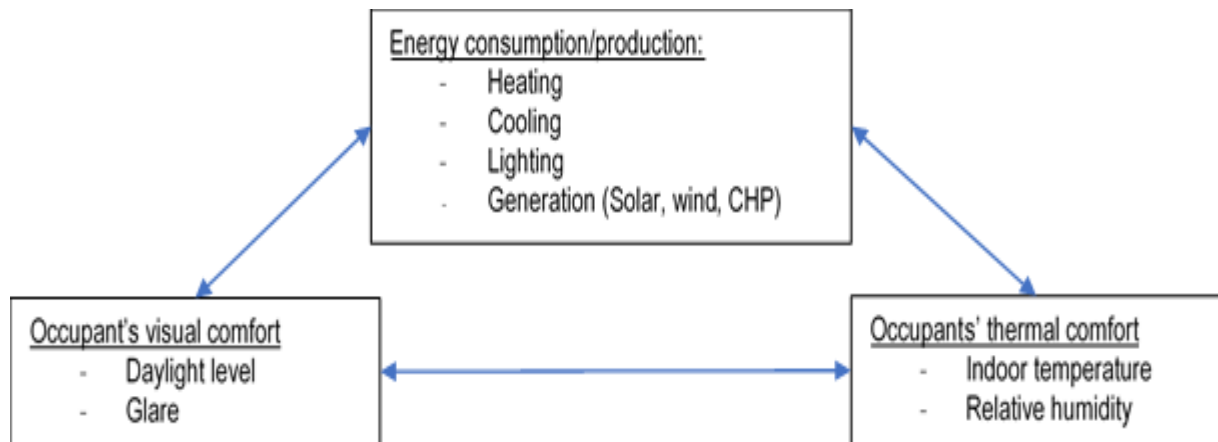
Figure 6.1: Main criteria considered in the design phase of a building

Most of the criteria cited above are affected by the transparent BIPV modules. Hence, in order to assess the impact of the products on the building energy needs, an overall indicator must be found. To aggregate the impacted criterion into a single value, the following sum is proposed:

$$E_{need} = E_{heat} + E_{cool} + E_{light} - E_{BIPV} \qquad \textbf{Eq. 18}$$

with:

E_{need} the indicator aggregating all the impacted criteria and used to assess the impact of BIPV on the building energy needs.

E_{heat} the amount of energy that needs to be brought to the building zones to meet the temperature set-point.

E_{cool} the amount of energy that needs to be extracted from the building zones to meet the temperature set-point.

E_{light} the artificial lighting energy needs. It is computed based on the daylight calculation, on the desired lighting level (e.g. 300 lux for office) and on the lighting equipment performance (e.g. W/100lux).

E_{BIPV} the semitransparent BIPV electricity production.

6.2 The ideal building geometry and operation

Two authors [1] and [3] studied the influence of semitransparent solar PV design on office building for middle east climate. They proposed the following "typical building":
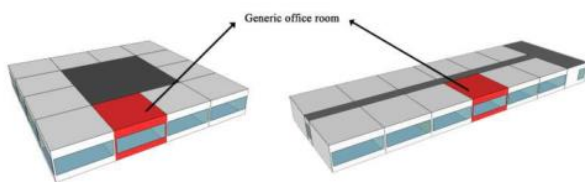
Figure 6.2: Chinese ideal building [1]
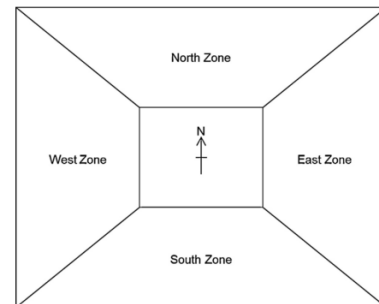
Figure 6.3: Singapore ideal building [3]

For the PVSITES study, we choose "an ideal building" that mixes both designs:
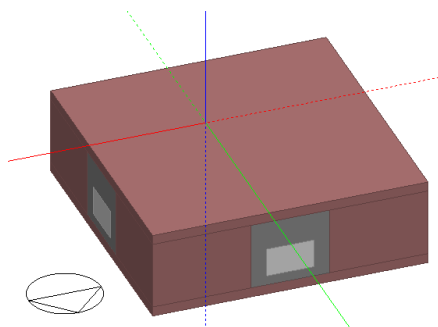
Figure 6.4: Overall 3D view
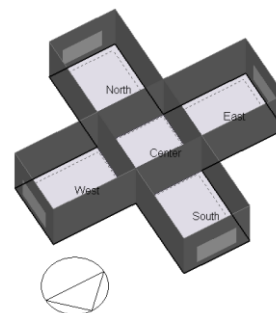
Figure 6.5: Thermal zone view

The following hypotheses are considered:
- With the exception of the external walls holding the BIPV modules and the partition that separates the office zone from the centre, the room surfaces are considered adiabatic. The modelled rooms represent generic office spaces on generic floors oriented according to the cardinal points.
- The building is considered to be occupied from 8AM to 6PM during the weekday and is empty during the weekends. A density of 0.2person/m² is considered [3].

- The office "generic" equipment are modelled with an internal heat gain of 8W/m² that is activated during the building occupation [3].
- For artificial lighting, a maximal heat gain of 10W/m² (2W/m².100lux) is considered. This amount of artificial lighting is modulated depending on the daylight availability. In each thermal zone, a sensor located at the centre of the zone and at a height of 0.7m maintains a constant illuminance of 500lux on the workplan (0.7m from the ground) during building occupation.
- A infiltration rate of 0.1 ACH [3].
- For the mechanical ventilation, the French mandatory airflow for office space is considered (25m³/h.pers). The fans are only active during building occupation [11].
- The temperature set point during winter period is set to 19°C and to 26°C during the summer time [11]. Heating and cooling are activated during occupation, set back temperatures are set to 15 and 32°C.
- For external walls, the layer composition is derived from the ASHRAE value; it's a non-structural light wall made of plaster and insulation material. The heat transfer coefficient is 0.361W/m².K.
- BIPV properties have been measured by Tecnalia using ONYX sample. An equivalent glazing is defined for every tested PVR according to the hypothesis made in "*corresponding chapter*".
- In this ideal case, frame and divider are neglected.
- Electricity production is simulated using a simple model with a 15% constant efficiency and an ideal converter (efficiency = 1).

6.3 Design parameters

Previous studies identified and studied the following parameters:
- The Windows to Wall Ratio (WWR) varying from 0.2 up to 0.7 [1] and from 0.7 up to 1 [3].
- The PV cell occupancy (PVR) from 0.1 up to 0.8.
- The room dimensions, with depth varying from 4m up to 13m.
- The climates.

Considering that room depth is related to architectural design, only the 3 parameters related to the BIPV modules will be used. For the 4 thermal zones:
1- The WWR will be varied from 0.2 up to 1 with a step of 0.1.
2- The PVR will vary from 0.2 up to 0.8 with a step of 0.1.
3- European climates are selected: Copenhagen (Denmark) for Northern Europe, Lyon (France) for Central Europe, Madrid (Spain) for Southern Europe.

| 0.2 | 0.5 | 0.9 |
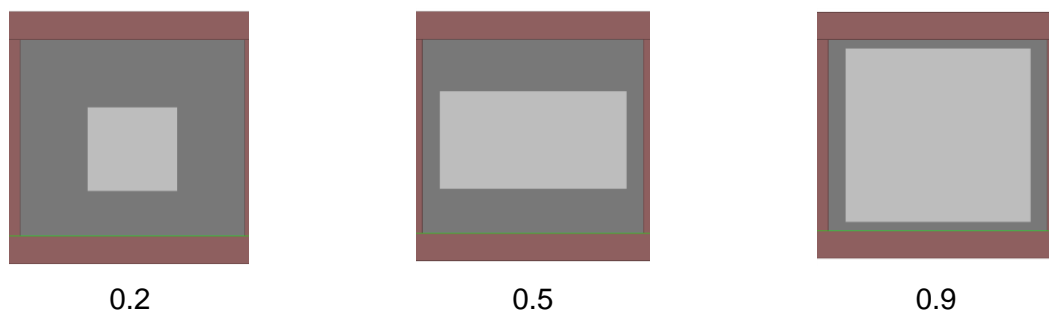
Figure 6.6: WWR from 0.2 up to 0.9 - graphical representation

6.4 Study and results

Parametric simulations are cast to assess the impact of the parameters on the previously described E_{need} indicator. Python scripts are use with the Eppy library (http://pythonhosted.org/eppy) to perform 189 simulations, corresponding to every combination of WWR, PVR and weather. The results are aggregated at zone and building level to get the indicators for every combination. The objective is to observe if "optimal" designs (WWR, PVR) exist to minimise the building energy needs depending on the climate and on the rooms' orientations.

Results exploitation is not an easy task. Heating/cooling needs, lighting consumption, and PV productions have to be observed for each climate and for each orientation. To get the best overview of the design possibilities, several representations from box plot to heat map are used.

The first paragraph compares the design possibilities for each climate at "building level". It will help to understand the challenges and the main energy need items for each city. A second paragraph compares the design efficiency based on the E_{need} indicator at room level and for each climate.

6.4.1 Climate study

The following box plot presents the distribution of all the "possible design" E_{need} for each climate (a design is a combination of WWR and PVR).
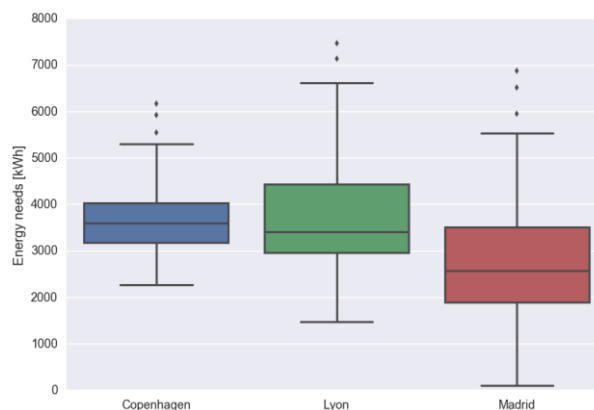
Figure 6.7: E_{need} box plot

The median is displayed; the coloured box shows the Inter Quartile Range (IQR) that contains 50% of the designs. The whiskers shows the maximum and minimum values when the outliers are removed. Outliers are defined as solutions having a value greater than the 3rd quartile plus 1.5 time the IQR.

The graph shows that for all the possible designs, the average E_{need} varies from 3700kWh for cold climate to 2800kWh for hot climate. Depending on the city, the configuration with a minimum E_{need} requires between 39% and 93% less energy than its average design. The configuration with the highest E_{need} has an energy demand 166% to 246% higher than the average design. The dispersion of the solutions seems to be greater for hotter climates (Lyon and Madrid). Considering the extent of the box plots, bad design choices may lead to over consumption.

The following figures plot boxes for each energy need item and for each city for the whole building.
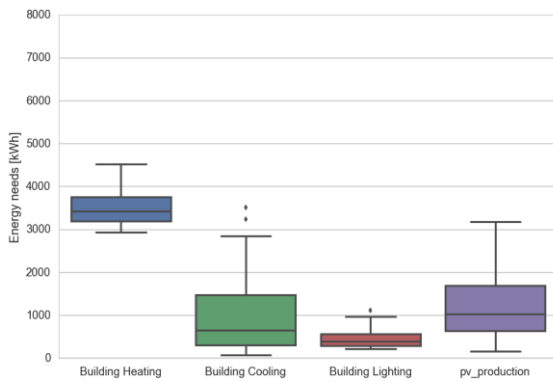
Figure 6.8: Energy need items Copenhagen
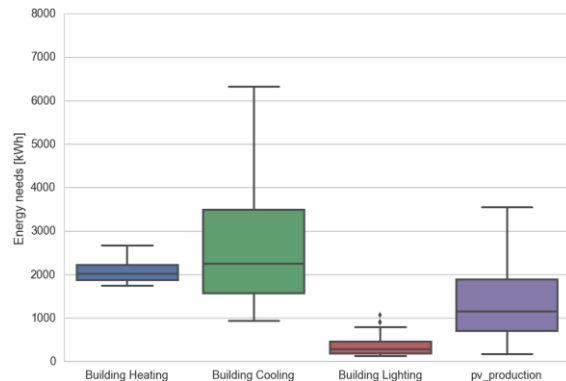
Figure 6.9: Energy need items Lyon
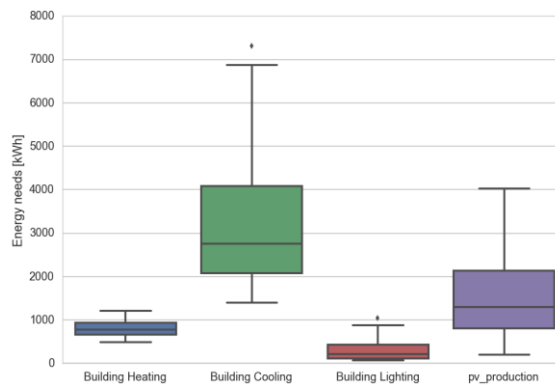
Figure 6.10: Energy need items Madrid

Heating need is one of the major energy need item. As one could expect, its importance decreases when the climate gets hotter. Moreover, this item has a small dispersion with a quartile coefficient of dispersion (QCD) that ranges from 0.08 for the city of Copenhagen to 0.16 for the city of Madrid. Compared to the other items, the design will have a lower influence on the heat need than on the other items.

A second major item is the cooling need. Its importance increases when the climate gets hotter. For cold climates cooling needs are inferior to heating needs; in tempered climates, the two items are equivalent, while in hot climates, cooling needs will dominate. Also, contrary to the heat needs, the cooling needs have a strong dispersion with QCD ranging from 0.32 to 0.65. It means that the cooling needs are strongly affected by the design choice and will probably guide the transparent BIPV sizing.

The third item is the artificial lighting need. No matter the climate, its value is low compared to the other energy needs. It slightly decreases when the climate gets hotter. This behaviour is probably due to the increase of solar radiations. The dispersion is high with a QCD ranging from 0.31 to 0.55. However, given the relative importance of this item it will not be of great influence on the design.

Finally, the PV energy production is rather important and exceeds cooling or heating needs in cold and hot climates. Given that the model is very simple (constant efficiency is assumed), the dispersion is constant for the 3 climates. This item will have a strong influence on the building design.

6.4.2 Design for different orientations

The amount of available solar radiation is very different for the 3 orientations. Also, the time of the day when radiation is available varies depending on the building location. For this reason, the "best designs" or combination of WWR and PVR will vary depending on the room azimuth and on the climate. Figure 6.11 below shows a room E_{need} box plot for the 4 main orientations.
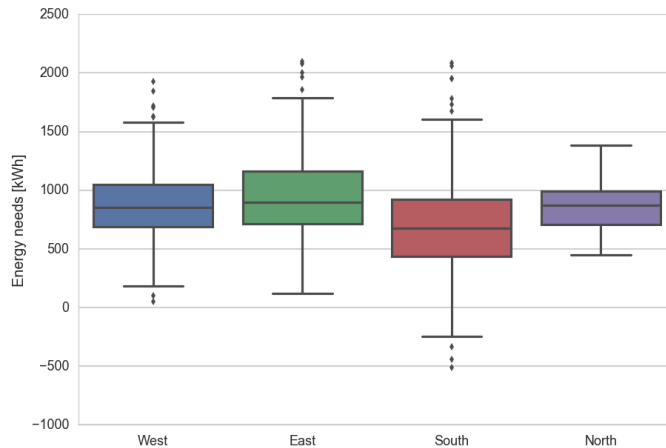
Figure 6.11: Room E_{need} dispersion according to azimuth

The figure above indicates that the average room energy need does not vary a lot no matter the room orientation. However, the dispersion due to design possibility is very different from an orientation to another. For north orientation, with a QCD of 0.16, the impact of the semitransparent BIPV will not greatly impact the E_{need}. On the other hand, with a QCD of 0.36, the south façade design choices will strongly impact building energy demand. For some design, the building will produce more energy than what is required for the south zone heating/cooling/lighting demand. With a QCD of 0.21 and 0.24, the eastern and western orientation design will have a moderate impact on the E_{need}. This difference of behaviour between the façades is obviously due to the variable amount of solar radiation.

The following sections try to find appropriate design for each orientation and climate. The study focuses on south room design that has a stronger impact on the overall building E_{need}.

6.4.2.1 South

The south façade is the orientation that receives the larger amount of solar radiation. For this azimuth, transparent BIPV design has a very strong impact on the room E_{need}. To represent the available combinations and support the selection of the appropriate design, two heat map figures per climates are given. Also, a box plot representing the energy need/production for each item and for each city is displayed.

6.4.2.1.1 Copenhagen

PVR [-]

		0.2	0.3	0.4	0.5	0.6	0.7	0.8
	20	797	777	764	759	762	776	810
	30	833	779	736	704	684	679	696
	40	911	821	741	676	629	601	600
WWR [%]	50	1007	878	763	664	585	531	507
	60	1115	948	796	663	551	469	422
	70	1228	1023	834	668	525	412	342
	80	1347	1105	882	679	506	363	270
	90	1467	1184	926	690	483	312	190
	100	1545	1237	954	696	469	279	139

Figure 6.12: E_{need} heat map for the south façade in the city of Copenhagen

PVR [-]

		0.2	0.3	0.4	0.5	0.6	0.7	0.8
	20	0%	0%	0%	0%	0%	0%	0%
	30	0%	0%	0%	0%	0%	0%	0%
	40	20%	0%	0%	0%	0%	0%	0%
WWR [%]	50	20%	0%	0%	0%	**-20%**	-20%	-20%
	60	20%	20%	0%	0%	-20%	-20%	-20%
	70	60%	20%	0%	0%	-20%	-20%	-20%
	80	60%	20%	20%	0%	-20%	-20%	-60%
	90	60%	60%	20%	0%	-20%	-20%	-60%
	100	60%	60%	20%	0%	-20%	-60%	**-60%**

Figure 6.13: PVR and WWR selection heat map for the south façade in the city of Copenhagen

The first heat map shows the E_{need} for the zone for all the simulated WWR and PVR configuration. A heat map blue/red/yellow is applied to visually compare the configuration that will minimise the south room energy need.

The second heat map categorises the different solutions to facilitate the design selection. 5 colour bins are defined according to the following figure:

60%	E_{need} is at least 60% superior to average E_{need}
20%	E_{need} is 20% to 60% superior to average E_{need}
0%	E_{need} is between 20% and -20% of average E_{need}
-20%	E_{need} is 20% to 60% inferior to average E_{need}
-60%	E_{need} is at least 60% inferior to average E_{need}

Figure 6.14: Design heat map colormap

In this document, only the designs that have a performance at least 20% superior to the average design have been considered. They are represented in blue and light blue.

For the city of Copenhagen, the best WWR and PVR combination is a curtain wall 80% covered by with PV cells. The "worst acceptable" design is a 50% WWR with a 0.6% PVR. Any design in between these values can be considered efficient. The two solutions are represented in bold colour on the "selection heat map" and plotted on the box plot below:
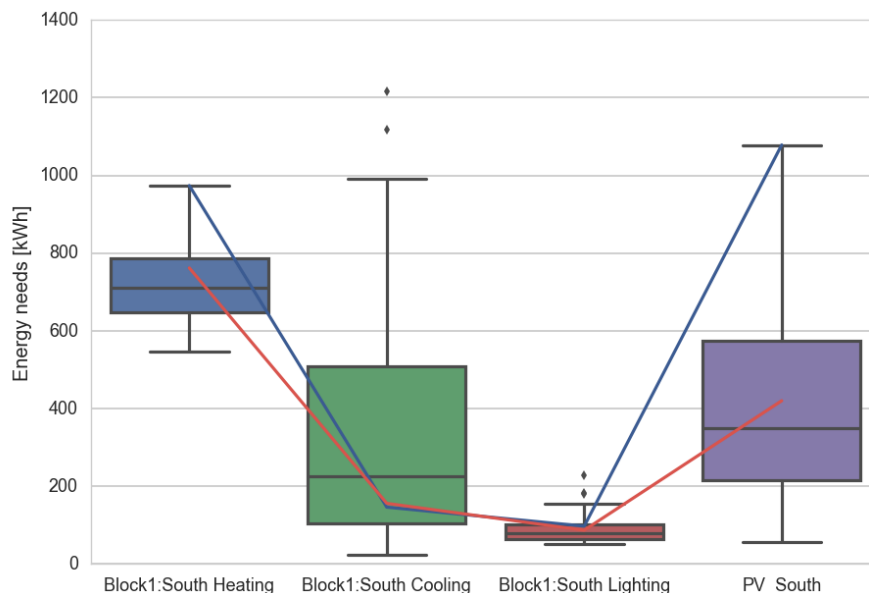
Figure 6.15: Copenhagen south orientation energy items box plot

On the above figure, the best design is represented with a blue line. The simulation shows that selecting a high WWR associated with a large PVR is the best solution for this orientation and this climate. During the winter, the windows heat losses are high, and the high PVR prevents the solar radiation from heating the building. It induces a very high heat need. However, during the summer, and for the same reason, the cooling needs are very low. Considering the large WWR associated to the greatest PVR available, electricity production is at its maximum and compensates the high heat needs. The artificial lightning needs is not a prevailing item.

The lowest "acceptable" design is plotted in red. It corresponds to a WWR of 50% and a PVR of 0.6. The configuration is a compromise between an average heat need and an average PV production. Windows surface is smaller diminishing the heat loss, and PVR is a bit reduced to allow a more important fraction of solar gain. Yet PV production is reduced. For this solution, cooling and lighting needs are similar to the previous case.

6.4.2.1.2 Lyon

	PVR [-]						
	0.2	**0.3**	**0.4**	**0.5**	**0.6**	**0.7**	**0.8**
20	823	775	734	698	676	669	690
30	946	853	769	695	633	587	572
40	1096	960	834	716	615	530	476
50	1258	1076	906	748	603	480	386
60	1428	1199	986	786	601	437	306
70	1602	1327	1069	827	603	400	233
80	1780	1461	1160	878	615	375	178
90	1952	1590	1245	920	618	340	105
100	2062	1673	1300	948	620	318	58

(WWR [%] is the vertical axis label for the rows)

Figure 6.16: E_{need} **heat map for the south façade in the city of Lyon**

	PVR [-]						
	0.2	**0.3**	**0.4**	**0.5**	**0.6**	**0.7**	**0.8**
20	0%	0%	0%	0%	0%	**-20%**	0%
30	0%	0%	0%	0%	-20%	-20%	-20%
40	20%	0%	0%	0%	-20%	-20%	-20%
50	20%	20%	0%	0%	-20%	-20%	-20%
60	60%	20%	0%	0%	-20%	-20%	-60%
70	60%	20%	20%	0%	-20%	-20%	-60%
80	60%	60%	20%	0%	-20%	-20%	-60%
90	60%	60%	20%	0%	-20%	-20%	-60%
100	60%	60%	20%	0%	-20%	-60%	-60%

(WWR [%] is the vertical axis label for the rows)

Figure 6.17: PVR and WWR selection heat map for the south façade in the city of Lyon
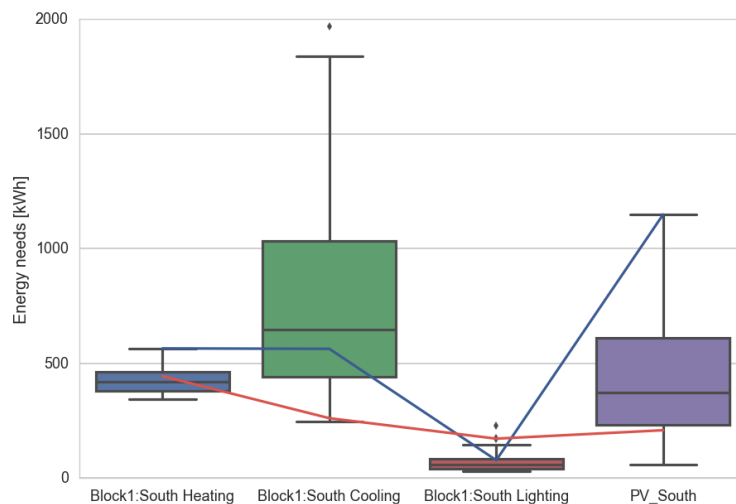
Figure 6.18: Lyon south orientation energy items box plot

As for the city of Copenhagen, for a more tempered climate, according to simulations, the best solution is a 100% WWR associated to a 0.8 PVR. The high heat needs are compensated by a fairly low cooling need and a maximal PV production.

On the opposite, the "worst acceptable design" features a very low WWR (20%) with a high PVR. This climate being hotter than Copenhagen, the solution is viable because it succeeds in limiting windows heat loss, while minimizing heat gain. It results in an average heat need and a very low cooling need. On the other hand, lighting consumption is elevated and PV production is low.

The following figures plot the heat needs, the cooling needs, the windows heat loss and the windows heat gains for both designs:
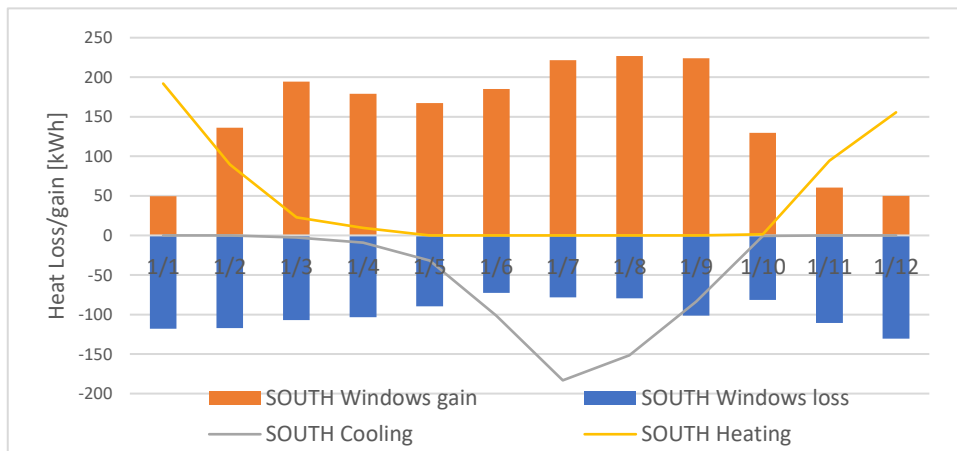
Figure 6.19: WWR100% PVR 0.8 Monthly windows heat gain/loss and heating/cooling needs
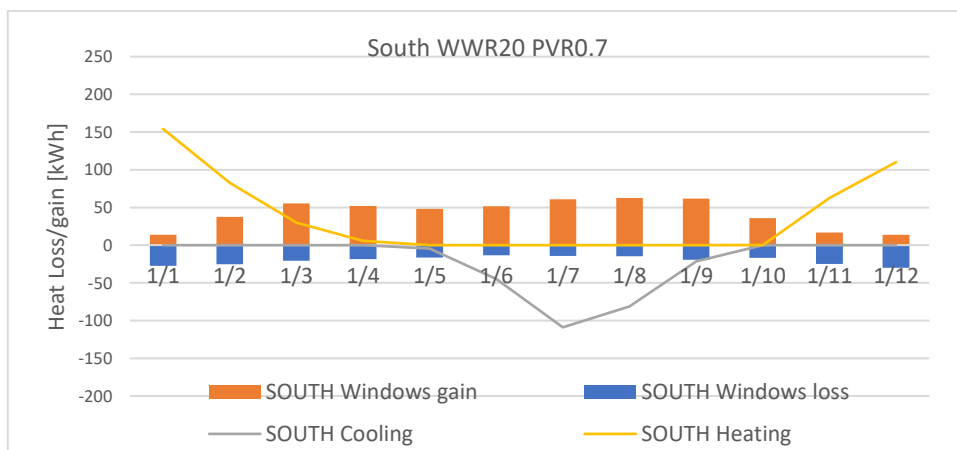
Figure 6.20: WWR20% PVR 0.7 Monthly windows heat gain/loss and heating/cooling needs

The first design clearly shows large windows heat loss in winter and a great amount of solar gain during the summer that leads to overall important heating/cooling needs. This design is made efficient by the important PV production. On the other hand, the second design shows that heat loss and solar gain have been reduced to a minimum, which leads to low heating/cooling needs.

6.4.2.1.3 Madrid

		PVR [-]						
		0.2	**0.3**	**0.4**	**0.5**	**0.6**	**0.7**	**0.8**
WWR [%]	**20**	571	522	482	453	438	441	467
	30	683	576	481	400	336	297	295
	40	854	680	527	391	275	186	143
	50	1058	819	599	403	233	92	-1
	60	1279	975	694	435	208	16	-129
	70	1506	1142	798	479	192	-52	-245
	80	1733	1316	915	540	197	-100	-333
	90	1950	1480	1026	594	194	-159	-442
	100	2088	1586	1098	630	194	-194	-511

Figure 6.21: E_{need} **heat map for the south façade in the city of Madrid**

		0.2	**0.3**	**0.4**	**0.5**	**0.6**	**0.7**	**0.8**
WWR [%]	**20**	0%	0%	0%	0%	0%	0%	0%
	30	20%	0%	0%	-20%	-20%	-20%	-20%
	40	20%	20%	0%	-20%	-20%	-60%	-60%
	50	60%	20%	0%	-20%	-20%	-60%	-60%
	60	60%	60%	20%	0%	-60%	-60%	-60%
	70	60%	60%	20%	0%	-60%	-60%	-60%
	80	60%	60%	60%	0%	-60%	-60%	-60%
	90	60%	60%	60%	0%	-60%	-60%	-60%
	100	60%	60%	60%	0%	-60%	-60%	-60%

Figure 6.22: PVR and WWR selection heat map for the south façade in the city of Madrid
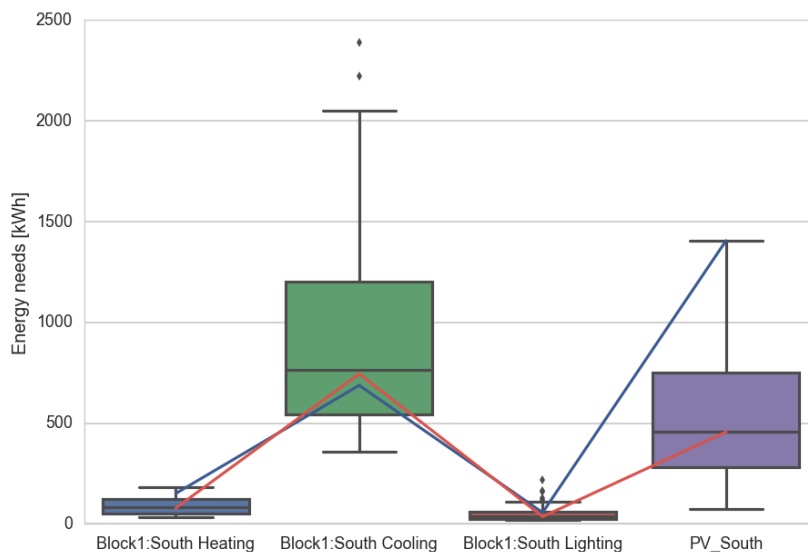
Figure 6.23: Madrid south orientation energy items box plot

For Madrid south orientation, the E_{need} can become negative for several configurations. For a PVR of 0.8 with WWR ranging from 100% to 60% and for PVR of 0.7 and WWR ranging from 100% to 70%, the room will produce more energy than its own needs. This is due to the very low heating needs and the strong PV production potential.

As for the other climates, the "best" and the "worst" acceptable designs are plotted in blue and red colours. The best performances are achieved using a 100% WWR and a 0.8 PVR that would maximise heating, minimise cooling and offer a strong PV production. The other design is obtained for a 50% WWR and 0.5 PVR. It has a slightly lower heat need and higher cooling need but a lower PV production.

For hotter climates strong contrasts appear between the possible design configurations. Considering the amount of solar radiations, high PVR that would limit the amount of heat gain and increase the PV production are recommended.

6.4.2.2 North orientation

WWR [%]	PVR [-]						
	0.2	0.3	0.4	0.5	0.6	0.7	0.8
20	0%	0%	0%	0%	0%	0%	0%
30	0%	0%	0%	0%	0%	0%	0%
40	0%	0%	0%	0%	0%	0%	0%
50	0%	0%	0%	0%	0%	0%	0%
60	0%	0%	0%	0%	0%	0%	0%
70	0%	0%	0%	0%	0%	0%	0%
80	0%	0%	0%	0%	0%	0%	0%
90	20%	0%	0%	0%	0%	0%	0%
100	20%	0%	0%	0%	0%	0%	**0%**
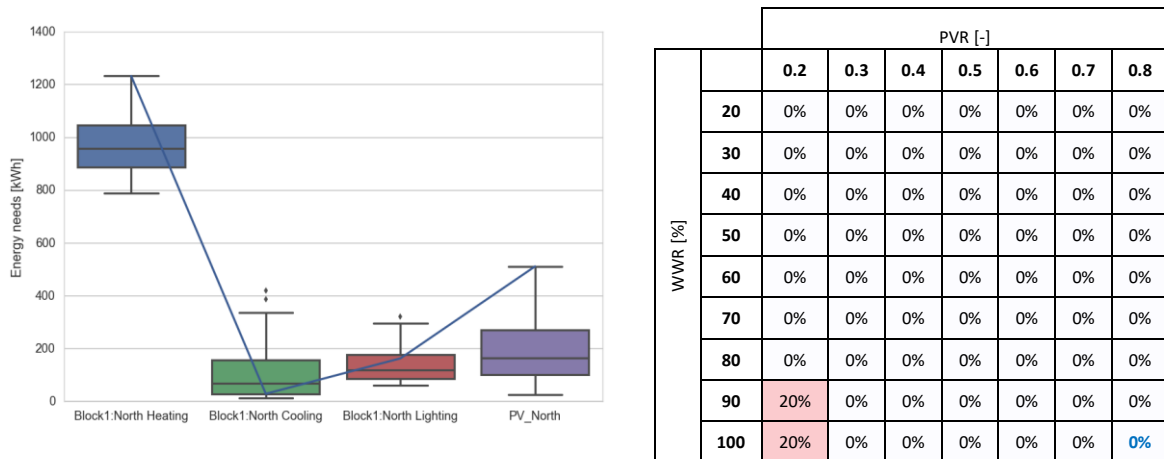
Figure 6.24: North Copenhagen Design selection

WWR [%]	PVR [-]						
	0.2	0.3	0.4	0.5	0.6	0.7	0.8
20	0%	0%	0%	0%	0%	0%	0%
30	0%	0%	0%	0%	0%	0%	0%
40	0%	0%	0%	0%	0%	0%	0%
50	0%	0%	0%	0%	0%	0%	0%
60	20%	0%	0%	0%	0%	0%	0%
70	20%	20%	0%	0%	0%	**-20%**	-20%
80	20%	20%	0%	0%	0%	-20%	-20%
90	20%	20%	0%	0%	0%	-20%	-20%
100	20%	20%	0%	0%	0%	-20%	**-20%**
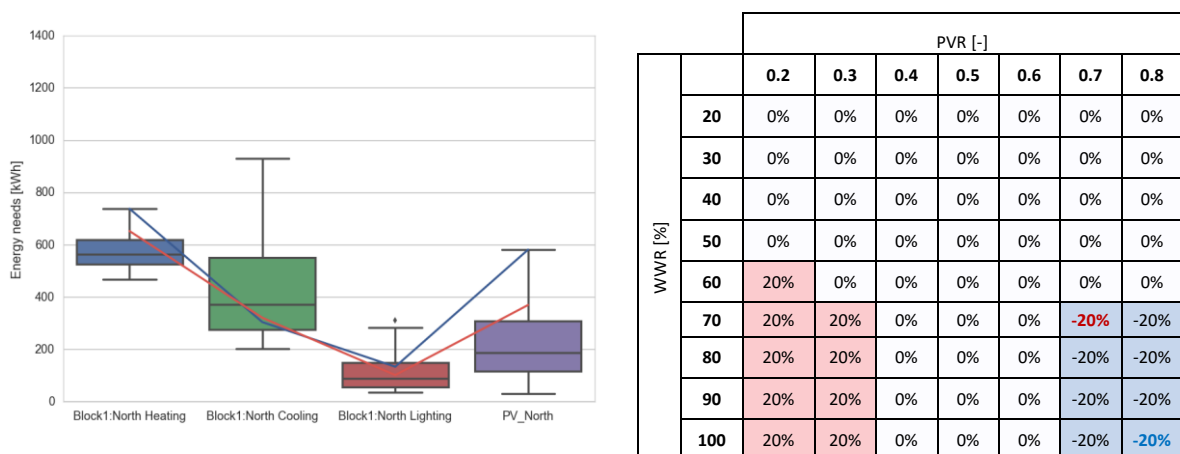
Figure 6.25: North Lyon Design selection
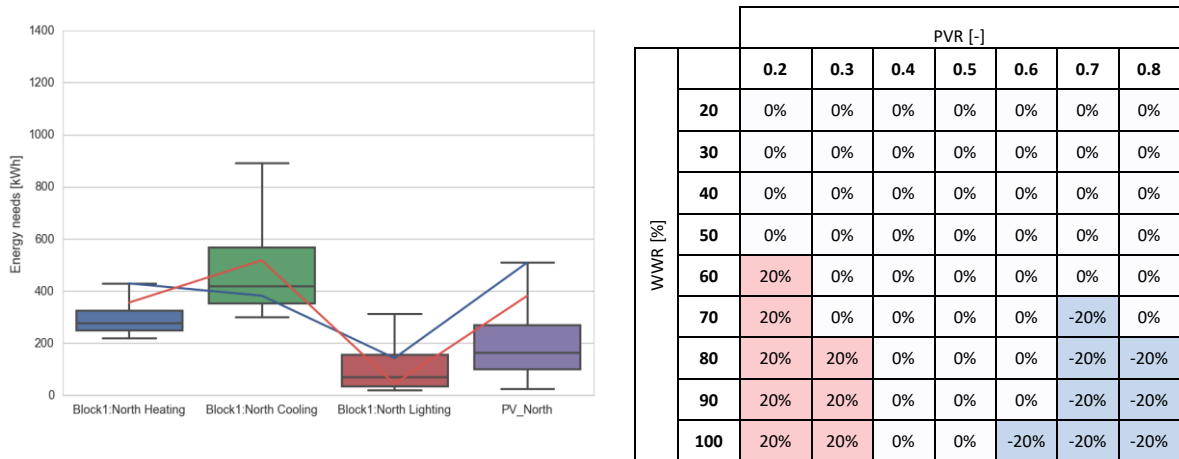
Figure 6.26: North Madrid Design selection

Simulations indicate that for this orientation, transparent BIPV design is less important regarding the room heat need. On the above "selection heat map", very few designs are classified as average design plus or minus 20%. The reason is a very low dispersion of the E_{need} indicator. For the north orientation, the QCD value of the E_{need} is in the range from 0.04 to 0.1 (Copenhagen and Madrid) whereas it was in a range from 0.22 to 0.61 for the south orientation.

However, as for the south orientations, the best design is a high WWR associated to a high PVR. Minimizing cooling needs and maximizing PV production even though heating needs and lighting needs are high, this appears to be the best compromise.

6.4.2.3 West and East orientation

West orientation

WWR [%]	PVR [-]						
	0.2	0.3	0.4	0.5	0.6	0.7	0.8
20	0%	0%	0%	0%	0%	0%	0%
30	0%	0%	0%	0%	0%	0%	0%
40	0%	0%	0%	0%	0%	0%	0%
50	0%	0%	0%	0%	0%	0%	0%
60	20%	0%	0%	0%	0%	0%	-20%
70	20%	20%	0%	0%	0%	-20%	-20%
80	20%	20%	0%	0%	0%	-20%	-20%
90	20%	20%	0%	0%	0%	-20%	-20%
100	60%	20%	20%	0%	0%	-20%	-20%

East orientation

WWR [%]	PVR [-]						
	0.2	0.3	0.4	0.5	0.6	0.7	0.8
20	0%	0%	0%	0%	0%	0%	0%
30	0%	0%	0%	0%	0%	0%	0%
40	0%	0%	0%	0%	0%	0%	0%
50	20%	0%	0%	0%	0%	0%	0%
60	20%	0%	0%	0%	0%	-20%	-20%
70	20%	20%	0%	0%	0%	-20%	-20%
80	20%	20%	0%	0%	0%	-20%	-20%
90	60%	20%	20%	0%	0%	-20%	-20%
100	60%	20%	20%	0%	0%	-20%	-20%
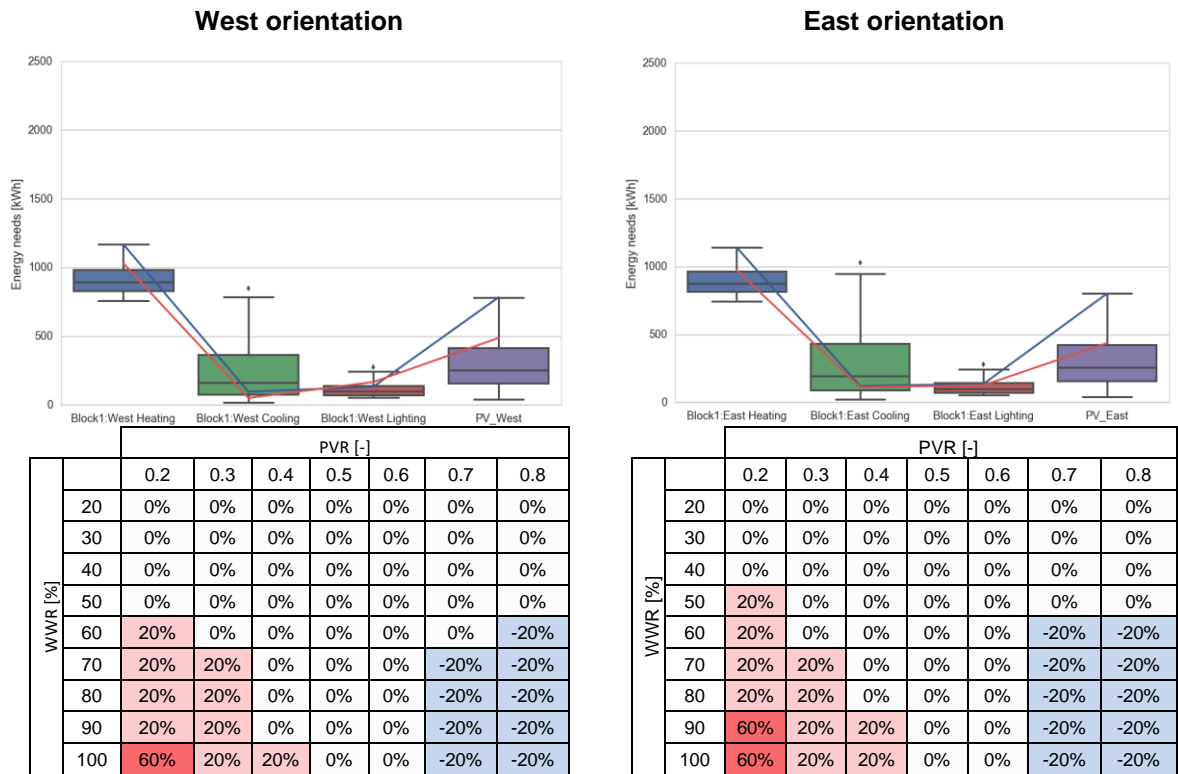
Figure 6.27: Copenhagen design selection

WWR [%]	PVR [-]						
	0.2	0.3	0.4	0.5	0.6	0.7	0.8
20	0%	0%	0%	0%	0%	0%	0%
30	0%	0%	0%	0%	0%	-20%	-20%
40	20%	0%	0%	0%	0%	-20%	-20%
50	20%	0%	0%	0%	**-20%**	-20%	-20%
60	20%	20%	0%	0%	0%	-20%	-20%
70	60%	20%	20%	0%	0%	-20%	-20%
80	60%	20%	20%	0%	0%	-20%	-20%
90	60%	60%	20%	0%	0%	-20%	-20%
100	60%	60%	20%	0%	0%	-20%	-60%

WWR [%]	PVR [-]						
	0.2	0.3	0.4	0.5	0.6	0.7	0.8
20	0%	0%	0%	0%	**-20%**	-20%	-20%
30	0%	0%	0%	0%	-20%	-20%	-20%
40	0%	0%	0%	0%	-20%	-20%	-20%
50	20%	0%	0%	0%	-20%	-20%	-20%
60	20%	20%	0%	0%	0%	-20%	-20%
70	60%	20%	20%	0%	0%	-20%	-20%
80	60%	20%	20%	0%	0%	-20%	-20%
90	60%	60%	20%	0%	0%	-20%	-20%
100	60%	60%	20%	0%	0%	-20%	-20%

Figure 6.28: East Lyon design selection

Report on simulation work for crystalline-silicon based BIPV elements

Figure 6.29: East Madrid design selection

The East and West façades are very similar. Concerning solar radiation, the "mean design" solar production does not vary by more than 3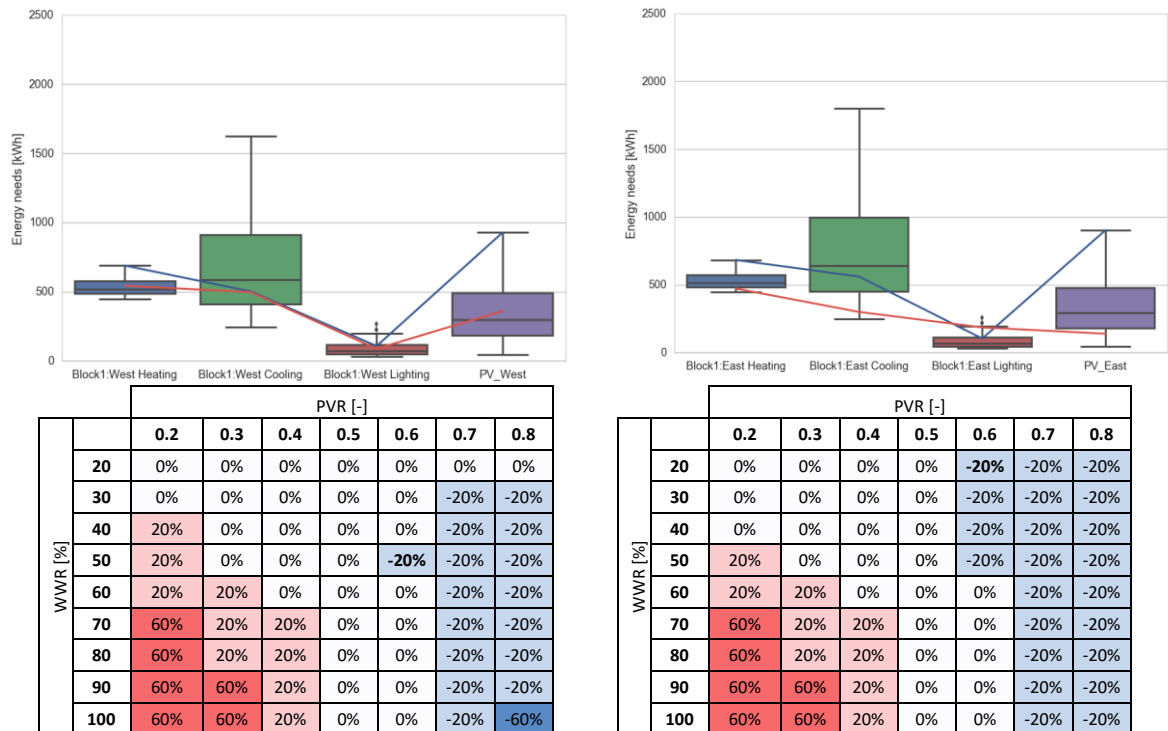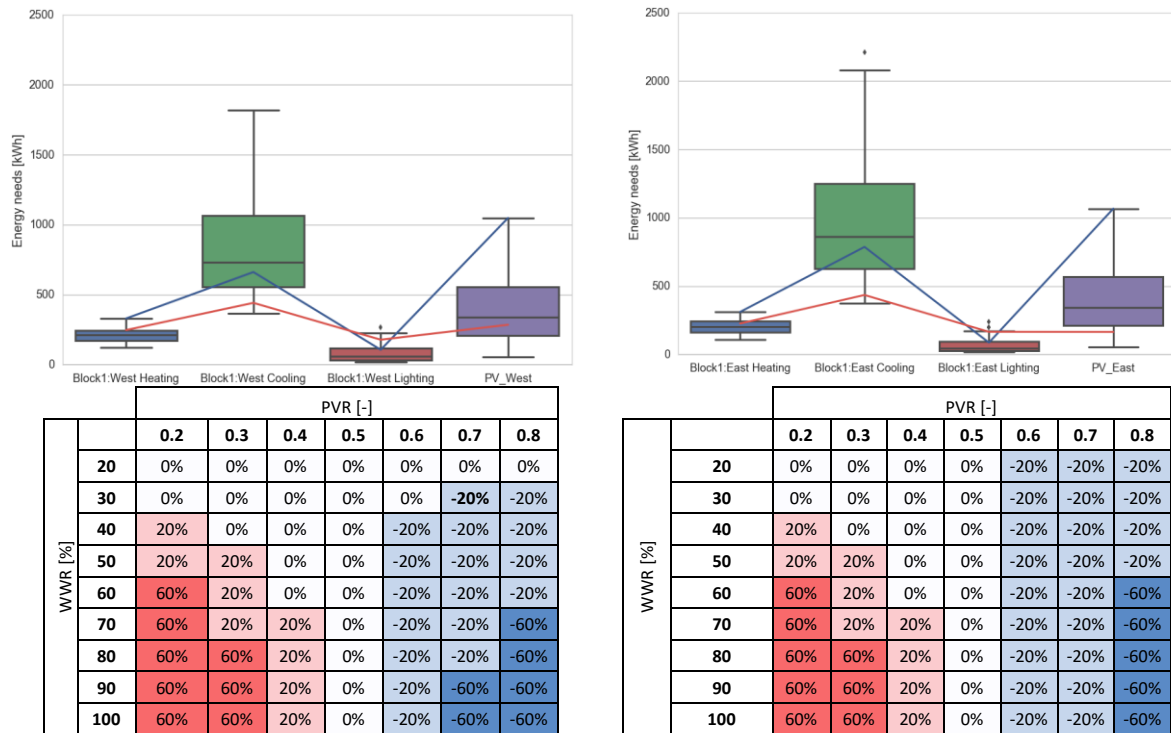% from an orientation to another. Consequently, minimum and maximum productions, respectively corresponding to [WWR = 20%, PVR = 0.2] and [WWR = 100%, PVR = 0.8], do not differ by more than 3%. Considering that the PV model is a constant efficiency coefficient, it means that these very small differences also correspond to the difference between the amount of solar radiation impacting the East and the West facades. From these observations, we can conclude that differences in the design performance between East and West orientations are due to the time of the day (morning or afternoon) when the radiations are available.

For the city of Copenhagen, for all the designs, heating needs are similar for both orientations. There is a small difference of 2% identified for mean design heat needs between the two orientations. However, regarding cooling needs, the mean design cooling need is around 20% higher for the West orientation. The lighting needs are nearly equal. For this climate, available designs are nearly identical. As for the other orientations, the best design is a curtain wall WWR 100% with a high PVR =0.8. Worst acceptable design is a high WWR (70%) associated to a high PVR (0.7).

For the city of Lyon, the results are similar, with an even smaller gap between cooling energy needs. However, given that the overall amount of solar radiation is higher for this climate, the energy needs item dispersion is slightly higher, and the design choices have a little more impact on the E_{need}. The "best" design is still a high WWR with a high PVR. But low WWR with high PVR that will minimise both heating and cooling needs are possible.

For Madrid climate, cooling needs and PV production potential lead the design. Similarly, the most efficient design maximises the heating needs, has low cooling needs and maximises the PV production. But other solutions limiting the WWR and keeping a high PVR can be considered.

6.5 Conclusions on the parametric study of semitransparent solar PV modules in an office building

At building level, the performed study proposes a methodology and a graphic representation to assess the impact of transparent BIPV on a building thermal behaviour. It aims at guiding the design using parametric simulations, and studying an overall heat need indicator. In the scope of this project, the methodology was applied to an "academic" simulation case, but it can easily be applied to actual buildings.

Regarding the results, one must keep in mind that the conclusions can be considered valid for this ideal case. For actual buildings, WWR and PVR might differ.

In this study, for any orientation and for any climate, best solutions are always high WWR and high PVR. Even though this configuration maximises the heat needs, it reduces the cooling needs and maximises the PV production making it the "best design". On the other hand, the worst solutions are high WWR and low PVR. This design implies high heat needs; high cooling needs and has a low electricity production. Between these extreme solutions, several combinations of WWR and PVR offer acceptable performance.

Finally, several notes can be made:

- The E_{need} indicator is based on cooling, heating needs and ideal electricity production. Taking into account the actual efficiency of a boiler, the coefficient of performance of a chiller or a more accurate model of a PV cell might strongly affect the results and the conclusions.

- The use of passive solutions to reduce the cooling needs such as internal blinds or night cooling may also alter the energy balance.

- The design is based on active cooling. Results would be entirely different for passive design. With this solution occupant thermal comfort indicators might be used.

7 REFERENCES

[1]   S. Xu, "Energy Evaluation and Optimal Design of Semi-transparent Photovoltaic Faç ade for Office Buildings in Central China," no. May, 2014.

[2]   P. W. Wong, Y. Shimoda, M. Nonaka, M. Inoue, and M. Mizuno, "Semi-transparent PV: Thermal performance, power generation, daylight modelling and energy saving potential in a residential application," *Renew. Energy*, vol. 33, no. 5, pp. 1024–1036, 2008.

[3]   P. K. Ng, N. Mithraratne, and H. W. Kua, "Energy analysis of semi-transparent BIPV in Singapore buildings," *Energy Build.*, vol. 66, pp. 274–281, 2013.

[4]   T. Baenas and M. Machado, "Optical model for multilayer glazing systems: Application to laminated glass and photovoltaic modules," *Sol. Energy*, vol. 125, pp. 256–266, 2016.

[5]   M. Machado, T. Baenas, and N. Yurrita, "Optical model for multilayer glazing systems: Experimental validation through the analytical prediction of encapsulation-induced variation of PV modules efficiency," *Sol. Energy*, vol. 135, pp. 77–83, 2016.

[6]   T. Baenas and M. Machado, "On the analytical calculation of the solar heat gain coefficient of a BIPV module," *Energy Build.*, vol. 151, pp. 146–156, 2017.

[7]   T. Y. Y. Fung and H. Yang, "Study on thermal performance of semi-transparent building-integrated photovoltaic glazings," *Energy Build.*, vol. 40, no. 3, pp. 341–350, 2008.

[8]   EnergyPlus, "Engineering Reference," *US Dep. Energy*, no. c, pp. 1–847, 2016.

[9]   ISO, "Thermal performance of windows, doors and shading devices - Detailed calculations," *ISO 150992003*, 2003.

[10]   G. Notton, C. Cristofari, M. Mattei, and P. Poggi, "Modelling of a double-glass photovoltaic module using finite differences," *Appl. Therm. Eng.*, vol. 25, no. 17–18, pp. 2854–2877, 2005.

[11]   Th-BCE, "Arrêté du 30 avril 2013 portant approbation de la méthode de calcul Th-BCE 2012 prévue aux articles 4, 5 et 6 de l'arrêté du 26 octobre 2010 relatif aux caractéristiques thermiques et aux exigences de performance énergétique des bâtiments nouveaux et des," *J. Off.*, vol. n°0106: 77, 2012.